CURRICULUM VITAE

Vidula Kolhatkar

(Degree and date to be conferred: Ph.D. 2011)

Education

Ph.D.	(pursuing since Aug 2006) Department of Pharmaceutical Sciences University of Maryland, Baltimore Advisor: Dr. James Polli
M.S. (Pharmaceutical Chemistry)	2000-2002 Institute of Chemical Technology Mumbai, India Advisor: Dr. Mariam Degani
B.S. (Pharmacy)	1996-2000 AISSMS College of Pharmacy Pune University, Pune, India

Work experience

Graduate Teaching Assistant Aug 2006-April 2007
University of Maryland, Baltimore
Assisted Pharm D students in Compounding lab and Pharmaceutics lab

Lecturer
AISSMS College of Pharmacy, Pune, India Aug. 2003-April 2004

- Conducted lectures and labs for second and third year Bachelor of Pharmacy students.
- Modules covered included:
  Structure, reactions and reaction mechanism of various classes of organic compounds
  Qualitative analysis of organic compounds, separation and identification of organic compounds in a binary mixture, synthesis of small molecules

Lecturer
Allana College of Pharmacy, Pune, India Nov. 2002 – April 2003

- Conducted lectures and labs for second and fourth year Bachelor of Pharmacy students.
- Modules covered included:
  Structure, reactions and reaction mechanism of various classes of organic compounds
  Design, discovery and Structure Activity Relationship studies of various classes of therapeutic agents
  Separation and identification of organic compounds in a binary mixture, synthesis of small molecules

Awards, honors and achievements

- Travel award from GlaxoSmithKline to attend 2010 FIP PSWC/AAPS Annual Meeting and Exposition in New Orleans, Louisiana.
- Junior Research Fellowship by University Grant Commission, New Delhi, India 2000
- Secured 99.36 percentile in the Nationwide Graduate Aptitude Test in Engineering-2000 (All India ranking 21)
- Rho Chi Honor Society Member

Leadership/Extracurricular activities

- AAPS Student Chapter treasurer 2009-2010
- Treasurer for Girls Hostel 2001-2002
- Received Foreign Pharmacy Graduate Examination Committee (FPGEC) Certification from National Association of Boards of Pharmacy
- Worked as Intern Pharmacist at a retail pharmacy store Aug 2005-Aug 2006
  Assisted Pharmacist in filling prescriptions, counseling patients and other routine Pharmacy duties

Abstracts and posters

- **Vidula Kolhatkar** and James Polli *Synthesis and in vitro evaluation of bile acid conjugate of 5-aminosalicylic acid for colon targeting* Accepted for AAPS Annual Meeting 2011.
- **Vidula Kolhatkar** and James Polli *Structural Requirements of the Human Apical Sodium Dependent Bile Acid Transporter Using Bile Acid Conjugates with Modifications of Steroidal Hydroxyl Groups* AAPS Transporter Workshop Bethesda, MD 2011
- **Vidula Kolhatkar** and James Polli *Effect of Structural Modifications of Steroidal Hydroxyl Groups on Bile Acid Interaction with Human Apical Sodium-Dependent Bile Acid Transporter* AAPS Annual Meeting, New Orleans, LA 2010
- **Vidula Kolhatkar** and James Polli *Inhibition of the human Apical Sodium-dependent Bile acid Transporter (hASBT) by 7-substituted Bile Acids* AAPS Annual Meeting, Los Angeles, CA 2009
- Vinita Kulkarni, **Vidula Vaze**, Mariam S. Degani *Novel method for synthesis of important intermediate of tiotropium* 5th International symposium on Innovations in Pharmaceutical Sciences and Technology, Mumbai, India 2003
- **Vidula Vaze**, Mariam S. Degani: *Microwave assisted thiamine catalyzed benzoin condensation type of reaction* IUPAC sponsored 14th International Conference on Organic Synthesis at Christchurch, New Zealand 2002

Manuscripts

- **Vidula Kolhatkar** and James Polli *Reliability of Inhibition Models to Correctly Identify Type of Inhibition* Pharmaceutical Research (2010) 27:2433–2445
- **Vidula Kolhatkar**, Lei Diao, Chayan Acharya, Alexander MacKerell and James Polli *Identification of novel non steroidal compounds as substrates or inhibitors of hASBT* Journal of Pharmaceutical Sciences 2011 (in press).
- **Vidula Kolhatkar** and James Polli *Synthesis and in vitro evaluation of bile acid conjugate of 5-aminosalicylic acid for colon targeting* (Submitted to Molecular Pharmaceutics)
- **Vidula Kolhatkar** and James Polli *Impact of C-7 chemical space on ursodeoxycholate interaction with bile acid transporters* (submitted to European Journal of Pharmaceutical Sciences))
- Seema Bag, **Vidula Vaze**, Mariam S. Degani. *Microwave assisted benzoin condensation using thiamine as catalyst* J. Chem. Research (2006) 4: 267-269.

ABSTRACT

Title of Dissertation: Elucidating structural requirements of bile acid transporters: prodrug design for oral delivery

Dissertation directed by: James E. Polli Ph.D.
Professor and Ralph F. Shangraw/Noxell Endowed Chair
Department of Pharmaceutical Sciences
School of Pharmacy
University of Maryland, Baltimore

Drug transporters play a key role in drug disposition and hold promise for improving pharmacotheapeutic outcomes. Inhibition studies are routinely performed to characterize transporters and identifying type of inhibition. Studies were performed to identify methods which can correctly determine inhibition type. For conventional inhibition data, nonlinear regression performed poorly, whereas Dixon-type data yielded moderately better results. Interestingly, a new approach denoted “nonconventional inhibition data” performed well.

Apical sodium dependent bile acid transporter (ASBT) and sodium-taurocholate cotransporting polypeptide (NTCP) are potential prodrug targets. Successful prodrug design is impeded by an incomplete understanding of structural requirements for these transporters. To evaluate the effect of C-3 and C-7 substitution on bile acid interaction with these transporters, 19 bile acid analogues were tested against ASBT and NTCP for binding and translocation. Results indicated that ASBT and NTCP accommodated a wide range of substituents for binding, but all major C-7 modifications resulted in analogues that did not demonstrate active uptake by either ASBT or NTCP. A C-3 modification that

was not tolerated at C-7 still afforded translocation via ASBT and NTCP, confirming the relative unacceptability of C-7 modification. Results suggest that drug conjugation to the C-3 hydroxyl group, rather than C-7, has potential for successful prodrug targeting of ASBT and NTCP. Based on these results a prodrug of 5-aminosalicylic acid (5-ASA), first-line therapy for treatment of ulcerative colitis, was designed that conjugated 5-ASA with glycoursodeoxycholic acid via an azo bond. In vitro studies demonstrated that the prodrug had a low permeability and it was selectively released 5-ASA in the colon.

Although bile acids are endogenous molecules and are considered safe, they have some limitations to use as pro-moities. Studies were performed to identify small molecules as pro-moities to target ASBT. This successfully identified two non-steroidal molecules that were substrates of ASBT. Results indicated, for the first time, that the bile acid steroid backbone and a negative charge are not required for ASBT translocation. Overall, this work may lead to successful design of prodrugs for better delivery of orally administered drugs.

Elucidating structural requirements of bile acid transporters: prodrug design for oral delivery

By

Vidula Kolhatkar

Dissertation submitted to the faculty of the Graduate School of the
University of Maryland, Baltimore in partial fulfillment
of the requirements for the degree of
Doctor of Philosophy
2011

This dissertation is dedicated to Rohit and Sanvi.

I appreciate all the help, support and understanding.

ACKNOWLEDGEMENTS

I owe my sincere gratitude to all those who supported me during my graduate studies and it is a pleasure to thank who have made this dissertation possible.

My deepest gratitude is to my advisor Dr. James Polli for his constant guidance, advice and support. He always encouraged me and set an example by constantly working hard himself. His patience and support helped me overcome many difficult situations and finish this dissertation. I am grateful for getting an opportunity to work with him.

I am thankful to my dissertation committee members Dr. Peter Swaan, Dr. Yan Shu, Dr. Hongbing Wang and Dr. Mark Ginski for their constructive comments, suggestions. They were always available when I needed their help.

I would like to thank to Dr. Steven Fletcher for his suggestions in chemistry. I would also like to thank Dr. Changxing Shao and Dr. Maureen Kane for their assistance with LC/MS work. Thanks to Dr. Kellie Hom for training and help with NMR. Thanks to Dr. Austin Yang and Dr. Stefani Thomas for allowing me to use the mass spectrometer in their facility.

Many thanks to my lab members Dr. Rana Rais, Dr. Xiowan Zheng, Dr. Pablo Gonzalez, Dr. Lei Diao, Dr. Bancha Chausuwan, Zhongqi Dong, Diana Johnson and Siddharth Raman. They all are very understanding and helpful. I will cherish the wonderful time we shared. I am also thankful to all my friends in school and outside school for their help and support.

I am grateful to my parents for their love, support and encouragement over the years. Thank you. I also appreciate all the help of my parents-in-law offered during this time. Most of all, I acknowledge Rohit for his constant support and encouragement. His help, patience and faithful support during the final stages of this Ph.D. is so appreciated. I cannot thank my daughter Sanvi enough. She made me forget most of my stress. Her cooperation with every move between the states made everything easier especially during the last one year.

LIST OF TABLES

LIST OF FIGURES

CHAPTER 1

INTRODUCTION AND OBJECTIVES

1.1 MEMBRANE TRANSPORTERS

Membrane transporters are proteins that govern the transport of various endogenous molecules such as amino acids, bile acids, glucose, electrolytes and hormones, as well as xenobiotics like drug molecules. Membrane transporters play a crucial role in oral drug absorption, distribution to specific organs, metabolism and excretion. Following oral administration, drug undergoes absorption by passive diffusion and possibly carrier-mediated transport. Passive diffusion is proportional to the concentration gradient, the lipid-water partition coefficient of the drug, and the membrane surface area available to the drug. In addition to the passive diffusion, carrier-mediated transport plays a key role in drug disposition and drug interaction, for drugs such as pravastatin, rosuvastatin, glyburude, digoxin to name a few (1-4). Depending on the physicochemical properties of drug and its metabolite, passive diffusion and carrier mediated transport regulates excretion of such moieties. The transporter white paper underlines the importance of transporters in drug absorption, distribution, metabolism and excretion (5, 6).

Carrier mediated transport by membrane proteins can be further classified as facilitated diffusion and active transport. As the name suggest, facilitated diffusion does not require energy input and transports substrates down the concentration gradient.

Two main transporter superfamilies are involved in drug disposition: the adenosine triphosphate (ATP)-binding cassette (ABC) transporter superfamily (efflux transporters) and the solute carrier (SLC) transporter superfamily (uptake transporters). The dynamic interplay between these influx and efflux transporters, along with passive disposition and drug metabolizing enzymes, decide the fate of drugs.

1.1.1 The ABC transporter superfamily

These are primary active transporters and require direct ATP hydrolysis for their function. Although they act as efflux transporters in eukaryotes, ABC influx and efflux transporters are present in prokaryotes. Despite the very wide expression range and a large variety of substrates, these transporters share conserved nucleotide binding domains and a signature motif (7, 8).

From a clinical perspective, P-glycoprotein (P-gp), multidrug resistance protein 1 (MRP1), breast cancer resistance protein (BCRP), bile salt export pump (BSEP) have a significant role in drug disposition, including as basis for drug interactions. Transporters in this class are responsible for translocation of a wide variety of endogenous compounds and xenobiotics. Various drugs such as digoxin, paclitaxel, fexofenadine, methotrexate, topotecan, and statins demonstrate interaction with ABC transporters and can elicit clinically significant changes in pharmacokinetic and pharmacodynamic respons of these drugs. Drugs with a low bioavailability and a narrow therapeutic index are expected to have the most significant clinical impact (6, 9, 10).

1.1.2 The SLC transporter superfamily

Unlike ABC superfamily, SLC superfamily transporters may be facilitated transporters or secondary (or tertiary) active symporters and antiporters. The secondary active transporters employ electrochemical potential of existing ionic gradient instead of direct ATP hydrolysis. A number of drugs as well as endogenous compounds are substrates and/or inhibitors of SLC transporters. Transportes such as those in the organic anion transporting polypeptide family including (e.g. OATP1B1, OATP1B3, OATP1A2,

OATP2B1), organic anion transporter 1 (e.g. OAT1), organic cation transporter 2 (e.g. OCT2), peptide transporter 1 (e.g. PEPT1) have clinically relevant role in drug disposition, including drug interactions. Changes in these interactions due to other substances/drugs can lead to potential differences in drug disposition (11).

Thus given the impact of transporters on pharmacokinetic and pharmacodynamic profiles of drugs, increasing number of studies now focus on screening drugs and new molecular entities for the interactions with transporters. This can also aid in identifying potential drug interactions (10).

1.2 IN VITRO TRANSPORTER ASSAYS

Despite the indispensable role of transporters in drug disposition, successful prediction of interactions with drug molecules is limited. Prediction of drug-transporter interaction is essential to designing new successful therapies. Understanding of these interactions is also central to rational design of drugs and prodrugs to target particular transporter to improve absorption and/or reduce adverse reactions. This approach has created an interest in elucidating structural requirements for the transporters and developing models to predict these interactions. However, in absence of suitable crystallization methods, only primary and secondary structures are known for most of these proteins. Under such conditions, homology modeling can be employed to model the transporter proteins. When a suitable template is not available, substrate based design can be an effective approach. This approach involves a series of experiments with substrates or inhibitors of the transporters where biological activity is correlated with structural features. With advances

in computational chemisrty, pharmacophore modeling and 3D- QSAR modeling can provide working knowledge of transporter-ligand interaction. A pharmacophore based model describes the molecular features required for biological activity (12-14). This approach has successfully identified structurally diverse drug molecules as novel inhibitors of transporters (15, 16). 3D QSAR model is another method that correlates changes in physicochemical properties of molecules to the biological activity. These models can be based on inhibitors describing the structural features that influence binding, or substrates that illustrate the features associated with translocation via the transporter. These computational modeling along with in vitro experiments represent a powerful tool to understand structure/function relationships of transporters.

Cell based transporter assays are routinely performed to evaluate interaction of various molecules with the transporter of interest. Such assays especially those performed in transfected cell-lines allow assessment of definitive interaction with the transporter protein with determination of kinetic parameters such as Ki, Kt and Jmax. Different types of assays performed include inhibition, uptake and transport assay.

1.2.1 Inhibition assay

The inhibition assay is a useful tool to determine affinity for a transporter and can be the first facile indicator of compound binding with the transporter. This assay measures the decrease in uptake of known substrate in presence of compound of interest. The assay can be performed to identify the percent decrease in uptake by a fixed concentration of inhibitor or inhibition constant Ki or half maximal inhibitory concentration (IC_{50}). IC_{50} value depends on amount of membrane protein present, concentration of substrate and

inhibitor used during assay. Ki on the other hand is an intrinsic value that depends on the transporter and inhibitor and independent of substrate concentration (17). This assay is typically performed with radiolabeled substrate making it a simple experimental design and higher throughput for each compound compared to the other assays described above. The data from inhibition can be successfully used to develop pharmacophore model or QSAR model and can aid in understanding transporter-ligand interactions.

Understanding the correct type of inhibition is necessary for developing an accurate computational model as two compounds that inhibit a transporter by differing mode may not bind to the same binding site. For example, enalapril was concluded to be a competitive inhibitor of glycylsarcosine transport by the high-affinity peptide transporter, whereas quinapril was concluded to be a noncompetitive inhibitor (18, 19). These conclusions suggested that enalapril and glycylsarcosine bind at the same binding site, whereas quinapril binds at a different binding site than glycylsarcosine. Thus, determining type of inhibition contributes towards transporter structure/function understanding.

1.2.1.1 Types of inhibition The three classical types of inhibition include competitive, noncompetitive and uncompetitive inhibition (20).

A. Competitive inhibition Competitive inhibition occurs when substrate (S) and inhibitor (I) compete for the same binding site. The inhibitor only binds the free enzyme/transporter (E).

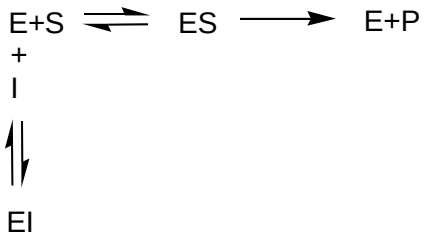

Competitive inhibition is represented by following equation.

$$J = \frac{J_{max} S}{K_t \left(1 + I / K_i\right) + S} P_p S \qquad \text{eqn 1.1}$$

where J is solute uptake, S is solute concentration, Jmax and Kt are the Michaelis-Menten constants for transporter-mediated uptake of the solute, Ki is the inhibition coefficient, I is inhibitor concentration and Pp is passive permeability.

B. Noncompetitive inhibition. In noncompetitive inhibition, S and I bind reversibly and independently at different sites. Thus I binds to both E and ES and S binds to E and EI.

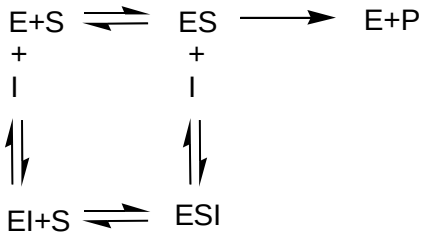

Noncompetitive inhibition is represented by following equation

$$J = \frac{J_{max} S}{\left(1 + I / K_i\right)(K_t + S)} P_p S \qquad \text{eqn 1.2}$$

C. Uncompetitive inhibition. In uncompetitive inhibition I binds only to the ES.

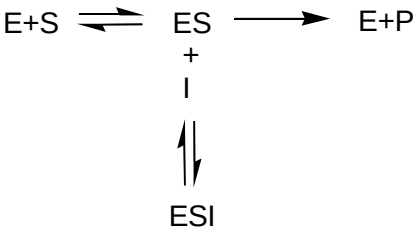

Uncompetitive inhibition is represented by following equation

$$J = \frac{J_{max} S}{K_t \left(1 + I / K_i\right) + S} + P_p S \qquad \text{eqn 1.3}$$

1.2.2 Uptake assay

In contrast to transport assay, the uptake assay measures the amount of compound translocated by a transporter (e.g. accumulation inside cell). The experiment should be performed to identify active and passive component of uptake to determine the substrate parameters. The saturable active component and passive component can be calculated by conducting a experiment the presence and absence of the driving force for active transport (e.g. Na^+ or H^+), or without and with known inhibitors. An approach can also employ studies at 37°C and 4°C respectively. The kinetic parameters are determined from net active flux across the monolayer using equation (1.4)

$$J = \frac{J_{max} S}{K_t + S} + P_p S \qquad \text{eqn 1.4}$$

where J is the flux rate, S is substrate concentration, Kt is Michaelis-Menten constant and Pp is passive permeability.

1.2.3 Transport assay

This assay measures the net permeability of a compound. The assay is best suited for polarized cells that form tight junction such as Caco-2 and Madin-Darby canine kidney (MDCK) cell lines. The cells are grown on membrane support system (e.g. polycarbonate or polyethylene terephthalate). The test compound is added to the apical side for apical-to-basolateral transport or to the basolateral compartment for basolateral-to-apical transport. Samples are collected at appropriate time to analyze concentrations in the apical and basolateral compartments by LC-UV or LC/MS. Permeability for reference compounds such as mannitol (for low permeability), and metoprolol for (for high permeability) is also assessed in parallel to evaluate monolayer integrity. Mannitol permeability < 2 x 10^{-6} cm/s is considered acceptable. Additionally, transepithelial electrical resistance (TEER) values can be measured before assay which indicates the degree of monolayer confluence and tight junction development (21, 22). The apparent permeability (Papp) of unidirectional flux can be calculated by eqn (1.5)

$$P_{app} \quad \frac{J}{A \times C_0} \qquad \text{eqn 1.5}$$

where J is the flux rate, A is the surface area and C_0 is concentration of drug in donor chamber.

1.3 PRODRUGS

Transporters interact with a range of molecules including nutrients and drug molecules and aid in absorption, metabolism and excretion of the same. Transporters not only play a

role in absorption but also control distribution of substances to various tissues. Transporters can be exploited to design specific molecules to be absorbed by specific tissues. The strategy has been successfully demonstrated to increase absorption of drugs such as valacyclovir, ganciclovir, midodrine via peptide transporters; gabapentin prodrug XP13512 that takes advantage of monocarboxylate transporter type 1 and a sodium-dependent multivitamin transporter is in clinical trials (23-27). Prodrugs by definition are bioreversible derivatives of drug molecules that undergo enzymatic and/or chemical transformation in vivo to release the active parent drug, which can then exert the desired pharmacological effect. With increased understanding and knowledge of carrier-mediated absorption, efforts are being made to rationally design prodrugs targeted to specific transporters. This involves attaching a drug to a promoiety, usually an endogenous substrate for the transporter, such that this promoiety-drug conjugate is absorbed by the transporter.

With increased diversity in the chemical structures of drug molecules, new strategies are needed to improve their oral bioavailability. Attaching drug molecules to endogenous ligands is being explored as a potential strategy. Various literature reports underline the prevalence of this approach to improve oral bioavailability of drug molecules (28-34). A rational approach to design prodrugs is more likely to be effective. To be an attractive prodrug target, a transporter should have high efficiency and capacity. Targeting a prodrug to a tissue specific transporter can reduce undesired side-effects and reduced dosage. Additionally, the natural ligand for the transporter should have suitable functional groups for a drug candidate conjugation. The transporter should have wide substrate specificity so these conjugates would be substrates for the transporter.

ASBT is one such transporter. It is a member of solute carrier superfamility (SLC 10A2). It is highly expressed in the terminal ileum and is a key component in absorption of bile acids from intestine and maintaining enterohepatic circulation. The intestinally absorbed bile acids then enter liver where they are absorbed across the basolateral membrane of hepatocytes mainly by NTCP. The bile acid pool of about 3-5 g, undergoes multiple cycles resulting in a turnover of 12-18 g of bile acid each day. Despite such high recycling, less than 0.5 g bile acids are lost in feces each day. Such high capacity and efficiency of ASBT and NTCP makes these transporters a prodrug target (35). Drug molecules can be conjugated to bile acids, the endogenous ligands of these transporters, such that the drug-bile acid conjugate will be absorbed by ASBT and NTCP. This can aid in increasing bioavailability of low permeability drugs. Absorption by NTCP can lead to liver targeting of the resulting prodrug. For successful design of prodrugs targeting these transporters it is necessary to understand the structural requirements of these transporters.

1.4 BILE ACID STRUCTURE AND FUNCTIONS

Bile acids are synthesized in liver by enzymatic catabolism of cholesterol. Cholic acid and chenodeoxycholic acid are the primary bile acids. These are further converted to secondary bile acids deoxycholic acid, lithocholic acid and ursodeoxycholic acid. Human bile acid pool consists mainly of cholic acid, chenodeoxycholic acid (CDCA) and deoxycholic acid (90%). Remaining 10% consists of lithocholic acid and ursodeoxycholic acid (UDCA). Bile acids do not exist as free C-24 carboxylic acids but as glycine or taurine conjugates in ratio 1:2. This conjugation reduces pKa of bile acids

from about 5 (unconjugated) to 4 and 2 for glycine and taurine conjugated bile acid respectively (36). Conjugation allows bile acids to exist as anions at physiological pH and limit the passive permeability. Figure 1 illustrates the general structure of bile acids in humans. Table 1 describes native bile acids and their structural differences.

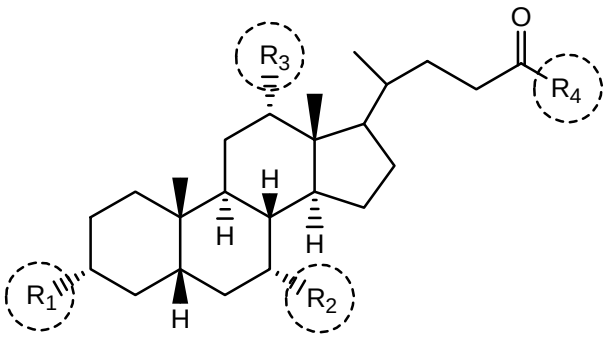

Figure 1.1 General structure of native bile acids.
Bile acids differ in hydroxylation pattern and amino acid conjugation pattern at the C-24 position.

Table 1.1 Bile acid nomenclature.

Bile acid	R_1	R_2	R_3	R_4
		Primary bile acids		
Cholate	OH	OH	OH	OH
Glycocholate	OH	OH	OH	$NHCH_2COOH$
Taurocholate	OH	OH	OH	$NH(CH_2)_2SO_3H$
Chenodeoxycholate	OH	OH	H	OH
Glycochenodeoxycholate	OH	OH	H	$NHCH_2COOH$
Taurochenodeoxycholate	OH	OH	H	$NH(CH_2)_2SO_3H$
		Secondary bile acids		
Deoxycholate	OH	H	OH	OH
Glycodeoxycholate	OH	H	OH	$NHCH_2COOH$

Taurodeoxycholate	OH	H	OH	$NH(CH_2)_2SO_3H$
Lithocholate	OH	H	H	OH
Glycolithocolate	OH	H	H	$NHCH_2COOH$
Taurolithocholate	OH	H	H	$NH(CH_2)_2SO_3H$
Ursodeoxycholate	OH	OH (β)	H	OH
Glycoursodeoxycholate	OH	OH (β)	H	$NHCH_2COOH$
Tauroursodeoxycholate	OH	OH (β)	H	$NH(CH_2)_2SO_3H$

Addition of hydroxyl groups converts the cholesterol to a more hydrophilic bile acid, allowing a more efficient interaction with water. The number and orientation of the hydroxyl groups determines the hydroplilicity of bile acids. In figure 2, the -OH groups in CDCA are located below the steroid nucleus and are axial whereas -OH group in UDCA is above the steroid nucleus and is equatorial to the plane of steroid nucleus. Among 3-, 7- dihydroxy bile acids, ursodeoxycholic acid (3 - and 7 - hydroxyl group) is more polar than chenodeoxycholic acid (3 .- and 7 .- hydroxyl group).

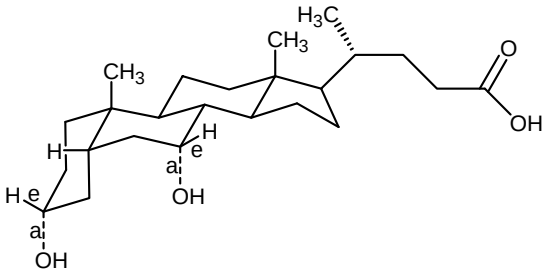

Chenodeoxycholic acid

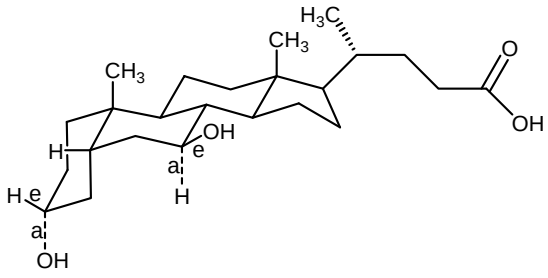

Ursodeoxycholic acid

Figure 1.2 Orientation of hydroxyl groups in chenodeoxycholic acid and ursodeoxycholic acid. Chenodeoxycholic acid has axially oriented hydroxyl groups at

1.4.1 Functions of bile acids

After their synthesis, bile acids are secreted into bile and stored in gall bladder. Following food intake, bile is secreted in the small intestine. Bile acids aid in the absorption of lipids, lipid soluble vitamins and cholesterol. Additionally, bile acids interact with various nuclear receptors and activate versatile signaling pathways.

Bile acids are lignads for nuclear receptors such as farnesoid X receptor, preganane X receptor and vitamin D receptor. This interaction with nuclear receptors results in regulation of bile acid synthesis as well as their metabolism and detoxification (37).

Bile acids also activate various cell signaling pathways in liver and gastrointestinal tract. Bile acids activate guanine nucleotide binding protein (G protein) coupled receptor TGR5. TGR5 is expressed in various organs and cells. TGR5 expression in monocytes and macrophages leads to immuno-modulatory bile acid activation. TGR5 activation also has hepatoprotective function, may help control glucose metabolism in liver and enhanced energy expenditure in brown adipose tissue (37-39).

Bile acids play a role in regulating their own synthesis, fatty acid, lipid and lipoprotein synthesis and glucose metabolism in liver. These important molecules are conserved and efficiently recovered by active and passive processes across intestinal epithelium and return to liver from where it is secreted in bile duct to enter intestine to complete enterohepatic circulation. Various transporters involved in this include the following (40):

- Ileal enterocyte
  - ASBT expressed on apical side

- Ileal bile acid binding protein (IBABP) facilitates intracellular transport across enterocyte.
- OST./OST expressed on basolateral side.

ƒ Hepatocyte

- NTCP expressed on basolateral side
- OATP1A2, OATP1B1, OATP1B3 expressed on basolateral side responsible for sodium independent uptake of bile acids.
- Bile salt export pump (BSEP) expressed on canalicular membrane of hepatocytes transports monovalent bile acids.
- Multidrug resistance protein MRP2 located on canalicular membrane of hepatocytes transports divalent acid or glucuronidated bile acids

1.5 PHYSIOLOGY AND FUNCTIONAL ASSESSMENT OF ASBT

ASBT is highly expressed on the apical membrane in ileum where it is responsible for 95% of reabsorption of bile acids. It is also expressed in renal proximal tubules and where it prevents urinary excretion of bile acids. Expressed in cholangiocytes, ASBT possibly functions in a cholehepatic shunt (41) or allows cholangiocytes to sample biliary bile acid concentrations in order to activate cellular signaling pathways (42, 43). Human ASBT (SLC10A2) is a seven transmembrane domain glycoprotein with apparent mass of 48 kDa and consists of 348 amino acids with Asn 10 representing the glycosylation site

(44). ASBT mediated transport of bile acids is electrogenic and is coupled with sodium (45).

Structural information on ASBT is limited to its primary and secondary structure. Like other polytopic membrane transporters no high resolution protein structure is available. There is limited information available about the structure activity relationships of this transporter with its ligands.

Prior to cloning of ASBT, studies were performed using everted gut sac and intestinal perfusion methods. Based on such studies, Lack proposed a model for bile acid transport (46).

This model suggested following generalization

1. For inhibition, there is an inverse relationship between number of steroidal hydroxyl groups and inhibitor affinity.
2. Trihydroxy bile acids are better transported than dihydroxy bile acids.
3. No one hydroxyl group in steroid ring is necessary. Among themselves the dihydroxy bile acids are equally well transported.
4. A single negative charge on the side chain is required and addition of a second negative charge aborted transport.

Swaan et al developed a low resolution model for substrate recognition by ASBT based on binding affinity studies performed in Caco-2 cells (47). This model had following features

1. A large electronegative region in the C-24 region of bile acids. Positive charge or neutral groups in this region diminish affinity for ASBT
2. There is flexibility towards substrates with altered C-24 sequence. There is positive effect on affinity with introduction of steric bulk at the end of C-24 side chain.
3. Three hydroxyl groups oriented in the same direction outline the hydrophilic region and number of hydroxyl groups in this region is directly related to affinity. Steric bulk in this region decreases affinity.
4. Orientation of methyl moieties on the steroid ring marks the lipophilic region.

Baringhaus et al developed a 3D QSAR pharmacophore model based on IC50 values of chemically diverse compounds. The study was performed in rabbitileal bile acid transporter expressed in CHO cells. This model was characterized by five features one hydrogen bond donor, one hydrogen bond acceptor and three hydrophobic features. Natural bile acids such as taurocholate, taurochenodeoxycholate or taurodeoxycholate were able to map four of these five features (48).

1. The five membered D ring and methyl group at position 18 map one hydrophobic site.
2. Methyl group at 21 maps the second hydrophobic site.
3. One of the .-oriented hydroxyl groups at 7- or 12- maps the hydrogen bond donor.
4. Negatively charged side chain functions as hydrogen bond acceptor.

4. Amino acids were conjugated bile acid indicated that a single negative charge is not essential binding with neutral and cationic CDCA conjugates exhibiting potent Ki. But only monoanionic conjugates demonstrated transport via ASBT (51).

5. Studies with aminopiperidine conjugates of glutamyl bile acids indicated these compounds to be strong inhibitors. Hydrophobicity, orientation of substituent on α-carboxylic acid, and partially compacted side chain conformation promoted inhibitory potency. Although these zwitter ions and cations were strong inhibitors they did not demonstrate transport across ASBT (52, 53).

6. Studies with monoanionic substituted aniline conjugates of glutamyl bile acids demonstrated strong affinity for ASBT with inhibition potency (Ki) as well as strong affinity for transport across ASBT. The Ki as well as Kt and Jmax were in the range of native bile acids. Dianionic bile acids had dramatically low Ki and Kt (53, 54).

7. Attaching pyridine with various substituents to glutamyl CDCA provided compounds with strong affinity for the transporter with Ki in the range of native bile acids. Most of these compounds were also substrates for ASBT (55).

All these studies involving substrate requirements for ASBT employed bile acid conjugates. All the models are therefore silent about non-steroidal small molecules being substrates of this transporter.

1.6 PHYSIOLOGY AND FUNCTIONAL ASSESSMENT OF NTCP

After intestinal absorption by ASBT, bile acids enter the portal blood. Na^+ dependent taurocholic cotransporting polypeptide (NTCP) is the major transporter for absorption of bile acids in liver. This transporter is expressed on the basolateral membrane of hepatocytes (40). Ntcp was found to be expressed in pancreatic acinar cells where it may be involved in clearing bile acids leaked into the terminal acini (56). Human NTCP (SLC10A1) consists of 349 amino acids with an apparent mass of 56kDa with two glycosylation sites Asn 5 and Asn 11 (57). Along with transport of conjugated and unconjugated bile acids NTCP also transports sulfated bile acids such as chenodeoxycholate-3-sulfate and taurocholate-3-sulfate, steroid sulfates such as oesterone-3-sulfate, chlorambucil taurocholate conjugate and rosuvastatin (58).

1.7 RESEARCH OBJECTIVES

The high capacity and efficiency of the bile acid transporters ASBT and NTCP to transport bile acids has potential to be exploited to improve oral delivery of drug candidates by making bile acid conjugated prodrug. Potential success of this prodrug strategy is impeded by incomplete understanding of structure and function requirements of these transporters. The objectives here included elucidating structural requirements for these transporters, identify suitable pro-moities, and design appropriate prodrugs for better delivery of orally administered drugs. Drugs with low or variable oral bioavailability such as methyldopa, furosemide, alendronate as well as drugs with liver as

site of action such as adefovir, ribavirin can benefit from prodrugs targeting ASBT and NTCP.

The evaluation of ligand binding to a transporter by an inhibition study is central to the comprehensive study of any transporter. Identifying the correct type of inhibition is an important yet challenging task. Chapter two explores this area with an aim to evaluate reliability of inhibition models to correctly identify type of inhibition. Two types of routinely performed studies were evaluated via simulations to identify their ability to correctly identify type of inhibition. Based on the results, a new method 'nonconventional inhibition' was also studied to recognize the method that can correctly identify the type of inhibition.

ASBT and NTCP are attractive prodrug targets with their high capacity to transport bile acids. For a successful prodrug targeting of these transporters, it is necessary to understand the structure activity relationships of these transporters and select candidate drug with such relationships in mind. Bile acid are versatile molecules in that drug molecules can be conjugated to various positions in bile acid molecules, such as any of the hydroxyl groups 3-, 7-, or 12- or at the C-24 carboxylic acid. Although literature reports may suggest conjugating drugs to the 7- position of bile acids, there are no reports of the influence of C-7 chemical space on interaction with bile acid transporters. Chapter three discusses the impact of C-7 chemical space on ursodeoxycholate and chenodeoxycholate interaction with bile acid transporters. Studies involved synthesis of a series of bile acid conjugates followed by evaluating interaction of these conjugates with ASBT and NTCP in terms of binding affinity as well as translocation. The studies were

performed in stably transfected ASBT-MDCK cell line and NTCP-HEK cell line to understand the structural requirements of these transporters.

Based on the results from chapter three which indicated that conjugating aromatic group to C-7 position of bile acids negatively impacts the interaction with ASBT and NTCP, a prodrug of 5-aminosalicylic acid (5-ASA) was designed. 5-ASA was conjugated to bile acid via azo bond at C-3 and C-7 positions to allow colon targeting of 5-ASA, first line treatment of ulcerative colitis. In vitro studies were performed to evaluate stability of the prodrug as well as release of the drug under appropriate conditions. Chapter four describes the findings.

Although bile acids are favorable promoities, they have certain limitations. These include their high molecular weight, limited water solubility and versatile signaling ability. In chapter five the aim was to identify nonsteroidal molecules as substrates of ASBT such that a drug can be conjugated to this promoiety to design prodrug to target ASBT. The project involved identifying molecules similar to bile acids, selecting molecules to screen for ASBT binding studies and evaluating uptake by ASBT for some of the hits to identify non-steroidal substrates. Two novel non-steroidal molecules were identified as ASBT substrates.

Overall, various in vitro studies were performed to understand the structural requirements of ASBT and NTCP to design prodrugs using bile acids as pro-moities. In addition, non-steroidal small molecules identified as substrates of ASBT for the first time have potential to lead to non-steroidal pro-moities to target ASBT. This work can aid in design of prodrugs for better delivery of orally administered drugs.

CHAPTER 2

Reliability of Inhibition Models to Correctly Identify Type of Inhibition

2.1 INTRODUCTION

Inhibition studies are routinely performed to gain insight into the structure and function of transporters, particularly when a transporter crystal structure is not available. For example, two project areas in our laboratory involve the apical sodium-dependent bile acid transporter (ASBT) and the organic cation/carnitine transporter (OCTN2), where transport inhibition studies by novel compounds and diverse drugs has yielded pharmacophore models and quantitative structure activity relationships (QSAR) (15, 16, 52, 53).

A simplifying assumption in proposing such pharmacophore or QSAR models is that inhibition data assumes the same type of inhibition, since two compounds that inhibit a transporter by differing mode may not bind to the same binding site. Hence, inhibition studies can benefit from elucidating the type of inhibition by which various compounds inhibit. Determining type of inhibition can also help in understanding of interaction of inhibitors at the binding site of transporter. For example, enalapril was concluded to be a competitive inhibitor of glycylsarcosine transport by the high-affinity peptide transporter(18), whereas quinapril was concluded to be a noncompetitive inhibitor (19). These conclusions suggested that enalapril and glycylsarcosine bind at the same binding site, whereas quinapril binds at a different binding site than glycylsarcosine. Thus, determining type of inhibition contributes towards transporter structure/function understanding.

Classic inhibition models include competitive, noncompetitive, and uncompetitive inhibition. Although these models have long-standing use, it has not been assessed when the competitive and noncompetitive models are reliable in correctly elucidating the type

of inhibition. One common approach to discern between competitive and noncompetitive inhibition is via nonlinear regression and selection of the better fitting model. For instance, Lau and Chang studied CYP2B6 inhibition by *Ginkgo biloba* extract (59). Mode of inhibition was determined through inhibition studies that used various inhibitor and substrate concentrations, followed by nonlinear regression for competitive, noncompetitive, mixed and uncompetitive inhibition. The result was verified by visual inspection of a Lineweaver-Burk plot and a Dixon plot. However, reliability of methods to identify the correct model has not been evaluated in such applications. The other approach to discern between types of inhibition involves measuring changes in substrate parameters Kt and Jmax with change in inhibitor concentration.

In this study three objectives were pursued that concerned the ability to correctly identify the correct type of inhibition. The first objective was to compare the abilities of the competitive, noncompetitive, and uncompetitive inhibition models to best fit simulated competitive and noncompetitive data, where data reflected conventional inhibition data. Conventional inhibition data entailed simulated data for the common situation where substrate concentration was fixed at a single level but inhibitor concentration varied. The second objective was identical to this first objective, but considered so-called Dixon-type data, where simulated data was larger in scope, in that both substrate concentration and inhibitor concentration were varied. These objectives were pursued by simulating uptake values for each competitive and noncompetitive inhibition model using an Excel spreadsheet; Gaussian error was then incorporated to the uptake values. These simulated data were subjected to nonlinear model fitting and the best fitting model was identified. Since results showed that nonlinear regression performed poorly in identifying the correct

inhibition model for conventional inhibition data, a third objective was pursued, which was to perform similar studies as per objective one, but for nonconventional inhibition data, where substrate concentration was varied and inhibitor concentration was fixed at a single level. Results from experimental inhibition data were also examined to challenge simulation observations. With recent progress in the filed of transporters it is now acknowledged that transporters play a key role during in vivo drug disposition. Elucidating type of inhibition is central to the study of transporters and aids in understanding how a new chemical entity interacts with a transporter. employing nonconventional inhibition a resource sparing study will be beneficial in high throughput environment such as pharmaceutical industry.

Overall findings here suggest caution in suggesting a specific inhibition model from various types of inhibition data, including conventional data and even the more comprehensive Dixon-type data. Additionally, results indicate that nonconventional inhibition data merits further consideration to identify type of inhibition, particularly since such an approach is resource sparing compared to Dixon-type data.

2.2 MATERIALS AND METHODS

To assess the ability to correctly identify type of inhibition, three objectives were pursued using simulated uptake data, where each objective differed in scope of data. The first objective employed simulated uptake where substrate concentration was fixed at a single level but inhibitor concentration varied (conventional inhibition data). The second objective employed simulated uptake where both substrate and inhibitor concentrations

were varied (Dixon-type data). The third objective employed simulated uptake where substrate concentration was varied but inhibitor concentration was fixed at a single level (nonconventional inhibition data). These objectives involved data simulation, followed by model fitting and comparison of model performance. Simulations were employed since only simulation can provide a basis to know with certainty the underlying inhibition type. Results from experimental inhibition data were also examined to challenge the observations from simulation studies.

2.2.1 Analysis of conventional inhibition data

2.2.1.1 Data simulation. Simulated uptake values were obtained from competitive and noncompetitive inhibition models. The competitive and noncompetitive inhibition models are shown in eqns 1 and 2.

$$J = \frac{J_{max} S}{K_t\left(1 + I/K_i\right) + S} \qquad \text{eqn 1}$$

$$J = \frac{J_{max} S}{\left(1 + I/K_i\right)(K_t + S)} \qquad \text{eqn 2}$$

where J is solute uptake, S is solute concentration, Jmax and Kt are the Michaelis-Menten constants for transporter-mediated uptake of solute, Ki is the inhibition coefficient, and I is inhibitor concentration. Passive flux was considered zero for simplicity. Simulations were performed with following parameters: Jmax = 0.0005nmol/s/cm^2; Kt = 5 μM; S = 2.5 μM. Three scenarios were studied. In the first scenario, simulated uptake values were obtained from the competitive model where Ki was 10 μM and inhibitor concentration varied from 0 to 100 μM. In the second scenario, simulated uptake values were obtained

from each competitive and noncompetitive model where Ki was 100μM and inhibitor concentration varied from 0 to 500μM, as well as from 0 to 1000μM. These values for Ki, I, Kt, and S were assessed since these values reflect typical ranges in the literature. Simulated uptake values were not obtained from the uncompetitive inhibition model, since this model is of less general interest than the other two models.

Uptake error was computed using Excel. Error in uptake was incorporated using a percent coefficient of variation (CV%) level of 30% and 10%, which reflects a higher and lower end of common level of variation. Error was added by multiplying the simulated uptake value from eqn 1 or 2 by a random number with mean 1.0 and standard deviation 0.3 or 0.1. Profiles were simulated to allow for each scenario to be evaluated 30 times (i.e. 30 occasions), which is a large sample size (60). For each occasion, simulations attempted to mimic experimental design using n = 3, such that each uptake value was simulated (with error) three times for each unique condition for each occasion.

2.2.1.2 Model fitting and identification of best fitting model. The competitive, noncompetitive, and uncompetitive inhibition models were fitted to the simulated data using WinNonlin 5.2 (Pharsight, Mountain View, CA). The competitive and noncompetitive models are eqn 1 and 2, respectively. The uncompetitive model is

$$J = \frac{J_{max} S}{K_t + S\left(1 + I/K_i\right)} \qquad \text{eqn 3}$$

Akaike Information Criterion (AIC) was used to select the best fitting model from the competing models(5).

$$AIC = n \cdot \ln\left(\sum_{i=1}^{n} w_i \left(Y_{obs,i} - Y_{cal,i}\right)^2\right) + 2p \qquad \text{eqn 4}$$

where n is the number of data points, i is the sequence sample number, wi is the weight (wi = 1), Yobs,i is the observed value, Ycal,i is the predicted value, and p is the number of model parameters.

Ki estimates from the correct model (even if not the best fitting model) were evaluated in terms of accuracy by comparing the Ki estimate to the true Ki (i.e. Ki value used to simulate the data).

2.2.2 Analysis of Dixon-type data

2.2.2.1 Data simulation. Simulated uptake values with error were obtained from competitive and noncompetitive inhibition models as above, using eqn 1 and 2. Simulations for two scenarios were conducted to mimic a matrix of inhibition studies involving three levels of substrate concentration, as well as four levels of inhibitor concentrations (i.e. conducted to mimic the large scope of data that is historically analyzed by Dixon plots). In the first simulation scenario, which covers a wide range of I/Ki, the following parameter ranges were used: Jmax was 0.0005nmol/s/cm^2; S was 1, 5, and 10 μM; when Ki was 1 μM, I = 0, 0.5, 2 and 5 μM; and when Ki = 100 μM, I = 0, 50, 200, and 500 μM. The ratio I/Ki ranged from 0 to 5.

The following parameter ranges were used in a second simulation scenario with a more narrow, but more experimentally-typical range, of I/Ki values: Jmax was 0.0002nmol/s/cm^2; Kt was 5 μM; S was 1, 2.5, and 5 μM; Ki = 58 μM; and I was 0, 10,

50, and 100 μM. The ratio I/Ki ranged from 0 to 1.7, which reflects the typical range of I/Ki values (61-66).

Error was incorporated using a CV% level of 20% or 30%, as described above. Uptake profiles were simulated to allow for each scenario to be evaluated 30 times (i.e. 30 occasions), which is a large sample size (60). For each occasion, simulations attempted to mimic experimental design using n = 3, such that each uptake value was simulated (with error) three times for each unique condition for each occasion.

2.2.2.2 Model fitting and identification of best fitting model. As above for objective one, primary analysis of this "Dixon-type data" was non-linear regression, and not Dixon plot analysis. For each the competitive, noncompetitive and uncompetitive inhibition models, fits of eqn 1, 2, and 3 to simulated data were conducted using WinNonlin. Simultaneous fitting of uptake versus inhibitor concentration was conducted across the three levels of substrate concentration. AIC was used in selecting the best fitting model. Ki estimates from the best fitting nonlinear regression model were also examined in terms of accuracy, by comparing to the Ki value used to simulate the data. As secondary analysis to nonlinear regression, simulated uptake data were plotted as Dixon plots; plots were visually assessed to determine type of inhibition.

2.2.3 Analysis of nonconventional inhibition data

As results below indicate, conventional inhibition data performed poorly in identifying the correct inhibition model. Additionally, Dixon-type data requires a large and comprehensive matrix of inhibition studies, which represents a practical barrier to routinely elucidate type of inhibition. Hence, nonconventional inhibition data – where

substrate concentration was varied but inhibitor concentration was fixed at a single level – was assessed for its ability to identify the correct inhibition model, even though such studies are generally not performed. Of note, data for this objective three was practically the same as for objective one (i.e. same simulation approach and same range of parameter values); objective one and three only differed in data groupings that were subjected to model regression, although were simulated separately.

2.2.3.1 Data simulation. Simulated uptake values with error were obtained from competitive and noncompetitive inhibition models as above, using eqn 1 and 2. Simulations were conducted over following parameter ranges: Jmax = 0.0005nmol/s/cm^2; Kt = 5 μM (as well as 500 μM for competitive model); S ranged from 0.2 times Kt to 100 times Kt; and I/Ki ranged from 0.01 to 100.

2.2.3.2 Model fitting and identification of best fitting model. The competitive, noncompetitive and uncompetitive inhibition models were fit to the simulated data using WinNonlin 5.2. AIC was used in selecting the best fitting model from the competing models.

2.2.4 Experimental data

2.2.4.1 Materials. Ursodeoxycholic acid was purchased from TCI America (Portland, OR, USA), taurocholic acid was purchased from Calbiochem (La Jolla, CA, USA) and (^{3}H) taurocholic acid was obtained from PerkinElmer (Waltham, MA, USA).

2.2.4.2 Inhibition studies. Inhibition studies were performed in ASBT-MDCK cell line as described previously (16). Briefly, the cells were exposed to donor solution containing taurocholate (spiked with ^{3}H taurocholate), and the inhibitor at 37 °C for 10 min. After 10

min cells were lysed and cell lysate was counted for associated radioactivity using a liquid scintillation counter.

Conventional inhibition data was obtained via an inhibition study using one fixed level of substrate concentration (i.e. 2.5 μM taurocholic acid). Ursodeoxycholic acid was used as inhibitor; inhibitor concentration ranged from 0 to 250 μM. Dixon-type data was obtained via an inhibition study using three taurocholate substrate concentrations (1, 2.5 and 5 μM) and four ursodeoxycholate concentrations (0, 25, 50 and 100 μM). Nonconventional inhibition data was obtained via an inhibition study performed at several taurocholate substrate concentrations ranging from 1 to 500 μM and one inhibitor (ursodeoxycholate) concentration. Two sets of nonconventional inhibition data were obtained: one at I/Ki = 1 and the other at I/Ki = 5.

Similar to eqn 1-3, inhibition data was fitted to the competitive, noncompetitive, and uncompetitive models, but allowed for a passive permeability component, per eqn 5-7:

$$J = \frac{J_{max} S}{K_t\left(1 + I/K_i\right) + S} + P_p S \qquad \text{eqn 5}$$

$$J = \frac{J_{max} S}{\left(1 + I/K_i\right)\left(K_t + S\right)} + P_p S \qquad \text{eqn 6}$$

$$J = \frac{J_{max} S}{K_t + S\left(1 + I/K_i\right)} + P_p S \qquad \text{eqn 7}$$

where Pp is the passive permeability.

2.3 RESULTS AND DISCUSSION

2.3.1 Analysis of conventional inhibition data

2.3.1.1 Simulated competitive model data. The first objective was to compare the abilities of competitive, noncompetitive, and uncompetitive inhibition models to best fit simulated competitive and noncompetitive data from conventional inhibition studies. Table 1 and Table 2 summarize results obtained from simulated competitive data and simulated noncompetitive data, respectively.

Table 2.1 Results from conventional inhibition data.
Data was simulated from competitive inhibition model, where Ki, maximum I/Ki, and random error were varied. Under "best fitting model", values are the percentage of times that the best fitting model was competitive, noncompetitive, or uncompetitive. Percentages are derived from simulations of 30 occasions (n = 3 per occasion). AIC was used to identify the best fitting model.

Ki (μM)	Maximum I/Ki	%CV error	Best fitting model		
			Competitive	Noncompetitive	Uncompetitive
10	10	10%	20.0%	13.3%	66.7%
10	10	30%	36.7%	16.6%	46.7%
100	5	30%	26.7%	23.3%	50%
100	10	30%	43.3%	20%	36.7%

In Table I, study variables were model used to fit data (competitive, noncompetitive, and uncompetitive), Ki (10 and 100 μM), maximum I/Ki ratio (5 and 10), and error level (%CV of 10% and 30%). When Ki = 10 μM, maximum I/Ki = 10, and error is 30%, the competitive model (i.e. the correct model) was the best fitting model only 36.7% of the time. The uncompetitive mode was the best fitting 46.7% of the time.

Figure 1 plots the simulated conventional inhibition data for two occasions. These data reflect conventional inhibition data, where uptake from a fixed, single concentration of substrate is reduced as inhibitor concentration is increased. Figure 1 shows the fits of all three models to simulated competitive data when Ki = 10 μM. In Figure 1 panel A, the uncompetitive model was the best fitting model, where r^2 was 0.900 for competitive, noncompetitive and uncompetitive fits. All three fit profiles were practically the same. For this simulation occasion (of the total of 30 independent occasions), AIC values did not determine the competitive model to be the best fitting model. Meanwhile, in panel B, the competitive model was the best fitting model per AIC, where r^2 was 0.818 for competitive, noncompetitive and uncompetitive fits. In general, all the competitive, noncompetitive, and uncompetitive fits were very similar from conventional inhibition data, as reflected in the two occasions in Fig. 1. It should be noted that r^2 values are reported here since r^2 values are frequently inspected as a measure of absolute quality of fit, even though AIC was used to identify the best fitting model.

In Table I, reducing error from 30% to 10% did not improve the ability to identify the competitive model as the correct model (compare 20.0% for %CV=10% to 36.7% for %CV=30%). Furthermore in Table I, when Ki was 100 μM and maximum I/Ki was 5 (i.e. inhibitor concentration ranged from 0 to 500 μM), the competitive model was the best fitting model only 26.7% of the time. Increasing the maximum I/Ki to 10 resulted in the competitive model to be correctly identified 43.3% of the time, which is still poor. This increase in maximum inhibitor concentration from 500 μM to 1000 μM enhanced the percent substrate inhibition from 76.9% to 86.9%, which may have contributed to the greater reliability to identify the correct model. Unfortunately, such high inhibitor

concentration may not be feasible in all cases because of limited inhibitor solubility. Also, changing the weighting from 1 (i.e. no weighting) to weighting of 1/observed^2 practically did not change the ability to identify the right model. Using weighting of 1/observed^2, the competitive, noncompetitive and uncompetitive models were the best fitting models 30.0%, 23.3%, and 46.7% of the time, respectively, compared to 36.7%, 16.6%, and 46.7% with weighting of 1 (Table I line 2). Similarly, using a different optimization algorithm and different initial conditions had no practical impact. Using the Nelder-Mead simplex algorithm (rather than Gauss-Newton algorithm with Levenberg and Hartley modification), the competitive, noncompetitive and uncompetitive models were the best fitting models 16.7%, 33.3%, and 50.0% of the time. Using initial conditions that differed from the original initial condition by being lower or higher than the estimated values, distribution was 40.0%, 40.0%, and 20.0%.

A

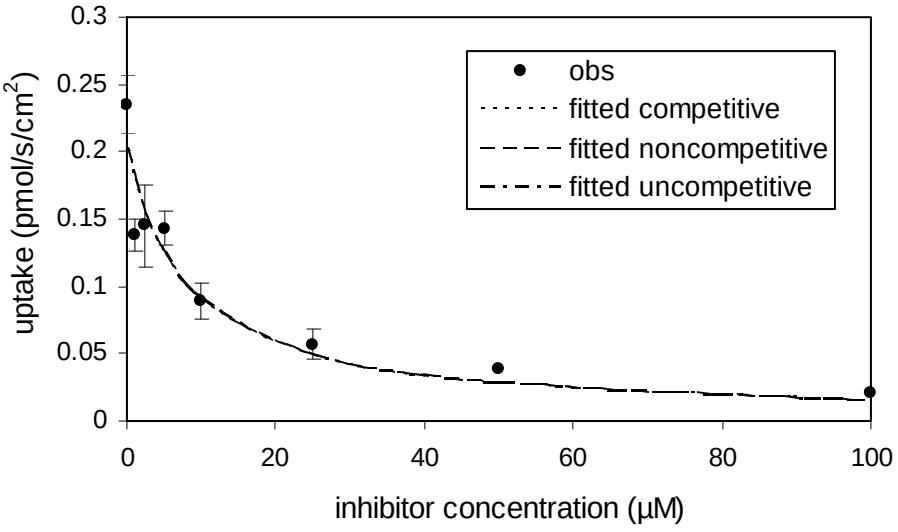

B

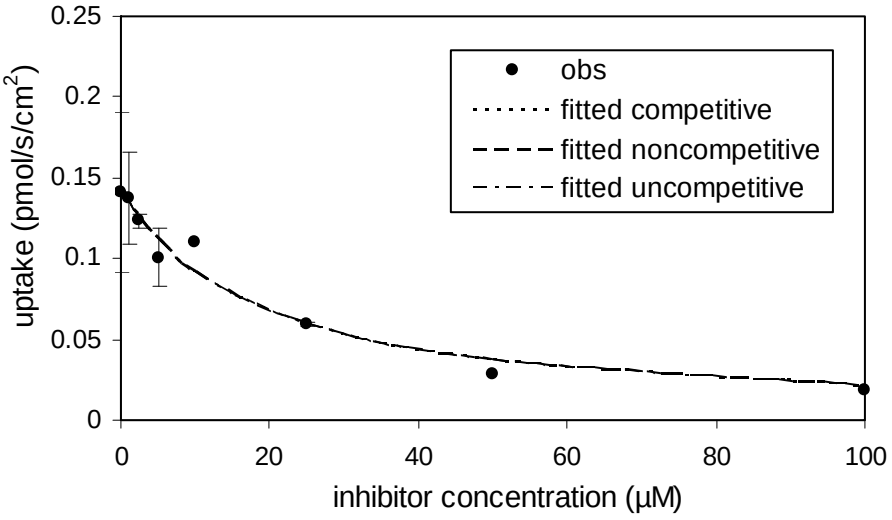

Figure 2.1 Fit of all three inhibition models to conventional inhibition data.
Data was simulated from competitive inhibition model, where Ki = 10μM and error was 30%. In panel A, the uncompetitive model was the best fitting model, although all three r^2 were about 0.90. In panel B, the competitive model was the best fitting model, although all three r^2 were about 0.82. Panels A and B each present one simulation occasion, of the 30 total independent occasions that were conducted. For each occasion, n=3 profiles were simulated. AIC was used to identify the best fitting model.

Notably, the accuracy of the competitive Ki estimate was dependent upon %CV, as expected, as well as upon Ki. The percent of occasions that Ki was accurate (i.e. within 20% of true competitive Ki) was 100%, 36.7%, 63.3%, and 66.7% for the four scenarios listed (top to bottom) in Table I, respectively. Hence, in Table I from conventional inhibition data, very infrequently was the correct model identified and Ki accurately estimated.

2.3.1.2 Simulated noncompetitive model data. Noncompetitive data were simulated for Ki = 100 μM. Results are summarized in Table II. When maximum ratio of I/Ki was 5, the noncompetitive model was correctly identified as the best fitting model only 23.3% of the time. When maximum ratio of I/Ki was increased to 10 (i.e. inhibitor concentration up to 1000 μM), noncompetitive model was correctly identified only 30% of the time. In

Table 2, Ki estimates for the noncompetitive model were accurate 50.0% and 56.7% of the time when inhibitor concentrations were up to 500 μM and 1000 μM, respectively. These poor results from noncompetitive data (Table 2) are practically the same as the poor results from competitive data (Table 1), indicating conventional inhibition data is a poor basis to determine type of inhibition.

Table 2.2 Results from conventional inhibition data.
Data was simulated from noncompetitive inhibition model, where Ki, maximum I/Ki, and random error were varied. Under "best fitting model", values are the percentage of times that the best fitting model was competitive, noncompetitive, or uncompetitive. Percentages are derived from simulations of 30 occasions (n=3 per occasion). AIC was used to identify the best fitting model.

Ki (μM)	Maximum I/Ki	%CV error	Best fitting model		
			Competitive	Noncompetitive	Uncompetitive
100	5	30%	40.0%	23.3%	33.3%
100	10	30%	30%	30%	40%

2.3.2 Analysis of Dixon-type data

The second objective was to compare the abilities of the competitive and noncompetitive inhibition models to best fit simulated data where substrate concentration and inhibitor concentration were varied. Varying both substrate concentration and inhibitor concentration is required for traditional Dixon plots, such that this data here is referred to as Dixon-type data. Because substrate concentration is also varied, Dixon-type data is several-fold larger in scope than traditional inhibition data (i.e. objective one above).

Two simulation scenarios were studied that differed in the extent of inhibition. In one scenario, I/Ki ranged from 0 to 5, which represent a wide range in inhibitor concentration, compared to typical literature reports. In the second scenario, I/Ki ranged from 0 to 1.7, which is a more narrow range, but one that better reflects common practice.

3.2.1 First simulation scenario. Simulations covered a range of I/Ki from 0 to 5, which reflects a high level of inhibition (i.e. large inhibition concentration, relative to Ki potency). In Table 3, results indicate that, when competitive inhibition data were simulated with 30% error, the competitive model was the best fitting model 76.7% of the time (Ki = 1 μM). Otherwise, the noncompetitive model was the best fitting model (23.3% of the time). The uncompetitive model was never the best fitting model.

Table 2.3 Results from Dixon-type data.
Data was simulated from either competitive or noncompetitive inhibition model, where maximum I/Ki=5 but Ki varied. Under "best fitting model", values are the percentage of times that the best fitting model was competitive, noncompetitive, or uncompetitive. Percentages are derived from simulations of 30 occasions (n = 3 per occasion). AIC was used to identify the best fitting model. Simulated data used 30% error.

Ki (μM)	Data origin	Best fitting model		
		Competitive	Noncompetitive	Uncompetitive
1	Competitive	76.7%	23.3%	0%
1	Noncompetitive	30.0%	66.7%	3.33%
100	Noncompetitive	16.7%	76.7%	6.67%

Figure 2 shows the simultaneous inhibition profile fits for each of the three substrate concentrations (i.e. 1, 5, and 10 μM). Panels A and B show results from two of the 30 occasions. In panel A, the competitive model was the best fitting model; meanwhile, the noncompetitive model was the best fitting model in panel B. Although the competitive model was usually (and correctly so) the best fitting model (76.7 % of the time), Figure 2 highlights that the quality of fits across all three inhibition models was very similar.

A

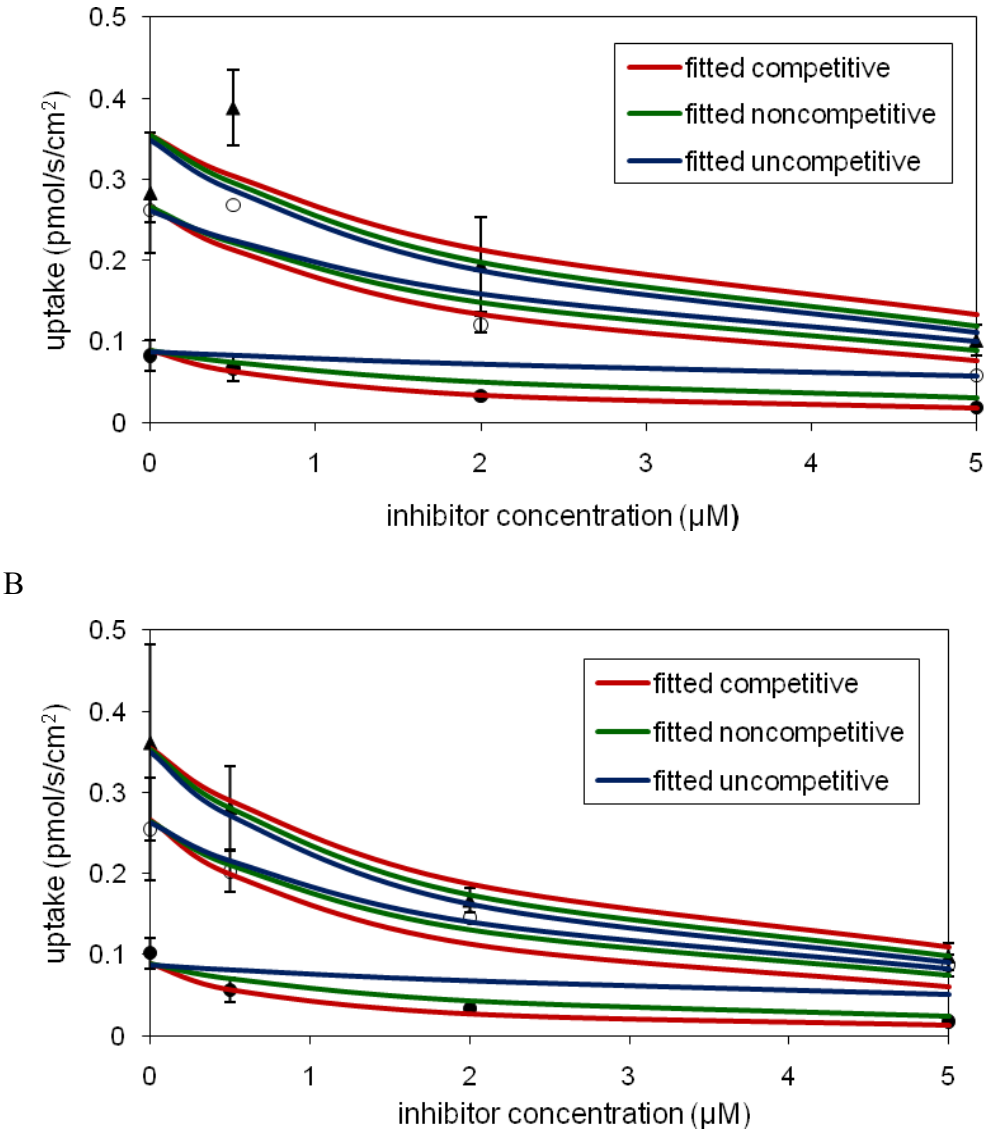

Figure 2.2 Simultaneous fits of the competitive inhibition model to Dixon-type data. Data was simulated from competitive inhibition model, where I/Ki ranged from 0-5 and error was 30%. In panel A, the competitive model was the best fitting model, although all three r^2 were about 0.68. In panel B, the noncompetitive model was the best fitting model, although all three r^2 were about 0.73. Panels A and B each present one simulation occasion, of the 30 total independent occasions that were conducted. For each occasion, n=3 profiles were simulated for each of the three levels of substrate 1µM (●), 2.5 µM (○), and 5 µM (▲). AIC was used to identify the best fitting model.

In Table 3, when noncompetitive inhibition data were simulated and Ki = 1µM, similar fits resulted, in that the correct model (i.e. noncompetitive model) was selected 66.7% of

the time. In Table 3, results were similarly successful from simulated noncompetitive inhibition data where Ki = 100 μM (76.7% correct). Similarity in results for Ki = 100 μM and Ki = 1 μM are due to inhibitor concentration being proportionally changed (i.e. I/Ki had the same 0 to 5 range). The extent of inhibition was the same whether Ki = 1 μM or Ki = 100 μM, such that these scenarios in Table 3 yield similar results. Ki estimates were accurate about 50-60% of the time, regardless whether the correct model was the best fitting model.

2.3.2.2 Second simulation scenario: nonlinear regression. Simulated experiments covered a range of I/Ki from 0 to 1.7, which reflects lower level of inhibition than the first simulation scenario. This more narrow range reflects the common ranges in the literature (6-11). Results for I/Ki from 0 to 1.7 in Table 4 broadly mimicked results for I/Ki from 0 to 5 in Table 3. Interestingly, when competitive inhibition data were simulated and 30% error added, the competitive model was the best fitting model 76.7% of the time, the noncompetitive model was best fitting 23.3% of the time, and the uncompetitive model was never the best fitting model. These results for I/Ki from 0 to 1.7 (Table 4) are identical to those results for I/Ki from 0 to 5 (Table 3). Comparing Table 3 and 4 for simulated noncompetitive inhibition data show the noncompetitive model was selected about 60-80% of the time. Table 4 also shows results when competitive data simulated with 20% error. There was no appreciable difference in results between 20% and 30% error (i.e. 80% correct versus 76.7% correct).

Table 2.4 Results from Dixon-type data.
Data was simulated from either competitive or noncompetitive inhibition model, where maximum I/Ki=1.7 and Ki=58. Under "best fitting model", values are the percentage of times that the best fitting model was competitive, noncompetitive, or uncompetitive.

Percentages are derived from simulations of 30 occasions (n=3 per occasion). AIC was used to identify the best fitting model.

Ki (μM)	%CV error	Data origin	Best fitting model		
			Competitive	Noncompetitive	Uncompetitive
58	20%	Competitive	80.0%	20.0%	0%
58	30%	Competitive	76.7%	23.3%	0%
58	30%	Noncompetitive	20.0%	60.0%	20.0%

Above results indicate that nonlinear regression was modestly successful in identifying the type of inhibition (range from 60.0% to 80.0% in Tables 3 and 4). Hence, we suggest caution in concluding inhibition type, even when employing comprehensive data where both substrate and inhibitor concentration are varied. Perhaps not surprising, level of success from this more compressive data was greater than from conventional inhibition data, where the success rate (20.0-43.3%) was poor.

Even in spite of this moderate success rate from Dixon-type data, nonlinear regression frequently did not estimate Ki accurately. For the simulated competitive and noncompetitive data with Ki = 1 μM with added 30% error (Table 3), an accurate estimate of Ki was obtained only 56.7% and 50.0% of the time, respectively. For the simulated noncompetitive data with Ki = 100 μM, an accurate estimate of Ki was obtained only 63.3% of the time.

2.3.2.3 Second simulation scenario: Dixon plot analysis. While nonlinear regression is the primary focus, secondary analysis is present here, where Dixon-type data is subjected to Dixon plot analysis. Linearized forms of inhibition models such as Dixon plots and Lineweaver-Burk plots are commonly used to elucidate type of inhibition and inhibition constant Ki. The Dixon plot has been reported to have some limitations and many authors have suggested use of nonlinear regression rather than the linearized form to

calculate Ki (67, 68). Yet, the Dixon plot is still frequently used to evaluate the mode of inhibition (69-71). Surprisingly, the accuracy of the Dixon plot to correctly identify the type of inhibition has never been assessed.

Figure 3 shows Dixon plots from simulated noncompetitive data. In a Dixon plot, noncompetitive inhibition provides profiles that intersect on the x-axis. In panel A of Fig. 3, inhibition appears to be competitive (i.e. incorrect conclusion), since the profiles intersect above the x-axis. In panel B, two profiles intersect above the x-axis, while two others intersect on the x-axis, such that the correct inhibition type (i.e. noncompetitive inhibition) was not easily concluded. In both panels A and B, this classic approach to assess for noncompetitive inhibition failed to conclude noncompetitive inhibition. From this graphical/visual approach to discriminate competitive versus noncompetitive versus uncompetitive inhibition, the noncompetitive model performed poorly. For simulated noncompetitive data with 30% error, the correct model was concluded only on two of 30 occasions. On 22 of the 30 occasions, it was not readily possible to identify the type of inhibition (i.e. appear like Figure 3 panel B). For simulated competitive data with either 20% or 30% added error, the correct model was identified only on four of the 30 occasions.

A

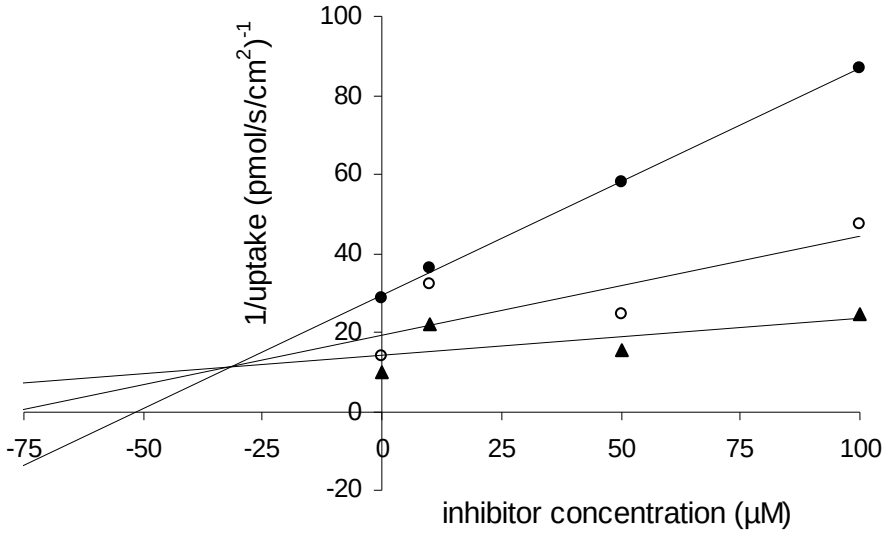

B

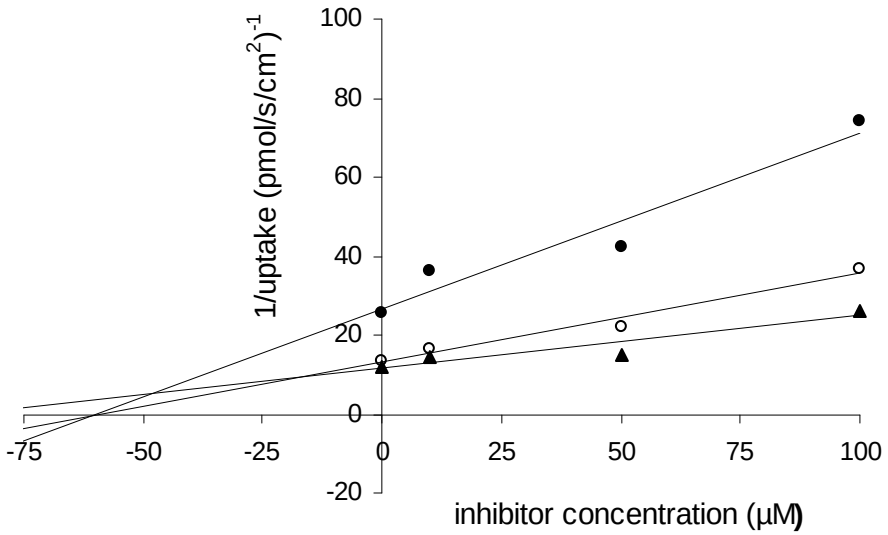

Figure 2.3 Dixon plots of Dixon-type data.
Data simulated from noncompetitive inhibition model, where I/Ki ranged from 0-1.7. Each panel A and B are data from separate occasions, of the 30 total independent occasions that were simulated. In spite of this sameness in data origin, panel A is visually different from panel B. In panel A, inhibition appears to be competitive, since the three lines intersect above the x-axis. In panel B, inhibition appears to be indeterminate, since two lines intersect above the x-axis, while another pair intersects on the x-axis. In each panel, substrate concentration is 1µM (●), 2.5 µM (○), and 5 µM (▲). Simulated data used 30% error. For each occasion, n=3 profiles were simulated for each of the three levels of substrate.

3.2.4 Second simulation scenario: summary. Overall results indicate that nonlinear regression was moderately successful in identifying the type of inhibition (about 60-80%

of the time). This level of reliability was observed for both the competitive and noncompetitive inhibition model, as well as for both 20% and 30% error. However, nonlinear regression often did not estimate Ki accurately (i.e. within 20% of true Ki). For the simulated competitive data with added 30% error, an accurate estimate of Ki was obtained only 30% of the time. When added error was reduced from 30% to 20%, performance improved, where Ki estimates were accurate 56.7% of the time. Meanwhile, for the noncompetitive data with added 30% error, accurate Ki was estimated only 50% of the time.

2.3.3 Analysis of nonconventional inhibition data

From objective one, conventional inhibition data performed poorly in identifying the correct model. This finding from this most common type of inhibition data (i.e. uptake from a single, fixed substrate concentration as a function of a range of inhibitor concentrations) motivated an analysis to assess whether similar inhibition data, but varying substrate concentration and not inhibitor concentration, could improve performance.

2.3.3.1 Simulated competitive model data. Table 5 summarizes results obtained from simulated competitive data where substrate concentration was varied and inhibitor concentration was fixed at a single level. Simulations involved 30% error and covered a range of scenarios, where Kt was 5 μM or 500 μM, and the ratio of I/Ki was 0.01, 1 or 100. All figures relating to objective three are in terms of substrate uptake versus substrate concentration; such inhibition plots are uncommon, since inhibitor concentration is fixed at a single level and not varied, while substrate concentration is varied. Figure 4 differs from Figure 1, which reflects conventional inhibition data.

Table 2.5 Results from nonconventional inhibition data.
Data was simulated from competitive inhibition model, where Kt and I/Ki were varied. Under "best fitting model", values are the percentage of times that the best fitting model was competitive, noncompetitive, or uncompetitive Percentages are derived from simulations of 30 occasions (n = 3 per occasion). AIC was used to identify the best fitting model. Simulated data used 30% error.

Kt (μM)	I/Ki	Best fitting model		
		Competitive	Noncompetitive	Uncompetitive
5	0.01	50.0%	16.7%	33.3%
5	1	100%	0%	0%
5	100	100%	0%	0%
500	0.01	50.0%	10.0%	40.0%
500	1	100%	0%	0%
500	100	100%	0%	0%

In Table 5, when I/Ki was 0.01, the competitive model was the best fitting model only 50% of the time for Kt = 5 μM or 500 μM. Figure 4 shows all three model fits to simulated competitive data on two separate occasions when Kt = 5 μM. In Figure 4 Panel A, the competitive model was the best fitting model, where r^2 = 0.894, 0.892 and 0.892 for competitive, noncompetitive and uncompetitive fits, respectively. In panel B, the uncompetitive model was the best fitting model, where r^2 = 0.728, 0.728, and 0.740 for competitive, noncompetitive and uncompetitive fits, respectively. In general, the noncompetitive fit was very similar to the competitive fit, such that noncompetitive was infrequently the best fitting model (i.e. less than 20% of time). Meanwhile, uncompetitive fits were similar to, but sufficiently different from, the other two models, such that it was best fitting about one-third of the time.

A

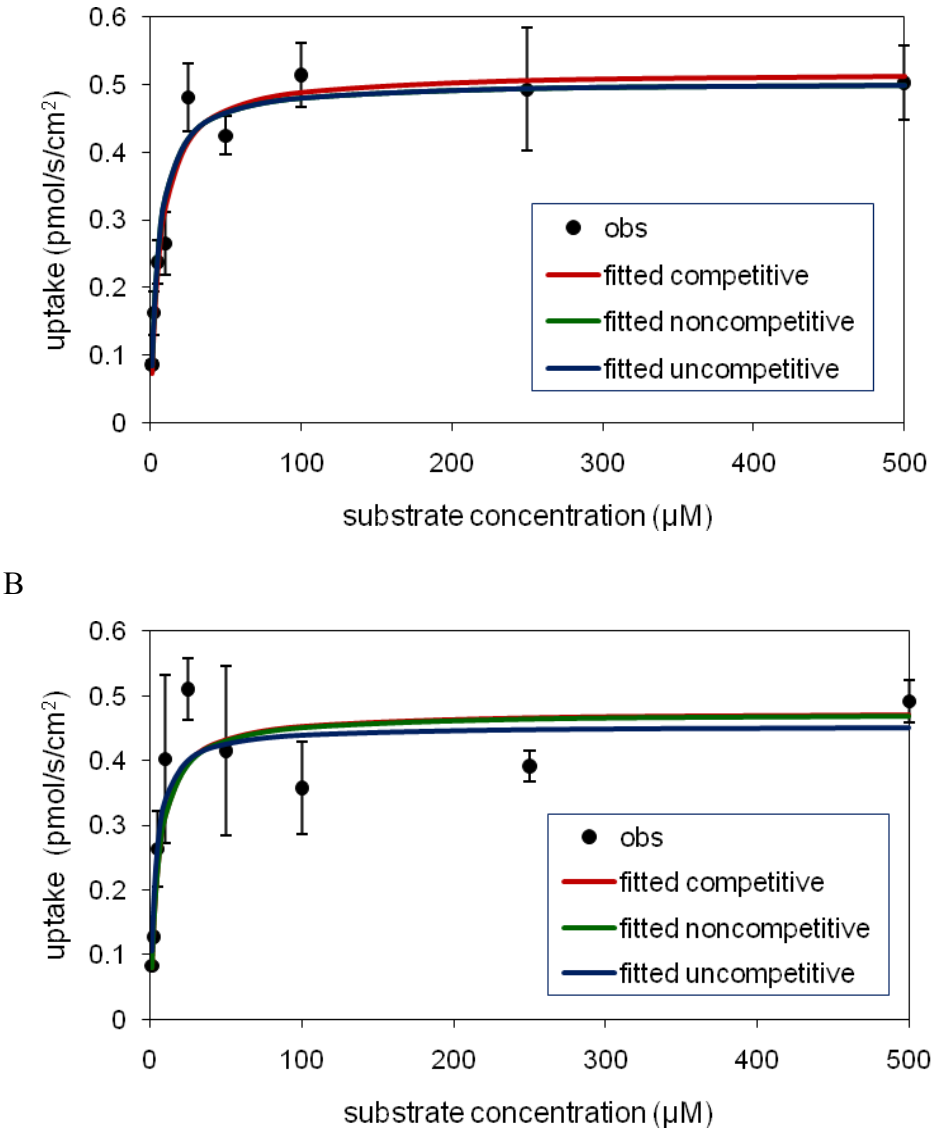

Figure 4. Fit of all three inhibition models to nonconventional inhibition data. Data was simulated from competitive inhibition model, where I/Ki = 0.01 and error was 30%. In panel A, the competitive model (red) was the best fitting model, although all three r^2 were about 0.73. The noncompetitive fit (green) overlaps with the uncompetitive fit (blue). In panel B, the uncompetitive model was the best fitting model, although all three r^2 were about 0.89. The competitive fit overlaps with the noncompetitive fit. Panels A and B each present one simulation occasion, of the 30 total independent occasions that were conducted. For each occasion, n = 3 profiles were simulated. AIC was used to identify the best fitting model.

In Table 5, the competitive model performed better when I/Ki was increased from 0.01 to 1 and 100, where the competitive model was always the best fitting model. Figure 5

shows all three fits to data simulated from the competitive inhibition model when ratio was 1. In Table 5, Kt did not have a notable impact. Results were similar whether Kt = 5 µM or 500 µM.

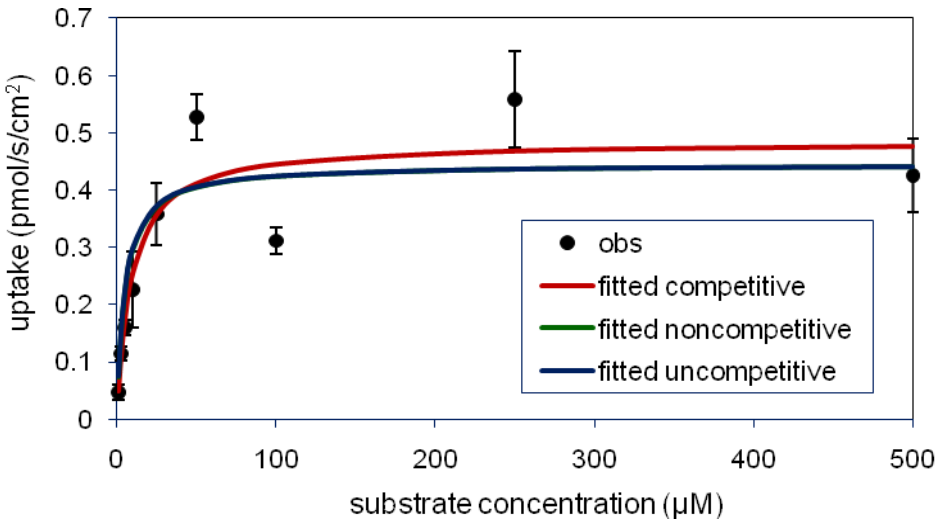

Figure 5. Fit of all three inhibition models to nonconventional inhibition data. Data was simulated from competitive inhibition model, where I/Ki = 1 and error was 30%. The competitive model was always the best fitting model, although all three r^2 were about 0.84. The noncompetitive and uncompetitive fits overlap. The plot presents one simulation occasion, of the 30 total independent occasions that were conducted. For each occasion, n=3 profiles were simulated. AIC was used to identify the best fitting model.

2.3.3.2 Simulated noncompetitive model data. Noncompetitive inhibition data were simulated with Kt = 5µM. Results are summarized in Table 6 and demonstrate the noncompetitive model is less frequently the best fitting model, compared to the competitive model (Table 5). However, as above, the correct model was always the best fitting model when I/Ki was large (i.e. I/Ki ≥ 10). Interestingly, when I/Ki ≤ 1, the noncompetitive model was infrequently the best model (3.33%). Unlike the simulated competitive data, I/Ki needed to be 10 (rather than 1) for the noncompetitive model to be the best fitting model 100% of the time. While the competitive model was always the best

fitting model when I/Ki = 1, the noncompetitive model was infrequently the best fitting model when I/Ki = 1.

Table 6. Results from nonconventional inhibition data.
Data was simulated from noncompetitive inhibition model, where I/Ki were varied and Kt=5 μM. Under "best fitting model", values are the percentage of times that the best fitting model was competitive, noncompetitive, or uncompetitive Percentages are derived from simulations of 30 occasions (n=3 per occasion). AIC was used to identify the best fitting model. Simulated data used 30% error.

Kt (μM)	Ratio (I/Ki)	Best fitting model		
		Competitive	Noncompetitive	Uncompetitive
5	0.01	60.0%	3.33%	36.7%
5	1	53.3%	3.33%	43.3%
5	10	0%	100%	0%
5	100	0%	100%	0%

3.3.3 Overall performance of nonconventional inhibition data. For objective three, overall results show that the use of nonconventional data had modest success in identifying the correct model. The level of success depended upon the ratio of I/Ki, where greater inhibition promoted higher reliability. When the competitive model was the correct model, success was 100% when I/Ki was 1 or larger. When the noncompetitive model was the correct model, success was 100% when I/Ki was 10 or larger. These results are a marked contrast to findings using conventional data, where success was 30-35%. Overall findings here suggest nonconventional data merits further examination as an approach to employ minimal data and determine inhibition type. Interestingly, nonconventional data was only a fraction in scope of the Dixon-type data, but performed better than analysis that used Dixon-type data.

A possible explanation of the better performance of the nonconventional data is the greater inhibition afforded by the nonconventional data. For example, for nonconventional data, the best fitting model being the correct model depended upon I/Ki,

where greater inhibition promoted higher reliability. For higher I/Ki, nonlinear regression with AIC frequently performed well, in terms of the correct model being the best fitting model, even when the absolute difference in AIC values and r^2 values between competing models were small. When data were simulated using a competitive inhibition model, nonlinear regression with AIC usually was able to identify the competitive inhibition model with moderate success (about 75% of the time). This level of success was about the same when data were noncompetitive, although noncompetitive data were more sensitive to the I/Ki ratio. For example, when I/Ki = 1 and 30% error, the extent of inhibition reached 45%, allowing the competitive inhibition model to be correctly identified all the time.

While the ability to reliably characterize competitive inhibition as competitive required only 45% inhibition, it should be recognized that low inhibitor solubility can limit achieving even this necessary level of inhibition (72). Compared to competitive inhibition with 30% error (Table 5), less desirable results were observed for the noncompetitive inhibition model with 30% error (Table 6). When I/Ki was even as high as 1 (i.e. 50% inhibition), the noncompetitive inhibition model was identified only 3.3% of the time; usually, the competitive inhibition model was incorrectly identified as the model. When I/Ki = 10, the extent of inhibition reached 90%, allowing the noncompetitive inhibition model to be correctly identified all the time. For both the competitive and noncompetitive models, a specific level of inhibition was required to reliably identify the correct model. For the competitive model, 45% inhibition was sufficient. For noncompetitive model, 50% inhibition was insufficient, but rather required 90% inhibition, which is a two-fold greater requirement. This high level of

inhibition may be problematic if a compound suffers from modest inhibition potency and/or low solubility.

2.3.4 Reflections from experimental data

Ursodeoxycholic acid is expected to bind to ASBT at the same binding site as taurocholic acid, since they are both native bile acids and share high chemical similarity. Moreover, ASBT is a relatively small transporter, with a molecular weight of 43kDa (35). The taurine conjugate of ursodeoxycholate has been identified as a competitive inhibitor of taurocholate (73).

3.4.1 Conventional inhibition data. Inhibition studies were performed over a range of ursodeoxycholate concentrations, while substrate (taurocholate) concentration was maintained at 2.5μM. The maximum ratio of I/Ki was 7.1, which was in the range of the simulations performed. Competitive Ki for ursodeoxycholate was found to be 35.2±2.67μM, which is similar to the previous report (49). Figure 6 panel A shows model fits to the conventional inhibition data. As expected from simulations, the competitive, noncompetitive and uncompetitive fits in Figure 6 panel A were very similar to each other. The noncompetitive model was the best fitting model, which we believe is an incorrect model. For simulations that were similar to this experimental condition (Table I where I/Ki = 10 and %CV = 10%), the competitive and noncompetitive models were best fitting 20.0% and 13.3% of the time).

3.4.2 Nonconventional inhibition data. Nonconventional inhibition data was obtained under two sets of conditions, where I/Ki was designed to vary, employing an expected Ki value of 35.2μM from the conventional inhibition results above. In both conditions,

taurocholate concentration ranged from 0 to 500μM, but where I/Ki = 1 in one set (i.e. I = 35.2 μM), while I/Ki = 5 in the second set (i.e. I = 176 μM).

When I/Ki=1, the noncompetitive model (incorrect model) was the best fitting model. When I/Ki=5, the competitive model (correct model) was the best fitting model; Figure 6 panel B plots the result. Experimental results are partially consistent with simulation results (Table V). Simulation result in Table 5 suggest very high accuracy to identify the competitive model as the correct model when I/Ki = 1 or higher (e.g. high accuracy when the percentage of inhibition reached 45.4% or greater). Here, the presumably correct model (i.e. competitive model) was concluded only when I/Ki = 5, where the percentage of inhibition reaches 80.6%. Overall, with the assumption that ursodeoxycholate competitively inhibits taurocholate, nonconventional inhibition data appears to have performed better than conventional inhibition data. However, these experimental results suggest that even simulation results, which anticipate modest ability for nonlinear regression to identify the correct model, may be too optimistic.

A

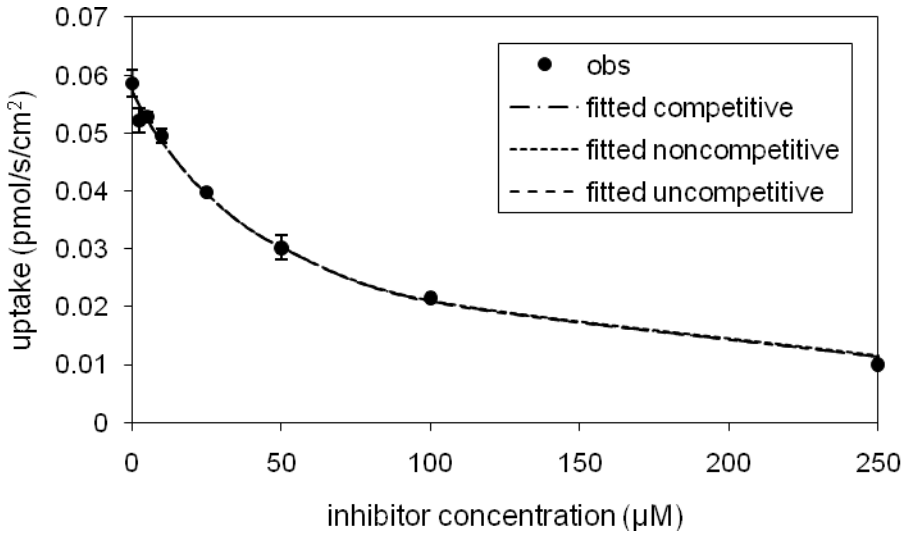

B

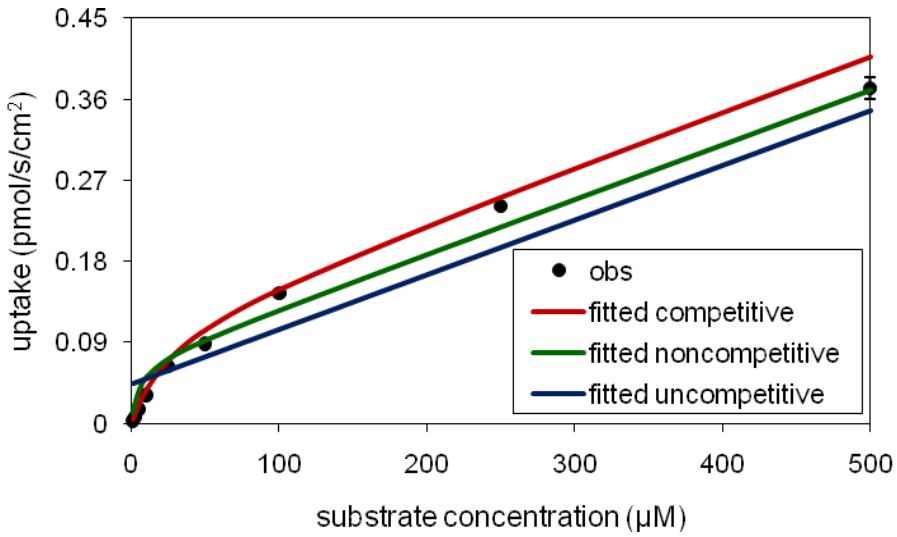

Figure 6. Results from experimental data.
Panel A shows model fits to conventional inhibition data, where substrate concentration is 2.5μM. The noncompetitive model was the best fitting model, although all three r^2 were about 0.99. Panel B shows fits to nonconventional inhibition data, when I/Ki = 5. The competitive model was the best fitting model, although r^2 was about 0.99 for competitive and noncompetitive fit and 0.98 for uncompetitive fit. Each point is mean ± SEM of three measurements.

3.4.3 Dixon-type data. Dixon-type data was generated by varying both inhibitor and substrate concentrations. Ursodeoxycholate concentrations were 0, 25, 50, and 100 μM (i.e. four levels). Taurocholate concentrations were 1, 2.5, and 5 μM (i.e. three levels). In

pooling uptake data from all 12 experimental conditions, simultaneous nonlinear regression was applied to this Dixon-type data. Figure 7 panel A shows the competitive, noncompetitive and uncompetitive fits. The competitive model was the best fitting model. Figure 7 panel B shows the traditional Dixon plot. All three profiles did not intersect at one point, as required for competitive inhibition. Two points of intersection were above the x-axis. Thus, the traditional Dixon plot appears to conclude competitive inhibition. It was not possible to measure Ki from the plot, since all the profiles did not intersect at one point.

A

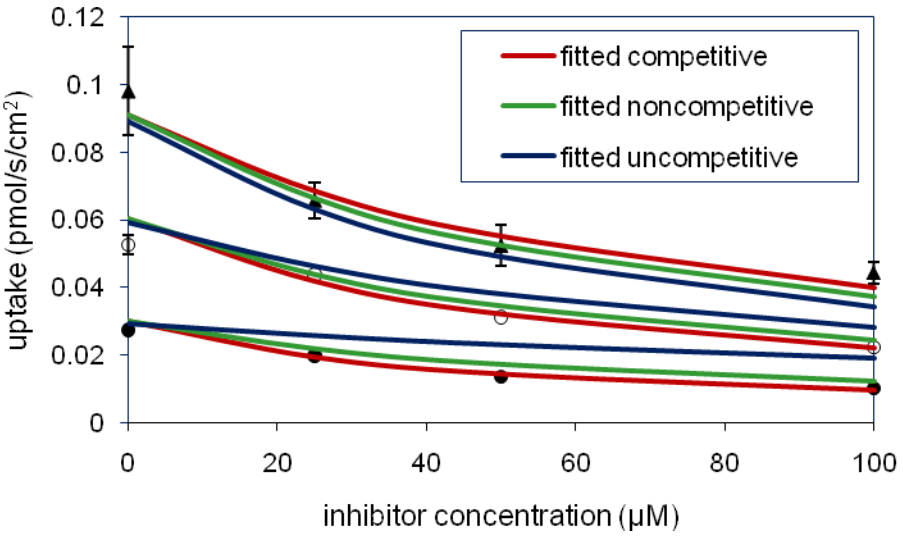

B

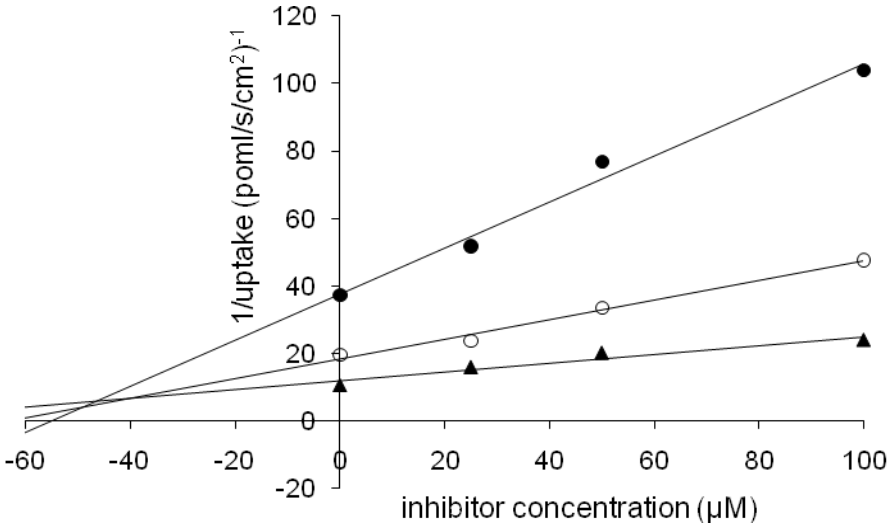

Figure 7. Results from experimental data.
Panel A shows simultaneous fits to Dixon-type data, where substrate concentration is 1µM (●), 2.5 µM (○), and 5 µM (▲). The competitive model was the best fitting model. Panel B shows the Dixon plot for the Dixon-type data. Competitive inhibition can be concluded, since all the profiles intersect above x-axis. Substrate concentration is 1µM (●), 2.5 µM (○), and 5 µM (▲). Each point is mean ± SEM of three measurements.

2.3.5 Comparison between conventional and nonconventional inhibition data

Findings here are notable in that nonconventional inhibition data appears more promising than conventional inhibition data in trying to identify the correct inhibition model from in vitro assessment. Hence, error-free simulations were performed. For conventional inhibition data, when there is no error added to uptake values and I/Ki=10, 98.5% inhibition occurs for competitive model while 99% inhibition occurs for noncompetitive model. However, the visual difference in simulated uptake between models is very small (Figure 8). This visual similarity, even under error-free conditions, explains the difficult to correctly identify the correct model from conventional inhibition data under this common situation.

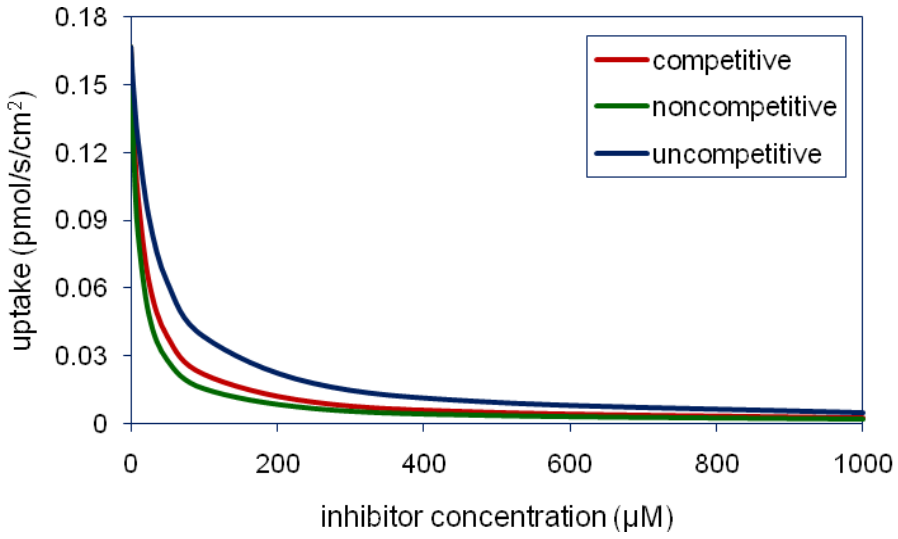

Figure 8. Inhibition profiles from error-free conventional inhibition data.
Ki = 10 μM and maximum I/Ki = 100 and S = 2.5 μM. All the inhibition models were visually very similar to each other.

Meanwhile, for nonconventional inhibition data, simulated uptake from competitive and noncompetitive models are more readily discernable from another. Figure 9 and fig. A1 in appendix illustrates error-free uptake over a range of I/Ki scenarios from competitive,

noncompetitive, and uncompetitive inhibitions. The difference between competitive and noncompetitive models is evident at even the low I/Ki ratio of 1. The difference between noncompetitive and uncompetitive models requires the higher I/Ki ratio of 10 (i.e. greater inhibition to discern these model differences). These error-free simulations support observations above from simulation and experimental findings that nonconventional inhibition data appears to be the better approach to collect data in order to elucidate type of inhibition. Further evaluation is merited.

A

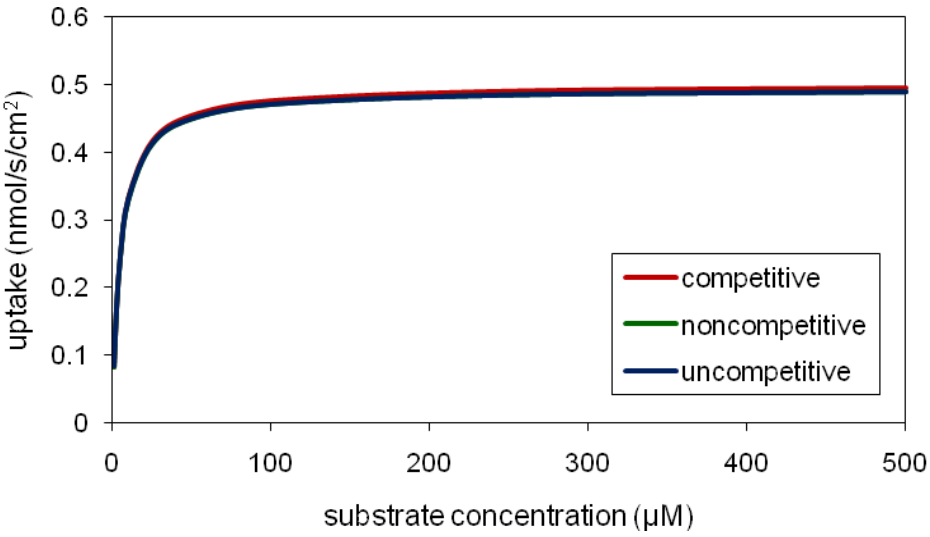
0.6
0.5
0.4
0.3
0.2
0.1
0
uptake (nmol/s/cm2)
0
100
200
300
400
500
substrate concentration (µM)
competitive
noncompetitive
uncompetitive

B

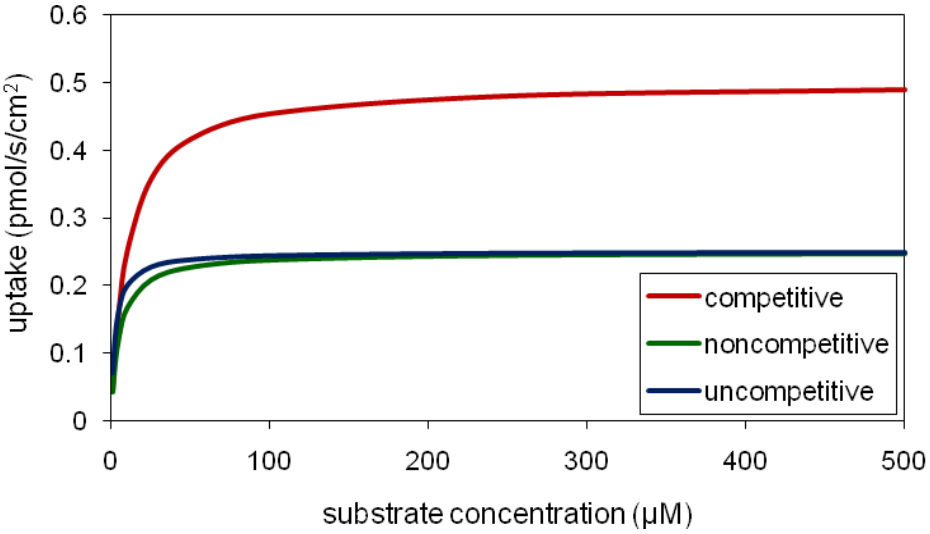
0.6
0.5
0.4
0.3
0.2
0.1
0
uptake (pmol/s/cm2)
0
100
200
300
400
500
substrate concentration (µM)
competitive
noncompetitive
uncompetitive

C

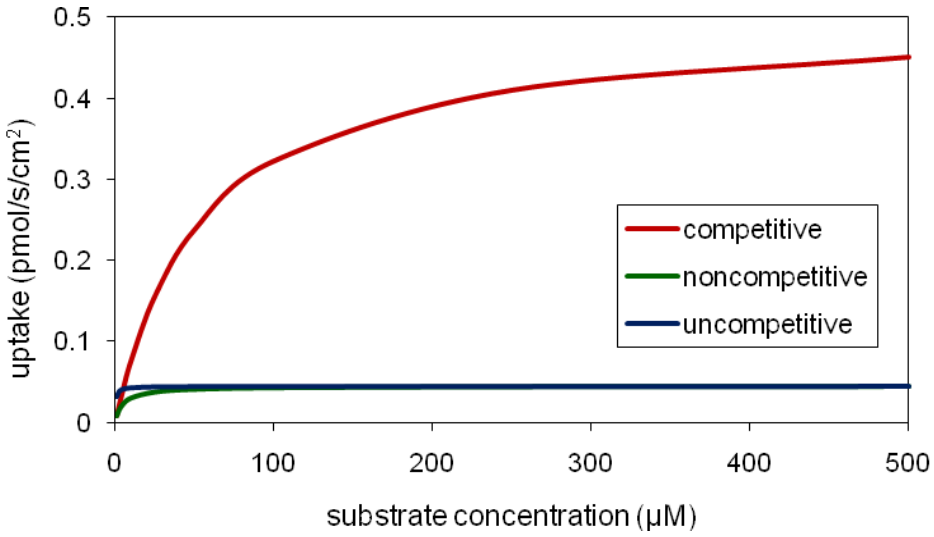

Figure 9. Inhibition profiles from error-free nonconventional inhibition data. Panel A shows the three profile are essentially identical where I/Ki = 0.01. Panel B employs I/Ki = 1 and shows the competitive model to be visually different from the noncompetitive and uncompetitive models at this higher I/Ki ratio. However, the noncompetitive and uncompetitive models were similar to one another. Panel C employs I/Ki = 10 and shows the competitive model is easily discernable from the other two models.

2.4 CONCLUSIONS

Analysis here examined the conditions and extent to which nonlinear regression results can be relied upon. For conventional inhibition data, nonlinear regression with AIC performed poorly for both the competitive and noncompetitive inhibition models. For Dixon-type data, nonlinear regression yielded moderately better results. Interestingly, nonconventional inhibition data performed well, with higher ratio of I/Ki providing better results. Nonconventional inhibition data merits further consideration.

CHAPTER 3

Structural requirements of bile acid transporters: C-3 and C-7 modifications of steroidal hydroxyl groups

3.1 INTRODUCTION

The human apical sodium dependent bile acid transporter (ASBT, SLC10A2), expressed at high levels in the terminal ileum, is one of the important transporters in the enterohepatic circulation. It is responsible for the active absorption of bile acids from the gut. Overall, a 3-5g bile acid pool results in the daily turnover of 12-18g and less than 0.5g is lost each day, reflecting the high capacity of this bile acid transporter. ASBT is thus an ideal prodrug target due to its high efficiency and capacity (35).

Despite being a prodrug target, the design of prodrugs is hampered by absence of the high resolution ASBT crystal structure and the lack of understanding of interactions at the molecular level. Our laboratory has taken a systematic approach to understand the structure-activity relationship of ASBT. Previous reports evaluated interaction of native bile acids with ASBT in the stably transfected ASBT-MDCK cell line (50). The evaluation of the C-24 chemical space has indicated that ASBT accommodates a range of substituents and charge conditions for binding. However, a single negative charge in the C-24 region promotes translocation across the transporter (51). ASBT also accommodates various drug-like single ring scaffolds with different substituents attached to the bile acid (52-55). Using C-24 bile acid linkage chemistry, bile acid-based prodrugs of gabapentin, ketoprofen, and niacin have been shown to be ASBT substrates (74, 75). In addition to this C-24 chemical space, the C-3 bile acid chemical space has also been explored, where various linkers and drugs have been conjugated to a bile acid at C-3, resulting in some prodrugs (29, 76).

After absorption by ASBT, bile acids are mostly extracted into hepatocytes by sodium-taurocholate cotransporting polypeptide (NTCP) at the basolateral surface of hepatocytes

(40). Liver specific expression of this transporter can be exploited for hepatocyte selective drug action. Some studies have evaluated the effect of conjugation at the C-3 and C-24 region of bile acid on interaction with NTCP (28, 77, 78). However, this strategy is impeded by limited understanding of structure activity relationships.

In addition to C-3 and C-24 positions, the C-7 location is often hydroxylated and represents a potential conjugation site in bile acid prodrug design (12, 79, 80). Cholic acid and chenodeoxycholic acid, the two most abundant bile acids in humans, contain a C-7 hydroxyl group (81). Interestingly, there are no reports of C-7 substitution on bile acid interaction with the bile acid transporters.

The objective of this study was to evaluate the effect of C-3 and C-7 substitution on bile acid interaction with bile acid transporters. Nineteen bile acid analogues were tested against ASBT and NTCP, using stably transfected ASBT-MDCK and NTCP-HEK monolayers. Results indicated that although ASBT and NTCP accommodated a wide range of substituents for binding, all major C-7 modifications resulted in analogues that were not translocated by either ASBT or NTCP. Interestingly, a C-3 modification that was not tolerated at C-7 still afforded translocation via ASBT and NTCP, further confirming the relative unacceptability of C-7 modification. Studies also characterize the relative promiscuity of ASBT and NTCP. Compared to ASBT, NTCP demonstrated a generally similar binding potency across compounds, although showed less binding affinity toward unconjugated bile acids with aromatic substitution at C-7. Results suggest that drug conjugation to the C-3 hydroxyl group, rather than C-7, has potential to serve as a bile acid transporter prodrug strategy.

3.2 MATERIALS AND METHODS

3.2.1 Materials

Ursodeoxycholic acid was obtained from TCI America (Portland, OR). Chenodeoxycholic acid was purchased from AK Scientific (Mountain View, CA). Geneticin, fetal bovine serum (FBS), trypsin, and DMEM were obtained from Invitrogen (Rockville, MD). [^{3}H]-Taurocholic acid was purchased from PerkinElmer Inc (Waltham, MA). Taurocholic acid, dehydrocholic acid (compound **13**), pyridine, and triethyl amine were obtained from Sigma Aldrich (St. Louis, MO). 7-oxo cholanic acid (compound **11**) was purchased from TCI America (Portland, OR). All other reagents and chemicals were of the highest purity commercially available.

3.2.2 Synthetic methods

Synthetic procedure overview. The carboxylic acid in the C-24 region was protected by methyl, methyl glycinate, or benzyl glycinate to yield C-24 protected bile acid (**Procedure A**). Selective monoacylation and diacylation of the free steroidal hydroxyl groups was then carried out by controlling the stoichiometry of the acyl chloride used during the reaction to obtain 3, 24 disubstituted or 3, 7, 24 trisubstituted bile acids. (**Procedure B**). Tri-substituted bile acids were then subjected to basic hydrolysis. Ease of ester hydrolysis was in following order C-3 > C-24 > C-7 (**Procedure C**). Thus compound **17** was obtained by selective hydrolysis only at C-3 while keeping esters at C-24 and C-7 intact while compounds **1-9** were obtained by selective hydrolysis at C-3 and C-24 position while keeping ester at C-7 intact. Compounds **16**, **18**, **19** were not subjected to basic hydrolysis to understand the effect of C-24 and C-3 substitution on

transporter interaction. Identity and purity of the final compounds was determined by TLC, ^{1}H NMR and mass spectroscopy.

3.2.2.1 Procedure A: Protection of C-24 carboxylic acid. Three different protecting groups were used for the synthesis of three groups of compounds. To synthesize compounds **1-6**, **16**, **18** and **19**, carboxylic acid was protected as methyl ester to get common intermediate (II) (Figure 1). To synthesize compounds **7-9**, and **17** methyl glycinate was used as protecting group to get common intermediate (V) (Figure 2) while for synthesis of compounds **10**, **12**, **14** and **15**, benzyl glycinate was used as protecting group to get common intermediate (X) (Figure 3). Below are the typical procedures used for the synthesis of intermediates II, V and X.

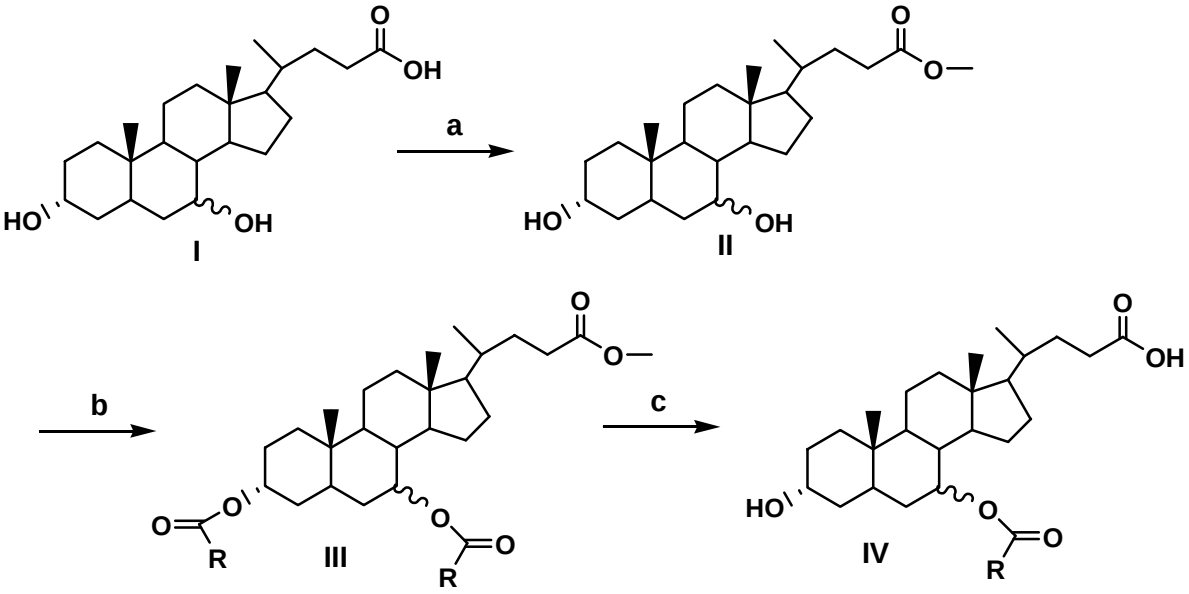

a. CH_3OH, $SOCl_2$. b. RCOCl, pyridine. c. KOH

Figure 1. Synthesis approach for compounds 1-6, 16, 18 and 19.

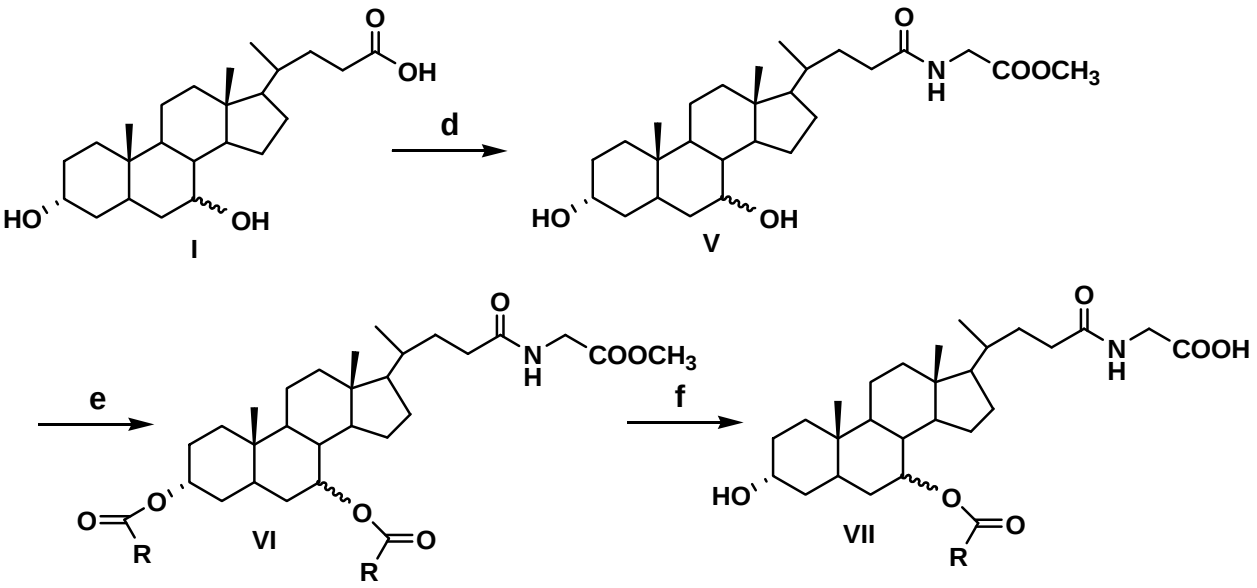

d. Methyl glycinate HCl, TEA, EEDQ. e. RCOCl, pyridine. f. KOH

Figure 2. Synthesis approach for compounds 7-9 and 17.

Synthesis of methyl ester of bile acid (II): Thionyl chloride (415 mg, 3.5 mmole) was added into a cold solution of ursodeoxycholic acid (UDCA) or chenodeoxycholic acid (CDCA) (500 mg, 1.3 mmole) in methanol. The reaction was allowed to warm to RT and stirred overnight. Methanol was then evaporated under vacuum to obtain the methyl ester of the respective bile acid (II) in quantitative yield. (MS, M+1 407.3).

Synthesis of glycine esters for bile acid (V and X): The glycine conjugate of the bile acid was synthesized, as described previously (82). Briefly, methyl glycinate hydrochloride (878 mg, 7 mmol) was stirred with triethylamine (1 ml) in ethyl acetate at RT for 30 min. Bile acid (1.96 g, 5 mmol) and EEDQ (1.73 g, 7 mmol) were added to the suspension. After 10 min, the reaction mixture was heated at 65 ºC and allowed to stir overnight. The ethyl acetate layer was then washed successively with water (25 ml), 0.5N NaOH (50 ml), water (25 ml), 0.5N HCl (2 X 50 ml), water (25 ml) and brine. The resulting ethyl acetate layer was evaporated under vacuum to yield methyl glycoursodeoxycholate or

methyl glycochenodeoxycholate. (MS M+1 464.3). Use of benzyl glycinate instead of methyl glycinate yielded common intermediate (X) (MS, M+1 540.2) which was used for the synthesis of compounds **10**, **14** and **15**.

3.2.2.2 Procedure B: Acylation of C-24 protected bile acid. Monoacylation at C-3 position of intermediate II and X with 2 equivalents of acid chloride (nicotinic acid chloride) yielded compound **18** and intermediate XI respectively (Figure 2 and 3) while reaction of intermediates II, V with excess (4 equivalents) of appropriate acyl chlorides yielded C-3, C-7-diacyl products III, VI respectively. Typical procedure used for diacylation is as follows: Acyl chloride (4 eq.) was added to a solution of C-24 protected bile acid (1eq.) in pyridine. The reaction mixture was stirred at 40-60 ºC for 2-8 hr. After cooling, the reaction mixture was poured over ice and acidified with concentrated HCl to pH 2. The suspension was extracted with dichloromethane. The organic layer was dried over sodium sulfate, and evaporated under vacuum to yield a crude mixture which was purified by flash column chromatography over silica gel using an appropriate mixture of ethyl acetate and hexane as eluent.

3.2.2.3 Procedure C: Selective hydrolysis of 3,7,24-trisubstituted bile acid derivatives. Intermediates III, VI were subjected to basic conditions to achieve selective hydrolysis (83). Selective hydrolysis at C-3 and C-24 positions of III yielded compounds **1-6**. Selective hydrolysis at C-3 and C-24 positions of intermediate VI yielded compounds **7-9** while selective hydrolysis of intermediate VI at C-3 position yielded compound **17**. A typical procedure for hydrolysis is as follows: The 3, 7, 24-trisubstituted bile acid (1 eq.) was dissolved in methanol. A 50% aqueous KOH solution (0.5 ml) was then added to it. The reaction was heated at 40-60 ºC for 2-10 hr. After the reaction was complete as

indicated by TLC and MS, methanol was evaporated under vacuum to yield a white residue which was dissolved in water and acidified with concentrated HCl to pH 2. The crude product was extracted with dichloromethane. The organic layer was dried over anhydrous sodium sulfate and evaporated under vacuum to obtain final compounds which were purified by column chromatography over silica gel column using an appropriate mixture of ethyl acetate and hexane.

3.2.2.4 Procedure D: Formation of hemisuccinate (compound **14**). C-24 protected CDCA (6.3 mmol) was suspended in 25 ml ethyl acetate with succinic anhydride (3 g, 30 mmol), triethylamine (0.63 ml, 6.3 mmol), and DMAP (70 mg, 0.6 mmol). The reaction was heated at 65 °C for 48 hr. It was then extracted with water, followed by wash with acidic water (pH 1) (84). Ethyl acetate was then dried over sodium sulfate, filtered and evaporated under vacuum to get a crude product which was purified by column chromatography over silica gel, using 20% hexane in ethyl acetate as an eluent to get compound **14**.

3.2.2.5 Procedure E: Deprotection of benzyl group. Intermediates X, XI and compound **14** were subjected to catalytic hydrogentation to obtain compounds **12**, **10** and **15** respectively. A typical procedure used for catalytic hydrogenation is as follows: Benzyl protected compound was dissolved in ethanol and subjected to catalytic hydrogenation in a Parr hydrogenator using Pd/C as catalyst. Hydrogenation was performed overnight at 45 psi and at RT. The suspension was filtered using celite and organic solvents evaporated under vacuum to obtain final products.

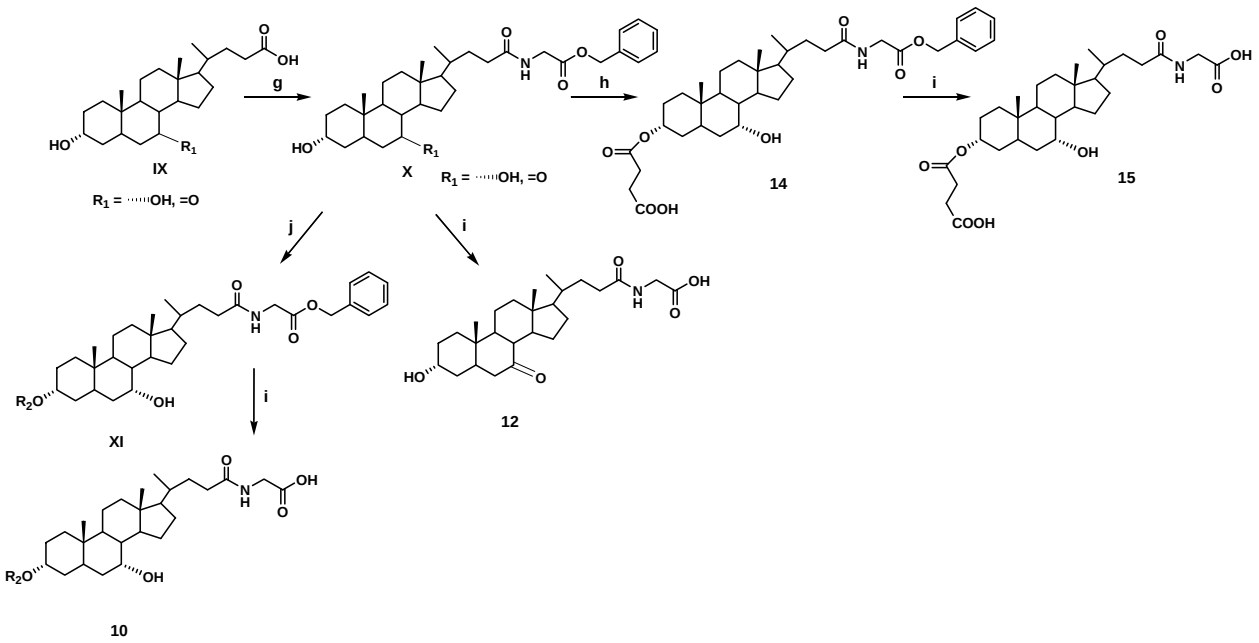

g. Benzyl glycinate HCl, TEA, EEDQ. h. Succinic anhydride, DMAP. i. H_2, Pd/C j. R_1COCl, Pyridine

Figure 3. Synthesis approach for compounds 10, 12, 14 and 15.

3.2.3 Cell culture.

Stably transfected ASBT-MDCK and NTCP-HEK cells were cultured as previously described (49, 85). Briefly, cells were grown at 37 ºC, 90% relative humidity, 5% CO_2 atmosphere, and fed every two days. Culture media consisted of DMEM supplemented with 10% FBS, 50 units/ml penicillin, and 50 µg/ml streptomycin. Geneticin (1 mg/ml) and hygromycin (100 µg/ml) were added to maintain selection pressure for ASBT-MDCK and NTCP-HEK cells, respectively. Cells were passaged after four days or after reaching 90% confluency.

3.2.3.1 Inhibition study in ASBT-MDCK monolayers. To characterize ASBT binding affinities, taurocholate uptake inhibition studies were conducted. Taurocholate is a potent ASBT substrate. Stably-transfected ASBT-MDCK cells were grown on 12-well

plates (3.8 cm^2, Corning, Corning, NY) under conditions described above. Cells were seeded at a density of 1.5 million/well and induced with 10 mM sodium butyrate 12–15 hr at 37 °C prior to study on day 4. Cells were washed three times with Hank's balanced salt solution (HBSS) prior to assay. Studies were conducted at 37 °C, 50 rpm for 10 min in an orbital shaker. Uptake buffer consisted of HBSS, which contained 137 mM NaCl (pH 6.8) and was supplemented with 1 g/L of glucose. Cells were exposed to the donor solution containing 0.5 μCi/ml [^{3}H]-taurocholate (TCA), 2.5 μM cold TCA, with varying concentrations of the analogues (from 0 μM to up to 500 μM) for 10 min at 37˚C at 50 rpm. After this time, donor solution was removed and cells were washed three times with chilled sodium-free buffer (SFB) where NaCl was replaced by 137 mM tetraethylammonium chloride. Cells were lysed using 250 μl of 1N NaOH and allowed to stand for at least 2 hr. After that time, cell lysate was neutralized with 250 μl of 1N HCl. Lysate was then counted for associated radioactivity (i.e [^{3}H]-taurocholate) using an LS6500 liquid scintillation counter (Beckmann Instruments, Inc., Fullerton, CA). Inhibition data was regressed using a modified Michaelis-Menten equation (eqn 1) to determine the inhibition constant Ki, as previously described (52).

$$J = \frac{P_{ABL} \cdot \left(\dfrac{J_{\max}}{K_t\left(1 + \dfrac{I}{K_i}\right) + S} + P_p \right)}{P_{ABL} + \dfrac{J_{\max}}{K_t\left(1 + \dfrac{I}{K_i}\right) + S} + P_p} \cdot S$$

eqn 1

where I is inhibitor concentration, Ki is inhibition constant, J is taurocholate flux, Jmax and Kt are the Michaelis-Menten constants, S is taurocholate concentration (i.e. 2.5 μM), Pp is passive taurocholate permeability, and P_{ABL} is aqueous boundary layer permeability. Kt was set to 5.03 μM, as obtained from pooled kinetic analysis of historical taurocholate uptake studies. P_{ABL} was set to 1.5×10^{-4} cm/s (86). Parallel studies were performed on each occasion to estimate Jmax and Pp for taurocholic acid. Pp was estimated from taurocholate uptake studies in absence of sodium. Ki was estimated by using nonlinear regression fitting performed by WinNonlin Professional (Pharsight; Mountain View, CA). Compounds with Ki up to 25 μM are considered strong inhibitors. Ki between 25 μM - 100 μM are denoted moderate inhibitors. Ki above 100 μM are weak inhibitors.

3.2.3.2 Uptake study in ASBT-MDCK monolayers. Analogue uptake by ASBT was evaluated. Cells were seeded as above for inhibition studies. Uptake studies employed HBSS buffer or modified HBSS buffer (i.e., sodium-free buffer). Since ASBT is a sodium-dependent transporter, studies using sodium-free buffer enabled passive permeability measurement of analogue (45, 54). Cells were exposed to a solution in HBSS or SFB containing a range of analogue concentrations (from 1 μM to up to 250 μM) for 10 min. Subsequently, cells were lysed by adding 300 μl acetonitrile to each well. After two hr, acetonitrile was evaporated at RT. A solution (1 ml) containing 50% water and 50% acetonitrile was added to each well for 15 min (54, 72). Samples were stored in -80 °C until analysis by LC/MS. Additionally, taurocholate Jmax was measured on each occasion, as taurocholate is a reference ASBT substrate. For each analogue, Jmax was normalized to the observed taurocholate Jmax to yield substrate normalized Jmax,

denoted normJmax. normJmax measures transporter capacity for analogue, while accommodating variable ASBT protein expression across occasions. Uptake data was fitted to the modified Michaelis-Menten equation (eqn 2) to yield estimates for Km and Jmax. Data from sodium free studies were fitted to eqn 3, which represents the passive transport.

$$J = \frac{P_{ABL}\left(\frac{J_{\max}}{K_t + S} + P_p\right)}{P_{ABL} + \frac{J_{\max}}{K_t + S} + P_p} \cdot S \qquad \text{eqn 2}$$

$$J = \frac{P_{ABL} P_p S}{P_{ABL} + P_p} \qquad \text{eqn 3}$$

Kinetic parameters were estimated via nonlinear regression by WinNonlin Professional.

3.2.3.3 Inhibition study in NTCP-HEK monolayer. The taurocholate uptake inhibition studies were performed in NTCP-HEK cells to characterize compound binding affinity with NTCP, as described above for ASBT. Stably-transfected NTCP-HEK cells were grown on BioCoat poly-D-lysine-coated 24-well plates (2 cm^2, BD, Franklin Lakes, NJ) under conditions described above. Cells were seeded at a density of 2.5 X 10^5 cells/well at 37°C. After culturing for two days, cells were washed three times with HBSS prior to assay. Cells were exposed to the donor solution containing 0.5 μCi/ml [^{3}H]-taurocholate, 2.5 μM cold taurocholate, with varying concentrations of the analogues (from 0 μM to up to 500 μM) for five min at 37˚C at 50 rpm. After this time, donor solution was removed and cells were washed three times with chilled sodium-free buffer. Cells were lysed by adding 150 μl acetonitrile to each well. Following evaporation at RT for about 2 hr, 250 μl of DPBS was added and 125 μl was then counted for associated radioactivity using an

LS6500 liquid scintillation counter. Inhibition data was regressed using a modified Michaelis-Menten equation (eqn 1) to determine the inhibition constant Ki. Kt was set to 5.31 μM. Parallel studies were performed on each occasion to estimate Jmax and Pp for taurocholic acid.

3.2.3.4 Uptake study in NTCP-HEK monolayers. The uptake of analogues by NTCP was performed, as described above for ASBT. Since NTCP is a sodium-dependent transporter, uptake studies employed HBSS buffer or sodium free buffer. Cells were exposed to a solution containing a range of analogue concentrations (from 1 μM to up to 250 μM) in HBSS or sodium free buffer. Subsequently, cells were lysed by adding 150 μl acetonitrile to each well. After two hr, acetonitrile was evaporated at RT. A solution (500 μl) containing 50% water and 50% acetonitrile was added to each well for 15 min. Samples were stored in -80 °C until analysis by LC/MS. Additionally, taurocholate Jmax was measured on each occasion. For each analogue, Jmax was normalized to observed taurocholate Jmax to yield substrate normalized Jmax, denoted normJmax. Kinetic data was subjected to eqn 2 and 3.

3.2.4 Analytical method.

Analogues were quantified by LC/MS on a Thermo Finnigan Surveyor HPLC system, equipped with a Thermo Finnigan Surveyor autosampler and a Thermo TSQ quantum mass spectrometer (Thermo Fisher Scientific Inc., Waltham, MA). The column was a Phenomenex Luna C8 (50 × 2.0 mm, 3 μm; Phenomenex; Torrance, CA, USA). The mobile phase was water and acetonitrile. Formic acid (0.1%) was used as modifier in each mobile phase. A flow rate of 0.4 ml/min was used with an injection volume of 10 μl. Detection was achieved under positive or negative ion electrospray, depending on the

approach that provided maximum sensitivity. The limit of quantification for all analogues was between 1 and 10 nM.

3.2.5 Assessment of inhibition type.

7-nicotinoyl glycoursodeoxycholate (Compound **8**) inhibited both ASBT and NTCP. In order to assess type of inhibition (i.e. competitive, noncompetitive, or uncompetitive), an additional ASBT inhibition study and an additional NTCP inhibition study was performed for 7-nicotinoyl glycoursodeoxycholate, using ASBT-MDCK and NTCP-HEK monolayers. Inhibition studies were performed as described above, except inhibitor concentration was fixed at one level (i.e. ten times Ki) and substrate concentration was varied. This approach is denoted the nonconventional inhibition study, since it differs from the conventional approach where inhibitor concentration is varied and substrate concentration is fixed(28). Cells were exposed to the donor solution containing 152 μM (for ASBT-MDCK) and 118 μM (for NTCP-HEK study) inhibitor and 1-200 μM taurocholate with 0.5 μCi/ml [^{3}H]-taurocholate. The inhibition data were fitted to the competitive, noncompetitive, and uncompetitive models per eqn 4, 5, and 6 using WinNonlin Professional (87).

$$J = \frac{J_{\max} S}{K_t\left(1 + I/K_i\right) + S} + P_p S \qquad \text{eqn 4}$$

$$J = \frac{J_{\max} S}{\left(1 + I/K_i\right)(K_t + S)} + P_p S \qquad \text{eqn 5}$$

$$J = \frac{J_{\max} S}{K_t + S\left(1 + I/K_i\right)} + P_p S \qquad \text{eqn 6}$$

3.3 RESULTS

3.3.1 Synthesis

Seventeen conjugates were successfully synthesized in moderate to high yield. Compounds **11** and **13** were purchased. Table 1 identifies the 19 compounds. A majority (i.e. 12; compounds **1-9**, **11**, **12**, **17**) were C-7 analogues. Compounds **1-9** were C-7 conjugates that differ in their substitution patter on the C-7 aromatic ring. Four compounds were C-3 conjugates (compounds **10**, **14**, **15**, and **18**). Compounds **13** and **19** were both C-3 and C-7 analogues. Compound **16** lacked conjugation at C-3 and C-17. Of the 19 compounds, 11 employed UDCA as the bile acid and five employed CDCA as the bile acid. UDCA is the 7-β epimer of the primary bile acid CDCA. Identity and purity of all the compounds was confirmed by TLC, mass spectroscopy and ^{1}H NMR.

3.3.2 Inhibition study

Table 1 lists compound Ki values against ASBT and NTCP. Binding affinity ranged from strong inhibition with Ki in the single micromolar range, to non-inhibitor. Figure 4 illustrates the inhibition of taurocholate by 7-(4-fluorobenzoyloxy) ursodeoxycholate [compound **3**] in ASBT-MDCK monolayers. Taurocholate uptake was inhibited by relatively low concentrations of 7-(4-fluorobenzoyloxy) ursodeoxycholate, which is a C-7 conjugate of UDCA.

Table 1. Structures and Ki values of bile acid conjugates.

Inhibitory Ki value was measured against ASBT and NTCP. Compounds varied in terms of structural features at C-3, C-7 and the C-24 region. Compounds **1** – **9** are C-7 conjugates with a negative change in the C-24 region. Ki ranged from single μM to non-inhibitor.

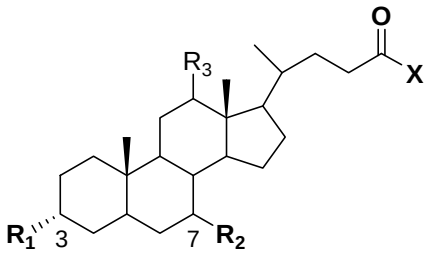

No.	Structure				Ki (μM)	
	R1	R2	R3	X	ASBT	NTCP
1	OH	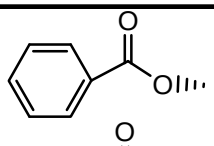	H	OH	5.79±0.80	15.4±2.7
2	OH	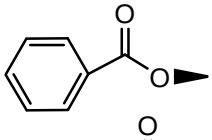	H	OH	8.19±1.56	24.4±4.5
3	OH	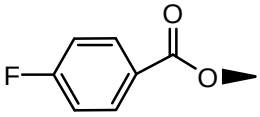	H	OH	10.3±1.1	183±32
4	OH	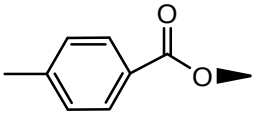	H	OH	13.4±2.6	198±72
5	OH	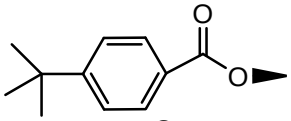	H	OH	30.8±6.8	264±82
6	OH	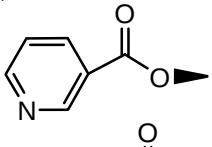	H	OH	34.2±4.0	11.7±2.5
7	OH	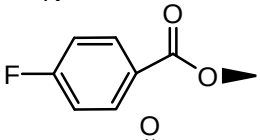	H	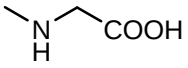	8.39±2.52	2.55±0.17
8	OH	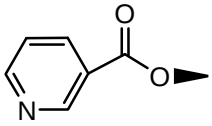	H	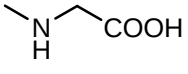	15.2±0.8	11.8±2.1
9	OH	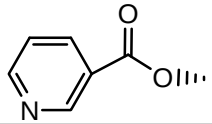	H	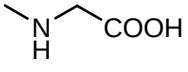	15.6±2.2	9.29±1.80

No.	Structure				Ki (μM)	
	R1	R2	R3	X	ASBT	NTCP
10	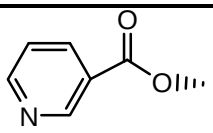		H	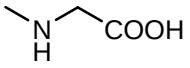	6.45±0.66	5.38±0.44
11	OH		H	OH	95.5±14.9	10.3±2.30
12	OH		H	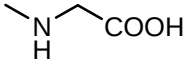	20.4±2.6	4.21±0.44
13				OH	No inhibition	355±59
14	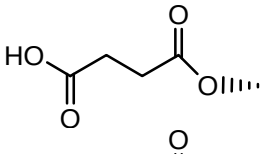		H	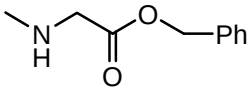	6.73±0.60	No inhibition
15	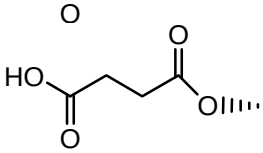		H	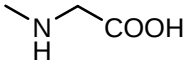	73.9±5.6	10.7±0.7
16	OH		H	OCH_3	29.8±5.1	1.22±0.10
17	OH	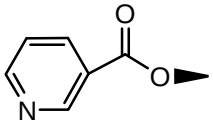	H	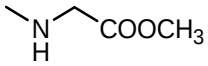	140±31.2	136±15
18	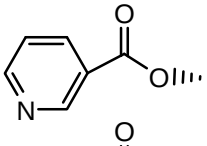		H	OCH_3	No inhibition	No inhibition
19	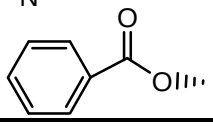	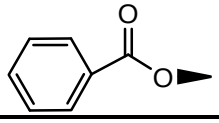	H	OCH_3	No inhibition	No inhibition

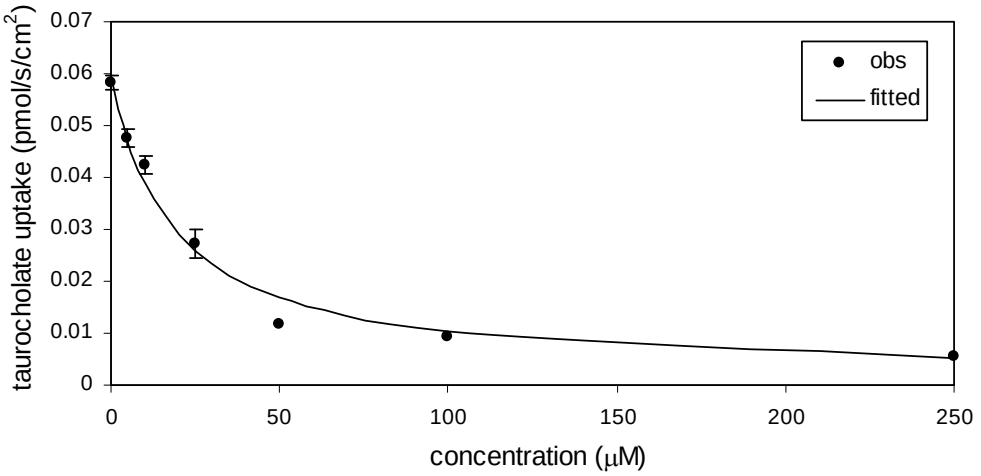

Figure 4. Inhibition profile for 7-(4-fluorobenzoyloxy) ursodeoxycholate [i.e. compound 3] in ASBT-MDCK monolayers.
Ki was 10.3 μM.

3.3.2.1 Conjugation at C-7. C-7 conjugation in CDCA (3α, 7α- dihydroxy bile acid) had negative impact on binding. Ki of CDCA against ASBT was 1.94 μM (50) and against NTCP was measured here to be 0.939 μM, which represent a very potent inhibition of each transporter. From compound **1**, conjugation at C-7 in CDCA minimally reduced ASBT inhibition potency to Ki = 5.79 μM, but reduced NTCP inhibition potency to a greater extent with Ki = 15.4 μM.

Meanwhile, C-7 conjugation in UDCA (3α-, 7β- dihydroxy bile acid) generally promoted inhibition potency in ASBT, but hindered NTCP binding affinity, as assessed using compounds **2**, **3**, and **4**. Ki of UDCA against ASBT was 22.6 μM (50) and against NTCP was measured here to be 4.90 μM, which represent strong inhibition of each transporter. Compounds **2**, **3**, and **4** modestly improved ASBT inhibition. Compounds **3** and **4** were weak NTCP inhibitors. Compound **6** with the C-7 nicotinoyl substituent did not practically differ from UDCA in terms of binding affinity for ASBT and NTCP.

Conjugation with glycine at C-24 dominated changes in C-7 steroidal substitution effects, for both ASBT and NTCP. Comparing compound **7** (Ki = 8.39 μM for ASBT and Ki = 2.55 μM for NTCP) to compound **3**, and comparing compound **8** (Ki = 15.2 μM for ASBT and Ki = 11.8 μM for NTCP) to compound **6**, binding potency was generally increased. The effect was most significant in the fluorobenzene moiety in compound **3** for NTCP, where Ki changed from 183 (±32) μM for C-24 unconjugated to 2.55 μM after glycine conjugation. This dramatic change in inhibition potency from weak to strong inhibitor highlights the favorable effect of C-24 conjugation on binding.

Of note, two pairs of C-7 conjugates differ in only the C-7 orientation. Compounds **1** and **2** are an epimer pair, derived from CDCA and UDCA respectively, and each being a C-7 benzoyl conjugate. Compound **1** is the C-7 α hydroxyl conjugate, where reactant CDCA possesses a C-7 α hydroxyl group (i.e. axially oriented) (38). Compound **2** is the C-7 β hydroxyl conjugate (i.e. equatorial orientation of the C-7 benzoyl conjugate). Compounds **8** and **9** are the second epimer pair. In each case, there was no epimer effect on ASBT or NTCP binding, and all four compounds were potent inhibitors.

Figure 5 shows the ASBT and NTCP inhibition profiles by 7-nicotinoyl glycoursodeoxycholate (compound **8**), which is a C-7 conjugate. Conjugation at C-7 resulted in competitive inhibition of each ASBT and NTCP, as indicated by the inhibition data of compound **8**. Figure 5 panel A plots the results for ASBT-MDCK cells, while panel B plots the results for NTCP-HEK cells. The studies were performed at I/Ki = 10, which is a preferred condition in order to correctly identify the type of inhibition (87). The competitive model was the best fitting model in both cases, indicating this compound to be a competitive inhibitor of each ASBT and NTCP.

A

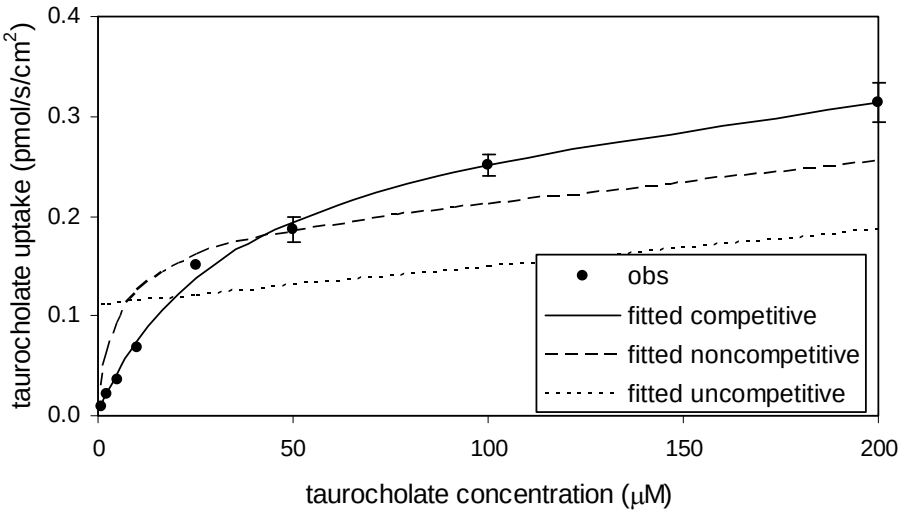

B

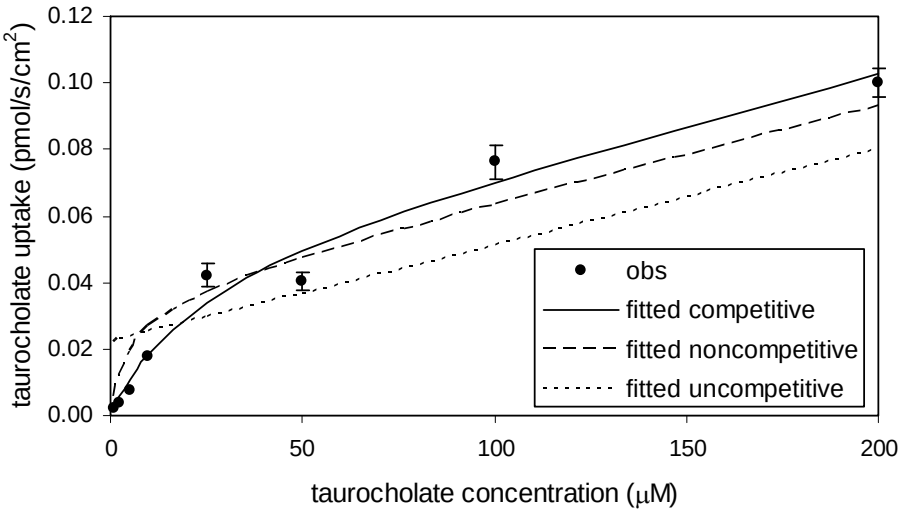

Figure 5. Nonconventional inhibition data for 7-nicotinoyl glycoursodeoxycholate [Compound 8] in (A) ASBT-MDCK monolayers and (B) NTCP-HEK monolayers. Inhibitor concentration was 152 μM and 118 μM in ASBT and NTCP studies, whereas taurocholate concentration varied from 1-200 μM. The competitive model was the best fitting model in both cases.

3.3.2.2 Oxidation of C-7 hydroxyl to keto. 7-oxo cholanic acid (compound **11**) was less potent with only moderate binding affinity (Ki = 95.5 μM) to ASBT, compared to its 7-hydroxyl counterparts (i.e. CDCA and UDCA). Although compound **11** was a strong inhibitor of NTCP (Ki = 10.3 μM), this Ki was higher than CDCA and UDCA.

Conjugation of compound **11** with glycine (i.e. compound **12**) increased inhibition potency to 20.4 (±2.6) μM and 4.21 (±0.44) μM in ASBT and NTCP, respectively, in agreement with C-24 glyco-conjugation effect on C-7 analogues. In Table 1, dehydrocholic acid (compound **13**) did not inhibit ASBT and was a weak inhibitor of NTCP.

3.3.2.3 Structural changes in C-3 region. Compounds **10**, **14**, **15**, and **18** were C-3 conjugates. Conjugation of a nicotinoyl group at C-3 of glycochenodeoxycholate (i.e. compound **10**) yielded strong inhibition of ASBT and NTCP.

The introduction of a hemisuccinate group at C-3 in compound **14** and **15** allowed for the study of the effect of a negative charge at C-3. For compound **14**, the carboxylic acid in the C-24 region was protected by a benzyl group, such that compound **14** was monoanionic by virtue of the negative charge at C-3. Compound **15** was dianionic, with one charge at C-3 and the other in the C-24 region. Compound **14** was a strong inhibitor of ASBT with Ki = 6.73 μM, but did not inhibit NTCP. Interestingly, compound **15** was a moderate inhibitor of ASBT, and a strong inhibitor of NTCP.

Compound **18** was not an inhibitor of either ASBT or NTCP, even though compound **18** has similarity to compound **6** and compound **10**, which were each much stronger inhibitors. For example, compound **18** has the same nicotinoyl group conjugated at C-3 instead to C-7 in compound **6**. However, compound **18** differs from compounds **6** and **10** by it being a methyl ester (i.e. neutral).

One compound studied that was neither a C-3 nor C-7 conjugate was compound **16**. Esterification of the C-24 carboxylate with methyl (compound **16**) did not change binding affinity, compared to compound UDCA. Ki of compound **16** was 29.8 μM and 1.22 μM

in ASBT and NTCP, respectively, which are similar to that of UDCA for these transporters. This lack of effect on C-24 esterification on ASBT inhibition has been observed previously and is the general case (51), which further affords the lack of inhibition by compound **18** even more surprising.

3.3.2.4 Effect of modification at both C-3 and C-7. Compounds **13** and **19** were both C-3 and C-7 analogues, although they substantially differed chemically. Compound **13** was a tri-keto analogue of cholic acid. It did not inhibit ASBT and only weakly inhibited NTCP. Compound **19,** which lacks steroidal hydroxyl groups inhibited neither, ASBT nor NTCP.

3.3.3 Uptake study

Uptake studies into ASBT and NTCP were performed for compounds **1**, **5**, **6**, **8**, **9**, **10**, **12**, and **14** (only ASBT for compound **14**). These compounds showed inhibition of ASBT and NTCP, except compound **14** did not inhibit NTCP. Table 2 lists uptake parameters Kt, normalized Jmax, and Pp. Of these eight compounds, six are C-7 analogues (i.e. compounds **1**, **5**, **6**, **8**, **9**, and **12**); while two are C-3 analogues (i.e. compound **10** and **14**). In spite of all being ASBT and NTCP inhibitors, none of the C-7 acyl analogues were apparently translocated by ASBT or NTCP. In Table 2, kinetic parameters reflect that they did not demonstrate active transport. Figure 6 shows practically the same uptake of 7-nicotinoyl glycoursodeoxycholate (compound **8**) in presence and absence of sodium in ASBT-MDCK monolayers. Thus, compound **8** was not a substrate of ASBT. Qualitatively similar plots were obtained for uptake of this and other compounds (**1**, **5**, **6**, **8**, **9**, **a**nd **14**) in ASBT-MDCK and NTCP-HEK cells. Pp ranged from 0.254 x 10^{-6} to

21.3 x 10^{-6} cm/s in ASBT-MDCK, and ranged from 0.727 x 10^{-6} to 85.6 x 10^{-6} cm/s in NTCP-HEK.

Based on Pp of a compound, its highest Kt that was detectable was estimated (see appendix). Subsequently, analogues were classified as non-substrate (NS) or not determinable (ND). Non-substrates are denoted to demonstratively not to be substrates. Not determinable denotes that apparent uptake was not observed, but that being a substrate could not be excluded, since sufficiently high passive permeability may possibly obscure active uptake.

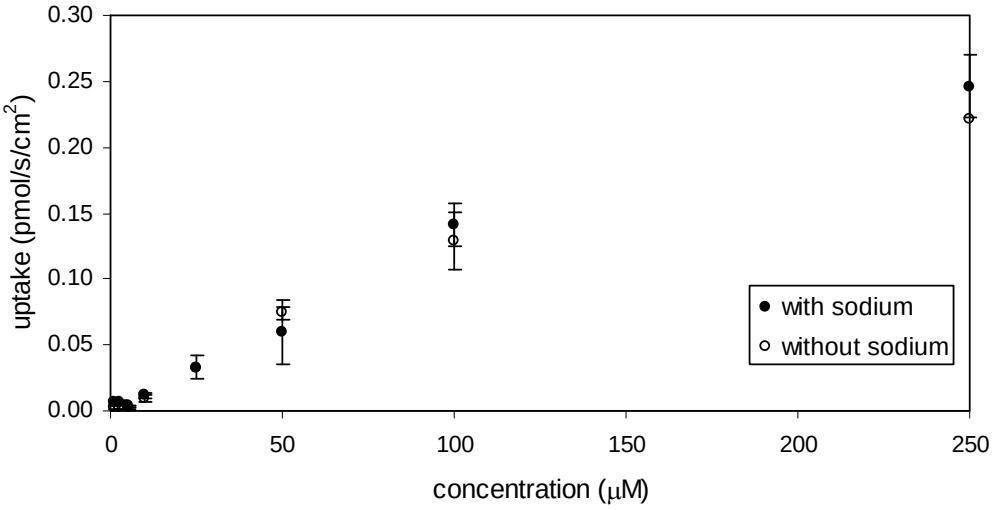

Figure 6. Concentration-dependent uptake profile for 7-nicotinoyl glycoursodeoxycholate [i.e. compound 8] into ASBT-MDCK monolayers. Compound **8** was not an ASBT substrate since it exhibited similar uptakes in the presence (●) and in the absence (○) of sodium.

Table 2. Structures and uptake kinetic parameters of bile acid conjugates.
Uptake was measured across ASBT and NTCP. Kt, norm Jmax, and Pp are the transporter Michaelis-Menten parameters, transporter capacity parameter, and compound passive permeability. Compound **10** was the most potent ASBT substrate. Compound **10** and **12** were about equi-potent as NTCP substrates. C-7 conjugates were either non-substrates or could not be determined to be substrates, due to high passive permeability.

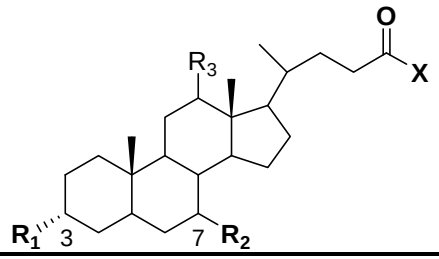

No	Structure			ASBT			NTCP		
	R1	R2	X	Kt (μM)	Norm Jmax	Pp*10^6 (cm/s)	Kt (μM)	Norm Jmax	Pp*10^6 (cm/s)
1	OH	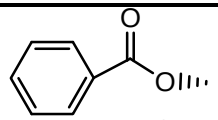	OH	NS	NS	21.3±1.8	ND	ND	85.6±14.3
5	OH	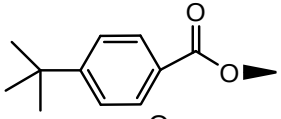	OH	NS	NS	2.41±0.27	NS	NS	2.17±0.09
6	OH	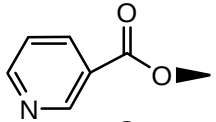	OH	NS	NS	21.2±0.9	NS	NS	7.11±0.23
8	OH	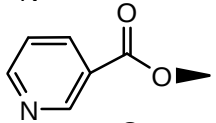	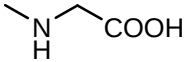	NS	NS	0.95±0.05	NS	NS	7.26±0.45
9	OH	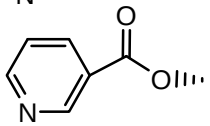	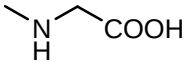	NS	NS	0.88±0.01	NS	NS	0.73±0.04

10	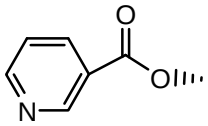	HO	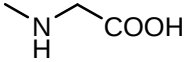	8.49±1.34	2.1	5.62±0.13	16.3±3.0	1.48	12.7±0.9
12	OH	O	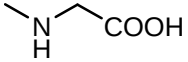	34.0±7.64	0.8	0.25±0.06	20.7±3.9	1.57	1.75±0.49
14	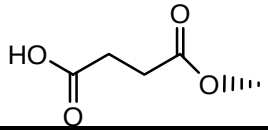	HO		NS	NS	24.9±1.1	-	-	-

ND = not determinable due to high passive permeability
NS= not substrate

In Figure 7, the uptake study for 3-nicotinoyl glycochenodeoxycholate (compound **10**) showed higher uptake with sodium than without sodium in both ASBT-MDCK monolayers and NTCP-HEK monolayers. Hence, compound **10** was a substrate of both transporters. Kinetic parameters (Table 2) were in the range of native bile acids. Kt was 8.49 μM for ASBT and 16.3 μM for NTCP, compared to taurocholate Kt of 5.03 μM and 5.31 μM, respectively. Jmax of compound **10** was 0.000242 nmol/s/cm^2 and 0.00298 nmol/s/cm^2 for ASBT and NTCP, respectively. As Jmax varies with transporter expression level, the Jmax values were normalized to the measured Jmax of taurocholate on the same study day, yielding normalized Jmax of compound **10** to be 2.11 and 1.48 for ASBT and NTCP, respectively. Hence, its Jmax was about twice than that of taurocholate for ASBT, and about 50% higher than that of taurocholate for NTCP. Of note, substitution with the same nicotinoyl group at position 7 (i.e. compound **9**) yielded a non-substrate.

Compound **12** was also a substrate of both ASBT and NTCP. Figure S1 shows the uptake profile in ASBT and NTCP. Its substrate parameters were comparable to native bile acids. Compound **14** was not an ASBT substrate. This finding was in accordance with previous observations that a single negative charge in C-24 region promotes transport by ASBT. This compound was not evaluated for uptake in NTCP-HEK cells since it did not show NTCP inhibition.

A

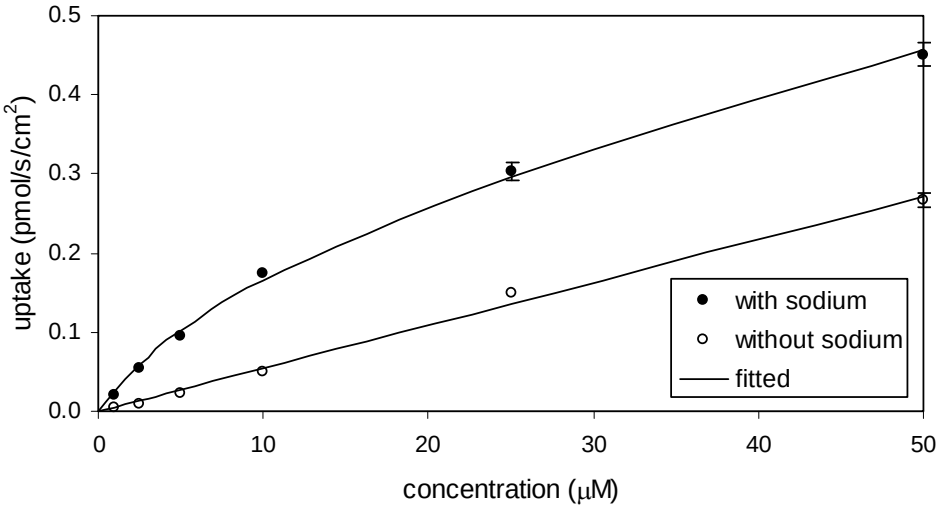

B

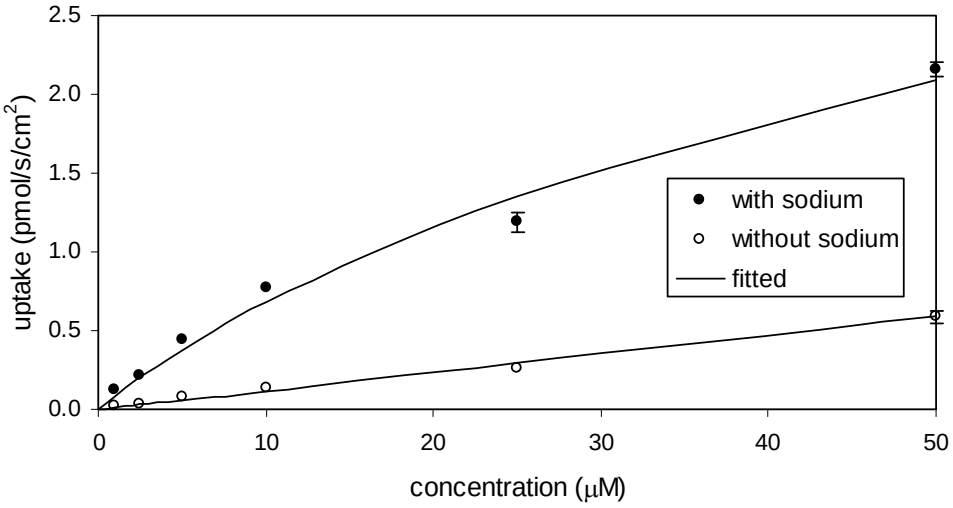

Figure 7. Concentration-dependent uptake profile for 3-nicotinoyl glycochenodeoxycholate [i.e. compound 9] into (A) ASBT-MDCK monolayers and (B) NTCP-HEK monolayers. For each transporter, uptake was greater in the presence of sodium (●) than in the absence (○) of sodium, indicating this compound to be both ASBT and NTCP substrate.

3.4 DISCUSSION

ASBT and NTCP represent the ileal and hepatic bile acid transporters that have a vital role in gut absorption and hepatic extraction of bile acids during enterohepatic recycling. These bile acid transporters have seven transmembrane domains with 35% sequence identity and 63% amino acid sequence similarity (35, 44, 57). Both transport native bile acids with high capacity and efficiency. It has been suggested that the hepatic bile acid transporter exhibits a much broader specificity for interaction than the ileal transporter, although little data has compared the substrate requirements of ASBT and NTCP (78, 88, 89). The present work was motivated in part to compare the ASBT and NTCP activities of a single set of compounds, in order to elucidate the similarities and differences between these transporters.

Studies here were also intended to evaluate structural modifications in C-7 chemical space. Prior reports investigating the ileal and hepatic bile acid transporters were limited to the structural changes in C-24 region or C-3 regions (28, 29, 48, 51-55, 76). No reports examined the effect of structural modifications in the C-7 chemical space on compound interactions with either ASBT or NTCP. Analogue modifications in this region were hypothesized to be able to modulate interaction with these transporters, including providing a new perspective to rational prodrug design that targets these transporters and liver-specific delivery.

3.4.1 Conjugate synthesis.

A total of 17 conjugates were synthesized. Substituted aromatic rings such as benzene and pyridine, the most common frames among existing drugs, were conjugated to bile acids CDCA or UDCA (90). Successful synthesis of C-7 acyl derivatives was based on

the difference in C-3 and C-7 hydroxyl groups reactivities(21). Most analogues employed UDCA, since UDCA is less toxic than CDCA (91).

3.4.2 Inhibition study.

Figure 8 plots log Ki in NTCP against log Ki in ASBT for all 19 compounds. The compounds that did not show inhibition were assigned Ki = 1000 μM. In Figure 8, there was a weak correlation between ASBT logKi and NTCP logKi (R^2 = 0.24). If plotted using Ki values that are not log transformed, R^2 = 0.46 due to effect of non-inhibitors. Compounds can be segregated into three groups, depending on relative inhibition affinities against ASBT and NTCP.

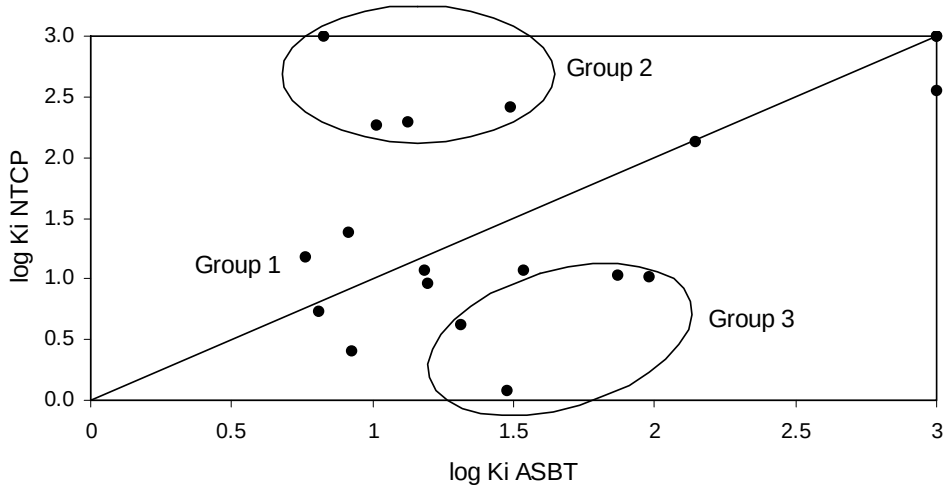

Figure 8. Plot of log Ki against NTCP versus log Ki against ASBT.
Inhibition data can be classified in three groups: equi-potent inhibitors, ASBT-preferred inhibitors, NTCP-preferred inhibitors.

3.4.2.1 Group 1: Equi-potent inhibitors. Most compounds showed similar affinities for ASBT and NTCP: compounds **1**, **2**, **6-10**, **13**, and **17-19**. For this subset of compounds, there was a strong correlation between ASBT logKi and NTCP logKi (R^2 = 0.88; R^2 = 0.88 if Ki values are not log transformed). Compound **1**, **2**, and **6** include unsubstituted aromatic groups conjugated at C-7 that showed strong-to-moderate inhibition of the transporters. For compounds **7-10**, glycine conjugation dominated the steroidal

substitution, resulting in potent inhibition. Compound **13** did not show any ASBT inhibition and was also a weak NTCP inhibitor; the distorted shape of its steroidal nucleus due to ketone substitution at 3, 7, and 12 may be responsible for its relative lack of affinity. For compounds **17**-**19**, which possess aromatic substitution at C-3 and/or C-7, steric hindrance at the possible binding sites may hamper activity.

3.4.2.2 Group 2: ASBT-preferred inhibitors. Four compounds showed higher affinity for ASBT than NTCP: compound **3**, **4**, **5**, and **14**. Although previous literature reports suggested NTCP exhibits much broader substrate specificity, these compounds showed a strong affinity for ASBT and demonstrated weak or no inhibition of NTCP. Among these four compounds, compounds **3**, **4**, and **5** are similar compounds that displayed the pattern where increased substituent size reduced ASBT and NTCP affinity (F < CH3 < t-butyl). The effect was more pronounced in NTCP, with NTCP Ki of about 200 μM or higher. Compound **14** has a benzyl ester in the C-24 region and carboxylate group in C-3 region. This compound was a strong inhibitor of ASBT but lacked affinity for NTCP. The lack of affinity may not be due to the charge in the C-3 region, but rather due to the presence of the bulky benzyl group in C-24 region, which may hinder interaction with the transporter binding site. Removal of this benzyl group (i.e. compound **15**) afforded a strong NTCP inhibitor. Strong ASBT inhibition by compound **14** but lack of NTCP inhibition suggests differences in binding sites between these transporters that involves the C-24 bile acid region.

3.4.2.3. Group 3: NTCP-preferred inhibitors. Five compounds showed higher affinity for NTCP than ASBT: compound **11**, **12**, **15** and **16**. Compound **11** was a strong NTCP inhibitor but a moderate ASBT inhibitor, indicating that oxidation of the 7-hydroxyl

group to ketone reduced affinity for ASBT. This observation was similar to that of Kramer *et al.* where oxidation of the 12-hydroxyl group in cholic acid to keto reduced affinity for the rabbit ileal bile acid transporter (88). Removal of this ketone functional group at C-7 and C-12 yields lithocholic acid and chenodeoxycholic acid, respectively, which each have a strong ASBT affinity (50). A ketone group perhaps distorts the steroid nucleus structure, reducing affinity for ASBT but not NTCP affinity. Although compound **11** was a strong inhibitor of NTCP, its Ki was higher than that of UDCA and CDCA in NTCP. As expected, conjugation with glycine (compound **12**) improved binding affinity of compound **11** in ASBT and NTCP.

Compound **15** was a strong inhibitor of NTCP but only a moderate inhibitor of ASBT. Compared to compound **14**, compound **15** involves the removal of the benzyl group at C-24, which allowed more potent interaction with NTCP, but reduced binding with ASBT.

Compound **16** was a strong inhibitor for ASBT and NTCP, although it possessed higher affinity for NTCP. Its Ki values were similar to that of UDCA. Compared to UDCA, compound **16** involves methyl esterification of the C-24 carboxylic acid, which did not affect affinity, especially when 3- and 7- hydroxyl groups were not conjugated.

3.4.3 Uptake study.

A C-3 analogue, compound **10** afforded active uptake by ASBT and NTCP, with substrate parameters comparable to that of native bile acids. Compound **12** also demonstrated active uptake by both transporters. None of the five C-7 conjugates (i.e. compounds **1**, **5**, **6**, **8**, and **9**) were a substrate of either ASBT or NTCP. The aromatic ring at C-7 in these five appears to disallow translocation. Meanwhile, the C-7 keto in compound **12** was translocated across both ASBT and NTCP, perhaps due to the smaller

size of the ketone functional group versus the aromatic ring, or a ketone allows similar interactions as a native hydroxyl group.

Interestingly, uptake results across ASBT and NTCP were similar, in spite of greater difference in inhibition data. Hence, results from combined inhibition and uptake studies suggest differences in initial binding sites between ASBT and NTCP, whereas solute translocation involves similar interaction in ASBT and NTCP.

NTCP has previously been shown to transport non-steroidal molecules, such as rosuvastatin (58). Substrate specificity of ASBT was though to be limited to bile acids. However, we recently identified non-bile acid small molecules as substrates of ASBT (92). Whether rosuvastatin is a substrate of ASBT remains to be examined. Nevertheless, such studies that compare inhibition, as well as uptake, in both transporters have the potential to provide insights into the solute interaction with these transporters.

3.5 Comparison to previous studies

Baringhaus *et al.* developed a pharmacophore model based on a training set of 17 diverse rabbit Asbt inhibitors (48). This model had five features: one hydrogen bond donor, one hydrogen bond acceptor, and three hydrophobic features. Native bile acids, including taurocholate, taurochenodeoxycholate and taurodeoxycholate, mapped only four of the five features. The model mapped the 12 α-hydroxy group in taurocholate as a hydrogen bond donor. The high affinity and uptake rate for CDCA (i.e. 3 α- and 7 α- hydroxyl bile acid) was explained by the 7 α-hydroxyl group as the hydrogen bond donor in absence of 12 α-hydroxy group. The 3 α-hydroxy group which is present in all native bile acids did not map any specific feature in the model. However, lithocholic acid, which lacks 12 α- and 7 α- hydroxyls and only possesses a 3 α- hydroxyl group, had high affinity and

uptake rates for ASBT (50). In addition to not mapping the 3 α- hydroxyl group, this model of Baringhaus *et al.* did not map any interaction with steroidal ring A and suggested that steroidal ring A or position 3 may serve as attachment for drug moieties for drug delivery.

However, Bhat *et al.* attached a substituted pyrazole to glycocholic acid (i.e. 7 α- and 12 α- hydroxyl bile acid) via steroidal ring A (89). The conjugate showed only weak interaction with ASBT. Another compound with substituted pyrazole attached to ring A but with no steroidal hydroxyl groups was a strong inhibitor of ASBT and NTCP, and was translocated by ASBT (89). No pharmacophore model has explained these results.

In conclusion, results show that ASBT and NTCP accommodate a wide range of substituents for binding, but that all major C-7 modifications resulted in analogues that were not translocated by either ASBT or NTCP. Interestingly, a C-3 modification that was not tolerated at C-7 still afforded translocation via ASBT and NTCP, further confirming the relative unacceptability of C-7 modification. Results also characterize the relative promiscuity of ASBT and NTCP. Compared to ASBT, NTCP demonstrated a generally similar binding potency across compounds, although showed less binding affinity toward C-24 unconjugated bile acids with aromatic substitution at C-7. Results suggest that drug conjugation of drug to the C-3 hydroxyl group, rather than C-7, has potential to provide as a bile acid transporter prodrug strategy.

3.5 APPENDIX

The objective was to identify a decision tool to conclude when a compound is a non-substrate.

3.5.1 Decision tool derivation.

Transport of a substrate across a transporter-expressing monolayer involves active and passive flux, as represented by eqn A1.

$$J_t = \frac{J_{\max} S}{K_t + S} + P_p S \qquad \text{eqn A1}$$

where J_t is total flux.

Distinguishing a substrate from a non-substrate depends on the ability to differentiate between total and passive flux. Passive flux depends on Pp and substrate concentration. Pp is generally independent of experimental conditions. Flux due to transporter-mediated translocation depends on K_t, transporter expression level, and substrate concentration. However, high Pp and/or high substrate concentration can cause inability to differentiate between the active and passive components, since passive flux can dominate. This inability to differentiate is most problematic for substrates with high K_t (i.e. low affinity substrates).

when $S = K_t$, eqn A1 yields

$$J_t = \frac{J_{\max}}{2} + J_p \qquad \text{eqn A3}$$

where Jp is the passive flux under this condition (i.e. $J_p = P_p \cdot K_t$).

Assuming $J_t = 2J_p$ and substituting into eqn A3,

$$2J_p = \frac{J_{\max}}{2} + J_p \qquad \text{eqn A4}$$

$$J_p = \frac{J_{\max}}{2} \qquad \text{eqn A5}$$

Substituting $J_p = P_p \cdot K_t$ into eqn A5

$$P_p K_t = \frac{J_{\max}}{2} \qquad \text{eqn A6}$$

$$K_t = \frac{J_{\max} / 2}{P_p} \qquad \text{eqn A7}$$

Eqn A7 delineates the requisite condition when total flux is twice the passive flux when S = Kt. Since it is assumed that substrates cannot be differentiated from non-substrates when $J_t < 2 \cdot P_p S$, eqn A7 identifies the highest Kt value that allows for substrates to be differentiated from non-substrates. Hence, eqn A7 is re-written

$$K_t^{\max} = \frac{J_{\max} / 2}{P_p} \qquad \text{eqn A8}$$

where K_t^{max} is not the actual Kt of the substrate, but the maximum allowable Kt that will allow $J_t \geq 2 \cdot P_p S$, when S = Kt.

Eqn A8 indicates that two factors promote the differentiation of substrates from non-substrates when S = Kt: high Jmax and low P. That is, compounds with low affinity (i.e. higher Kt) can be discerned as substrates or non-substrates, provided they have sufficiently high Jmax or low Pp.

Implications of eqn A8 were confirmed by simulations performed under varying Pp, Jmax values, and Kt values. Calculations confirmed that if $K_t > \frac{J_{\max} / 2}{P_p}$, then $J_t < 2 \cdot P_p S$, which presumably affords an experiment to not be able to differentiate a substrate from a non-substrate.

It should be noted that this above approach assumes that an experiment employs S = K_t. However, uptake studies often use substrate concentrations above K_t, which only makes

differentiating between substrates and non-substrates more difficult, due to an increasing relative contribution of passive flux.

3.5.2 Application.

Table 2 shows several compounds were concluded to not be substrates. From eqn A8, their estimated K_t^{max} ranged from about 10 – 1000 μM. Experiments below the estimated K_t^{max} found total flux was the same, either with or with sodium, such that non-substrate was concluded.

In Table 2, one compound (compound **1**) was not determinable – i.e. it was not possible to differentiate whether it was a non-substrate or that its active uptake was not measurable. The compound's high permeability (Pp = 85.6 x 10^{-6} cm/s) and assumed Jmax equal to taurcholate resulted in K_t^{max} equal to about 1 μM. An analytical method could not be developed to measure drug uptake from a donor concentration of 1 μM. Experiments using S = 10 μM found total flux was the same, either with or with sodium. However, since the S was above the estimated K_t^{max}, it was conservatively concluded that active uptake was not determinable, although perhaps others would conclude compound **1** not to be a substrate.

CHAPTER 4

Synthesis and in vitro evaluation of bile acid conjugate of 5-aminosalicylic acid for colon targeting

4.1 INTRODUCTION

Ulcerative colitis is an idiopathic inflammatory disorder that affects the lining of the colon and rectum. 5-aminosalicylic acid (5-ASA) is first-line therapy for mild to moderate ulcerative colitis, and is an anti-inflammatory agent that needs to be targeted to colon for successful treatment. Orally administered 5-ASA undergoes rapid absorption in the small intestine that can render the therapy ineffective. Various delivery systems and prodrugs are therefore designed for colon targeting of 5-ASA, such as pH sensitive coating (e.g. Lialda, Asacol) and delayed release formulation (e.g. Pentasa) (93-95).

Sulfasalazine is a prodrug of 5-ASA that targets the colon, and achieves targeting by colonic bacterial enzymes reducing the prodrug to 5-ASA and sulfapyridine. An azo bond between 5-ASA and the sulfapyridine moiety is activated by colonic bacteria to liberate 5-ASA. 5-ASA is mostly unabsorbed in colon (about 75%) and is eliminated in feces (95, 96). Meanwhile, the formed sulfapyridine is rapidly absorbed and undergoes extensive hepatic metabolism. About 10-45% of patients have side effects related to this sulfa moiety, including allergic reactions (95, 96). Olsalazine and balsalazide are also 5-ASA prodrugs conjugated to 5-ASA and 4-aminobenzoylalanine respectively, and employ an azo bond for colon targeting.

The objective of this study was to synthesize and characterize a prodrug of 5-ASA based on a bile acid conjugate with low permeability. In our laboratory, we are performing systematic studies to evaluate structure activity relationships for the ileal bile acid transporter, i.e. the apical sodium-dependent bile acid transporter (ASBT). These studies involve conjugating various drug-like probe molecules to different positions of bile acids

to assess how these structural changes impact solute interactions with ASBT. For example, conjugation of an aromatic ring at the C-7 position of chenodeoxycholic acid or ursodeoxycholic acid resulted in molecules with low passive permeability, and no translocation across ASBT (97). In the present study, we selected glycoursodeoxycholic acid to conjugate with 5-ASA, in order to design a 5-ASA prodrug that targets the colon and employs a linker between the bile acid and drug. The linker incorporated an azo bond.

4.2 MATERIALS AND METHODS

4.2.1 Materials

Ursodeoxycholic acid was obtained from TCI America (Portland, OR). p-aminobenzoic acid was purchased from USB corporation (Columbus, OH). Sodium nitrite was obtained from Sigma Aldrich (St. Louis, MO). 4-benzyloxycarbonylaminobenzoic acid was purchased from Medinoah Co. (Wallingford, CT). Geneticin, fetal bovine serum (FBS), trypsin, and DMEM were obtained from Invitrogen (Rockville, MD). [^{3}H]-Taurocholic acid was purchased from PerkinElmer Inc (Waltham, MA). Taurocholic acid was obtained from Sigma Aldrich (St. Louis, MO). All other reagents and chemicals were of the highest purity commercially available.

4.2.2 Synthetic procedure overview

The synthetic approach is depicted in Figure 1. The prodrug was synthesized in five steps. Ursodeoxycholic acid was conjugated to methyl ester of glycine. The C-3 and C-7 positions of glycoursodeoxycholate were acylated by 4-benzyloxycarbonylaminobenzoyl

chloride followed by deprotection, and diazotization. The diazonium salt was further reacted with salicylic acid to yield the prodrug.

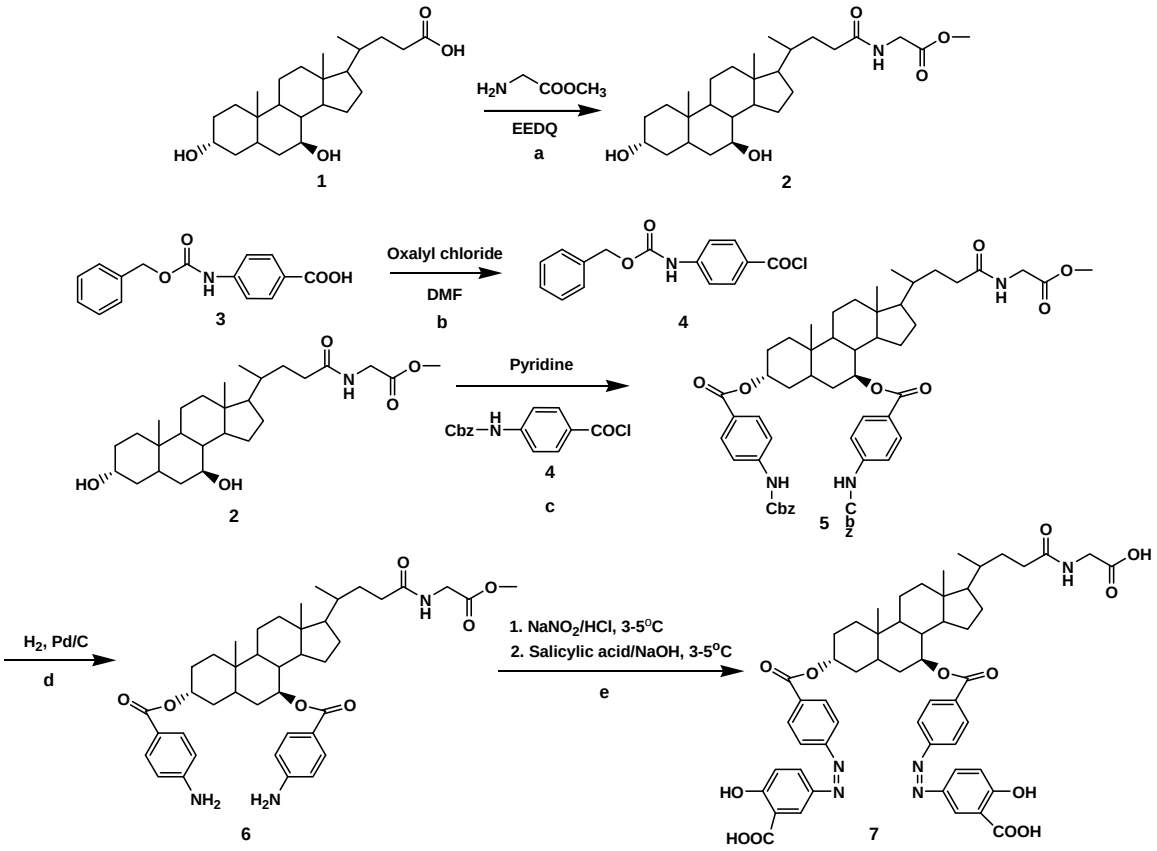

Figure 1. Prodrug synthesis.

4.2.2.1 Conjugation of ursodexycholic acid to meyhyl glycinate hydrochloride (step a). The glycine conjugate of bile acid was synthesized, as described earlier (82). Briefly, methyl glycinate hydrochloride (0.878g, 7mmol) was stirred with triethylamine (1ml, 7.1 mmol) in ethyl acetate (about 70 ml) at RT for 30 min. Ursodeoxycholic acid (1.96g, 5mmol) and N-ethoxycarbonyl-2-ethoxy-1,2-dihydroquinoline (1.73g, 7mmol) were added to the suspension. The reaction mixture was heated at 65 ºC for 15 hr. The suspension was then cooled to RT and washed with water (25 ml), 0.5N NaOH (50 ml),

water (25 ml), 0.5N HCl (50 ml X2) and water (25 ml). The resulting ethyl acetate layer was washed with brine and evaporated under vacuum to yield methyl glycoursodeoxycholate, which was used without further purification. Mass spectrometry (MS) showed appropriate peaks: [M+1] 464.2, [M+Na] 486.3.

4.2.2.2 Acid chloride formation (step b). 4-benzyloxycarbonylaminobenzoic acid (2.93g, 14 mmol) was suspended in anhydrous dichloromethane (40 ml). Oxalyl chloride (4.44g, 35mmol) was added to this suspension, followed by addition of a catalytic amount of dimethyl formamide. After 3 hr the clear solution was evaporated under vacuum to obtain the acid chloride (**4**).

4.2.2.3 Conjugation of protected p-aminobenzoic acid to methyl glycoursodeoxycholate (step c). To compound (**4**) (3.18g, 14mmol) was added a solution of methyl glycoursodeoxycholate (1.7g, 3.6mmol) in pyridine (12 ml). The reaction mixture was heated at 55-60 ºC for eight hours. After cooling, the reaction mixture was poured over ice and acidified with concentrated HCl to pH 2. The suspension was extracted three times with dichloromethane. The combined organic layer was dried over sodium sulfate and evaporated under vacuum to yield a crude mixture (83). The crude mixture was purified by column chromatography over silica gel using 50 % hexane in ethyl acetate as an eluent to obtain methyl ester of 3,7-di-(p-amino) benzoyl derivative (**5**). MS indicated appropriate peak: [M+1] 970.5.

4.2.2.4 Deprotection of methyl ester of 3,7-di-(4-amino) benzoyl derivative (step d). The purified diacyl derivative (**5**) was dissolved in ethanol and subjected to catalytic hydrogenation using 10% Pd/charcoal in ethanol at 45 psi for 15 hr. The suspension was

filtered through celite and solvent evaporated under vacuum to obtain methyl 3,7-di-(4-amino) benzoyl glycoursodeoxycholate (**6**). The product was pure as indicated by TLC analysis and was used in the next step without further purification. MS indicated appropriate peak: [M+1] 702.4.

4.2.2.5 Formation of azo bond (step e). Compound (**6**) (500mg, 0.7 mmol) was added to the aqueous solution of $NaNO_2$ (105 mg, 1.5 mmol). The mixture was stirred in an ice bath (3-5 °C) for 15 min and then acidified with 3M HCl and stirred (about 5 min) until tested positive for the presence of slight excess of nitrous acid, using potassium iodide/starch paper. The formed diazonium salt was added to an ice cold solution of salicylic acid (300 mg, 2.1 mmol) in 0.5M sodium hydroxide, and pH was adjusted to 10 using 1M sodium hydroxide. The reddish-brown solution was stirred for 30 min and then acidified with 3M HCl to separate the desired prodrug (**7**). The identity and purity of the final compound was confirmed by TLC, MS and NMR.

4.2.3 Stability and 5-ASA release studies

4.2.3.1 Chemical stability. Prodrug chemical stability was studied in 0.1M HCl and pH 6.8 Hank's balanced salt solution (HBSS) buffer for 3 hr. The prodrug (10 μM) was incubated in 0.1 M HCl at 37 °C for 3 hr in an orbital shaker. 100 μl samples were collected, neutralized with 0.1M sodium hydroxide, and diluted to 1 ml with cold DPBS buffer. For stability in pH 6.8 HBSS buffer, 100 μl samples were collected and diluted with cold DPBS buffer. Samples were analyzed by HPLC for disappearance of prodrug and appearance of drug.

4.2.3.2 Caco-2 homogenate stability. Caco-2 cells were grown in 225 cm^2 flasks for three weeks at 37 °C and 5% CO_2. The cells were grown in Dulbecco's modified Eagle medium (DMEM), 10% FBS, and 1% nonessential amino acids. The cells were washed with 10 ml of Dulbecco's phosphate buffered saline (DPBS) three times. The cells were scraped from the flasks on an ice tray and reconstituted in 10 ml of DPBS. The cell suspension was transferred to a sterile centrifuge tube and sonicated by using a sonic dismembrator (Model F60; Fisher Scientific, Pittsburgh, PA). Crude Caco-2 homogenates were centrifuged at 10,000 rpm for 10 min at 4°C. One ml aliquots of supernatant were collected in centrifuge tubes. Total protein was quantified using the Bradford protein assay (Bio-Rad Laboratories, Hercules, CA) and was about 0.46 mg/ml (75, 98).

The prodrug (10 μM) was incubated with cell homogenate at 37 °C for 5 hr in an orbital shaker (50 rpm). 100 μl samples were collected and added to 900 μl of ice cold DPBS. The samples were centrifuged at 10,000 rpm for 10 min at 4°C prior to analysis by HPLC for disappearance of prodrug and appearance of drug.

4.2.3.3 Stability in cecal contents. These studies were conducted in accordance of the University of Maryland Institutional Animal Care and Use Committee. The cecal segment of four C57BL mice intestines were surgically obtained and their contents were collected, pooled, weighed, and dispersed in nitrogen-bubbled PBS (pH 6.8) to yield a 20% w/v suspension of cecal contents. One ml of prodrug (250 μM) was mixed with one ml suspension. The mixture was incubated at 37 °C. At specified times points, the reaction was quenched by adding 400 μl of cold acetonitrile to the sample (200 μl). Samples were stored at -80 °C until further processing. The samples were centrifuged at 10,000 rpm for 10 min at 4 °C. Acetonitrile was evaporated under vacuum using a

speedvac (Thermo Savant SPD121P; Thermo Scientific, Waltham, MA) before sample analysis. Samples were analyzed by HPLC for disappearance of prodrug and appearance of drug.

4.2.4 ASBT inhibition study

Stably transfected ASBT–MDCK cells were cultured as previously described (49). Briefly, the cells were grown at 37 °C, 90% relative humidity, 5% CO_2 atmosphere, and fed every 2 days. Culture media consisted of DMEM supplemented with 10% FBS, 50 units/ml penicillin, and 50 μg/ml streptomycin. Geneticin was added at 1 mg/ml to maintain selection pressure. The cells were passaged after 4 days or after reaching 90% confluency.

To evaluate prodrug binding affinity for ASBT, a taurocholate uptake inhibition study was performed using ASBT-MDCK cells (53, 72). Cells were seeded at a density of 1.5 million/well in 12-well plates (3.8 cm^2, Corning, Corning, NY) and induced with 10 mM sodium butyrate 12–15 hr prior to study on day 4. Cells were washed thrice with Hank's balanced salt solution (HBSS) and exposed to donor solution containing taurocholic acid (2.5 μM with 0.5 μCi/ml ^{3}H-taurocholate) and conjugate (0-250 μM). The study was conducted at 37°C, 50 rpm for 10 min in an orbital shaker. After this time, donor solution was removed, and cells were washed three times with chilled sodium-free buffer. Cells were lysed by adding 300 μl acetonitrile to each well. Following evaporation at RT for about 2 hr, 500 μl of DPBS was added and 250 μl was then counted for associated radioactivity using an LS6500 liquid scintillation counter (Beckmann Instruments, Inc., Fullerton, CA). Inhibition data was regressed using a modified Michaelis-Menten

equation (eqn 1) to determine Ki as previously described (86). Parallel study was performed on the same occasion to estimate Jmax and Pp for taurocholic acid (86).

$$J = \frac{P_{ABL} \cdot \left(\frac{J_{\max}}{K_t\left(1+\frac{I}{K_i}\right)+S} + P_p \right)}{P_{ABL} + \frac{J_{\max}}{K_t\left(1+\frac{I}{K_i}\right)+S} + P_p} \cdot S \qquad \text{eqn 1}$$

where I is inhibitor concentration, Ki is inhibition constant, J is taurocholate flux, Jmax and Kt are the Michaelis-Menten constants, S is taurocholate concentration (i.e. 2.5 μM), Pp is passive taurocholate permeability, and P_{ABL} is aqueous boundary layer permeability. Kt was set to 5.03 μM, as obtained from pooled kinetic analysis of historical taurocholate uptake studies. P_{ABL} was set to 1.5×10^{-4} cm/s (86). Pp was estimated from taurocholate uptake studies in absence of sodium. Ki was estimated by using nonlinear regression fitting performed by WinNonlin Professional.

4.2.5 ASBT uptake study

Prodrug uptake by ASBT was performed in a similar manner to the above inhibition study (i.e. 12 well plate, where cells were seeded at a density of 1.5 million/well and induced with 10 mM sodium butyrate 12-15 hr prior to study on day 4).

Cells were washed three times with HBSS prior to the study. Uptake was initiated by exposing cells to donor solution of prodrug (2.5-50 μM) for 10 min. Cells were washed with cold sodium free buffer and lysed with acetonitrile, as described above. After evaporation of acetonitrile, the prodrug was extracted from the cell lysate by adding 1 ml

of 1:1 acetonitrile and water. Identical studies were performed without sodium, to measure passive uptake of the prodrug. Also, on the same occasion, taurocholate Vmax and passive permeability (Pp) were measured to normalize for ASBT expression. Uptake data was fitted to the modified Michaelis-Menten equation (eqn 2 and 3) to yield estimates for Kt and Jmax and Pp (54, 86).

$$J = \frac{P_{ABL} \cdot \left(\frac{J_{\max}}{K_t + S} + P_p \right)}{P_{ABL} + \frac{J_{\max}}{K_t + S} + P_p} \cdot S \qquad \text{eqn 2}$$

$$J = \frac{P_{ABL} P_p S}{P_{ABL} + P_p} \qquad \text{eqn 3}$$

Kinetic parameters were estimated by using nonlinear regression fitting performed by WinNonlin Professional.

4.2.6 Quantification of prodrug and 5-ASA

Quantification of prodrug and drug from chemical stability studies, Caco-2 homogenate stability studies, and cecal stability studies were performed using an HPLC-UV system consisting of a Waters 1525 binary pump, 717 autosampler, and 486 tunable absorbance detector (Waters Corp., Milford, MA). The detector was set at 215 nm. The column was a Phenomenex Luna [5µ C18(2) 150X4.6mm] column. The mobile phase consisted of methanol : 25mM phosphate buffer (4:96, v/v) pH 6.8.

Quantification of prodrug and drug from the uptake study was performed using a Waters Acquity UPLC system equipped with binary solvent manager, sample manager autosampler, and PDA detector. The column was a Phenomenex Luna [5µ C8(2)

50X2mm] column. Mobile phase consisted of acetonitrile : water (10:90, v/v), each with 0.1% formic acid.

4.3. RESULTS AND DISCUSSION

4.3.1 Prodrug synthesis

The prodrug was successfully synthesized in five steps, with overall yield of approximately 24%. The prodrug employed glycoursodeoxycholic acid because of its low passive permeability compared to ursodeoxycholic acid. p-aminobenzoic acid was selected as a linker based on the appropriate functional groups, in order to link to bile acid hydroxyls (i.e. carboxylate) and to 5-ASA (i.e. amine). Carboxybenzyl protected p-aminobenzoic acid was used to avoid self conjugation. The carboxylic acid of 4-benzyloxycarbonylaminobenzoic acid was converted to an acid chloride and conjugated to methyl glycoursodeoxycholate. Following deprotection of the amine group, this amine was diazotized using nitrous acid formed in situ by HCl and sodium nitrite. The aromatic amine facilitated the formation of diazonium salt. The diazonium salt was coupled at the para- position of salicylic acid by the para-directing phenolic hydroxyl group (99). The strongly basic conditions in this step also lead to the methyl ester hydrolysis of the methyl glycinate.

Identity and purity of the final compound was confirmed by TLC, MS and ^{13}C NMR. TLC showed a bright yellow spot in ethyl acetate : methanol : acetic acid (90:9:1). The MS indicated appropriate peak at 984.6 (M-1). ^{13}C NMR (methanol-d_4) provided: 12.72, 19.12, 22.54, 23.89, 27.76, 29.59, 33.19, 33.94, 34.26, 35.47, 35.69, 35.71, 35.76, 36.77, 40.96, 41.38, 41.75, 41.88, 43.80, 44.94, 45.46, 56.52, 59.59, 85.15, 86.17, 118.30 (2),

119.54, 120.22, 123.72 (2), 128.90, 129.84, 131.70, 131.83, 136.75 (2), 146.77 (2), 166.46, 166.92, 168.44, 168.59, 177.27 (2), 182.58 (2), 184.28, 184.88. A peak at 48.6 ppm was obscured by solvent.

4.3.2 Chemical stability, Caco-2 homogenate stability, and activation by cecal contents.

Figure 2 illustrates prodrug chemical stability and Caco-2 homogenate stability. Prodrug was essentially completely stable over 3 hr in 0.1M HCl, as well as in HBSS buffer pH 6.8. No drug was detected (LOQ = 0.7 μM). Prodrug was also stable in Caco-2 homogenate, with 89.2 (±2.8) percent remaining after 5 hr. In 0.1M HCl and in buffer pH 6.8, no drug was detected.

The prodrug was evaluated for drug release in mouse cecal contents. Figure 3 shows drug release increased with time over 8 hr. At 8 hr, 42.8 (±5.9) percent of drug was liberated from the prodrug. Compared to its stability in acid, pH 6.8 buffer, and cell homogenate, drug release in cecal content suggests potential success in targeting 5-ASA to the colon. In Figure 3, loss of prodrug was more rapid than generation of drug. For example, at 2 hr, about 76% of prodrug disappeared, with about 15% of 5-ASA release from prodrug. At 8 hr, about 81% of prodrug disappeared, and about 43% 5-ASA was formed. A potential explanation is more rapid ester hydrolysis than azo bond reduction, under these experimental conditions. It may be possible that initial ester hydrolysis between the linker and bile acid was followed by subsequent 5-ASA liberation via azo reduction.

A

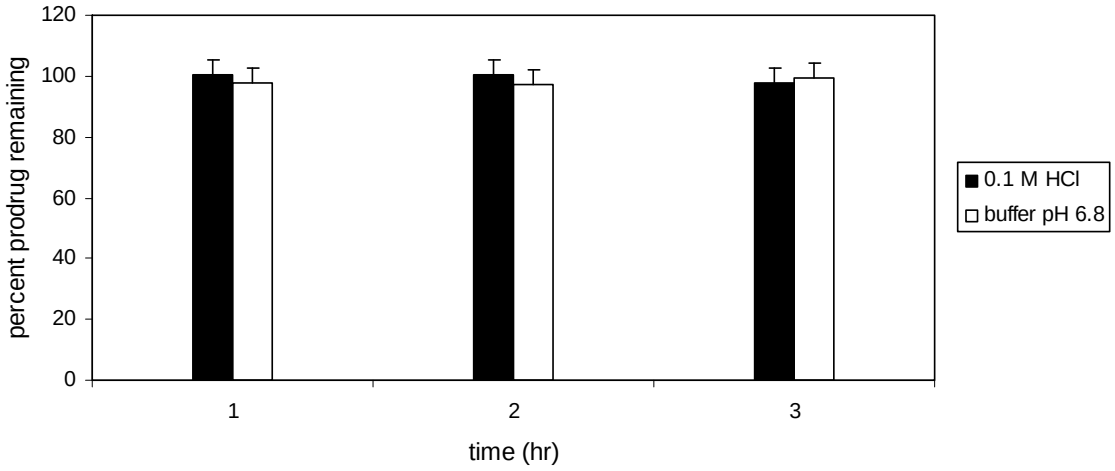

B

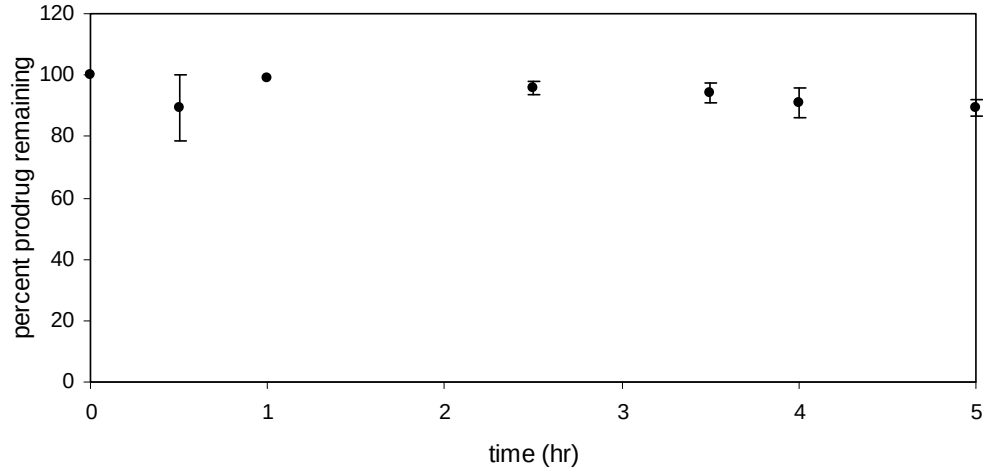

Figure 2. In vitro chemical and metabolic stability.
(A) Prodrug stability in 0.1M HCl and buffer pH 6.8. (B) Prodrug stability in Caco-2 homogenate. Prodrug was stable of the time course of studies.

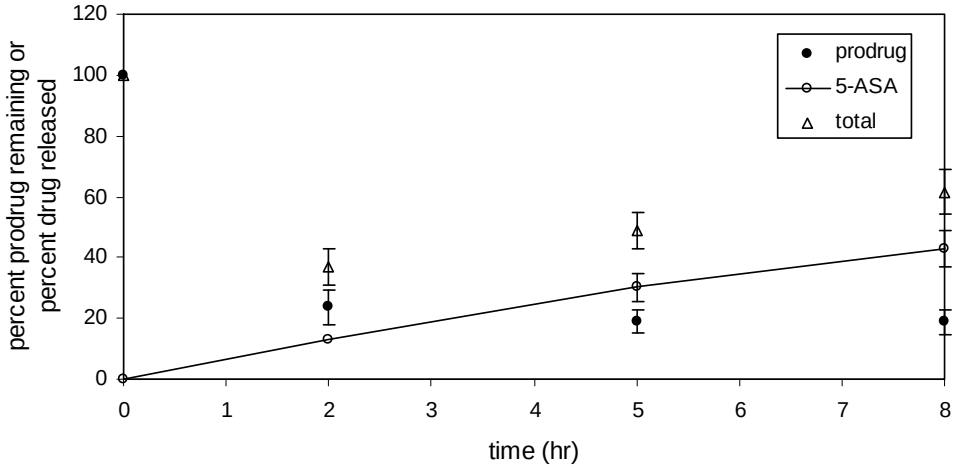

Figure 3. In vitro release profile of 5-ASA from the prodrug during incubation with mouse cecal content at 37 °C.
About 43% drug was released by 8 hr. Loss of prodrug, generation of 5-ASA, and their stoichiometric sum (i.e. total) suggest that prodrug was largely converted to an intermediate (e.g. hydrolysis product), which then yielded 5-ASA.

4.3.3 Prodrug Permeability into ASBT-MDCK monolayers

The prodrug was evaluated for its interaction with ASBT. The inhibition study demonstrated a potent Ki of 8.63±1.66 μM (Fig 3). This Ki value reflects tight binding of the prodrug to ASBT and is similar to Ki values for native bile acids (50).

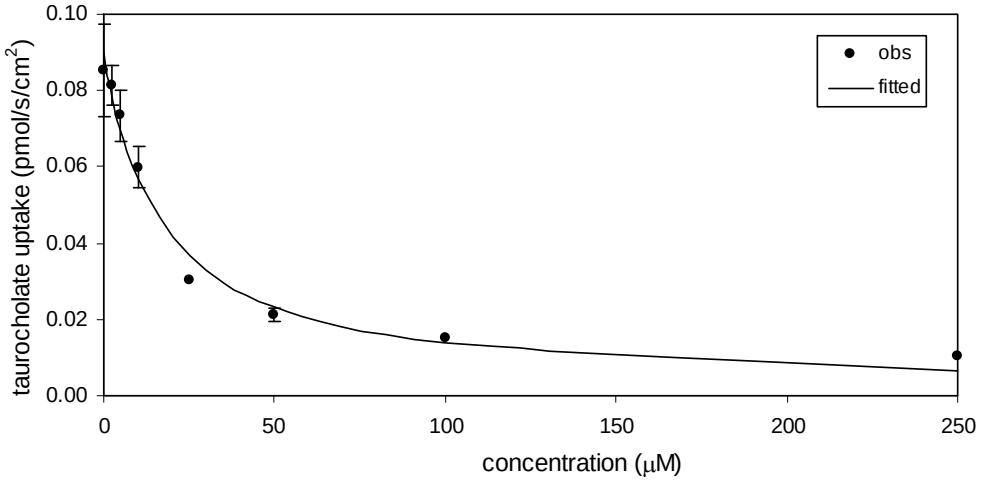

Figure 4. Inhibition profile of taurocholate uptake by prodrug in ASBT-MDCK.
The prodrug strongly inhibited ASBT, with a potent Ki of 8.63±1.66 μM.

Figure 5 illustrates prodrug uptake into ASBT-MDCK monolayers in the presence and absence of sodium. ASBT is a sodium-dependent transporter, such that the study without sodium was interpreted to reflect only passive prodrug permeability (45, 54). The prodrug was not an ASBT substrate since there was no practical difference in the uptake profiles of produg in the presence and absence of sodium. The prodrug was designed not to be an ASBT substrate through conjugation at the bile acid's C-7 hydroxyl group. Additionally, as expected, the prodrug exhibited a low passive permeability [Pp = 9.67 (±0.94) x 10^{-7} cm/s], since the prodrug contained three negative charges. The prodrug's combined low permeability and stability pattern anticipate potential success in targeting 5-ASA to the colon.

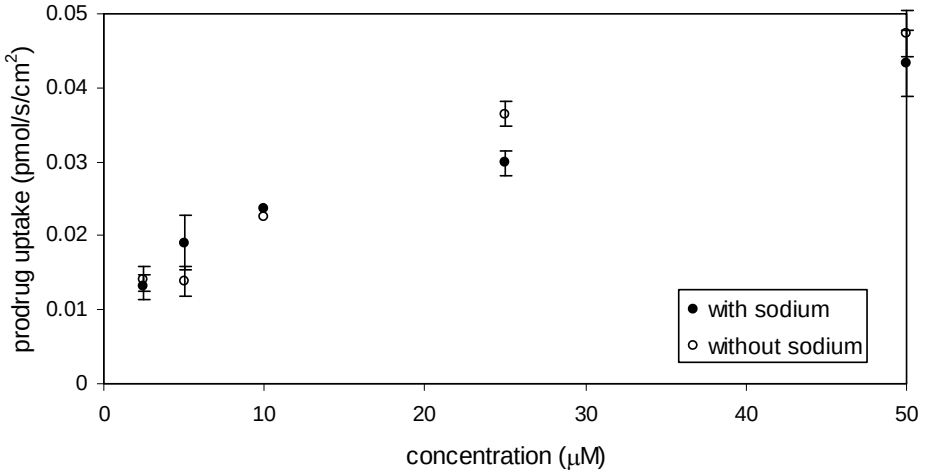

Figure 5. Uptake profile of prodrug into ASBT-MDCK monolayers.
The prodrug was not an ASBT substrate since it exhibited similar uptakes in the presence (●) and in the absence (○) of sodium. Low prodrug uptake also reflected low passive permeability of the prodrug.

4.3.4 Prodrug design

5-ASA continues to be first-line therapy for the treatment of mild to moderate ulcerative colitis. However, oral administration of free 5-ASA results in ineffective therapy. Various colon targeting strategies are employed for successful treatment outcome. Coupling 5-ASA to a carrier molecule by an azo bond limits absorption from the upper intestine and azo bond reduction in the colon releases drug within the colon. Sulfasalazine, balsalazide and olsalazine are 5-ASA prodrugs drugs that employ this azo bond strategy. Use of pH sensitive coating (e.g. Asacol) or delayed release formulation (e.g. Pentasa) also offers effective treatment choices. Treatment goals for ulcerative colitis include controlling acute exacerbations and maintaining remission, which requires chronic treatment. However, the long term use of 5-ASA based treatments can cause nephrotoxicity in some patients. This side effect has been associated with systemic absorption of 5-ASA, but is rare in patients taking azo-based prodrugs of 5-ASA (94, 100-102). Treatment with azo-based prodrugs balsalazide and olsalazide has shown better outcomes than outcomes from Asacol (i.e. pH dependent formulation) in clinical trials (103, 104).

However, the azo based pordrug sulfasalzine has been associated with a wide range of adverse reactions including headache, nausea, fatigue, rash, fever, Stevens-Johnson syndrome and reversible male infertility (95, 105, 106). These adverse reactions are dose dependent and related to the carrier molecule sulfapyridine, highlighting the importance of the carrier molecule in prodrug-based treatment.

Batta *et al* reported the synthesis and intestinal metabolism of 5-ASA conjugated to ursodeoxycholic acid by an amide bond via carboxylic acid at C-24 position of the bile

acid (107). The authors hypothesized the dianionic nature of this conjugate would limit its absorption, allowing it to reach colon and 5-ASA release by bacterial enzymes. However the pKa of 2.97 and 9.89 for -COOH and –OH, respectively, would anticipate the conjugate to only possess a single negative charge at physiological pH (108, 109). In vitro studies demonstrated loss of parent conjugate with quantitative generation of ursodeoxycholic acid, but appearance of 5-ASA was not investigated or discussed. Similarly, in vivo studies indicated 65% of intact conjugate was excreted in feces thus suggesting limited 5-ASA release.

In the current in vitro study, 5-ASA release was successfully quantified and no 5-ASA release occurred in 0.1M HCl, pH 6.8 buffer or Caco-2 homogenate. The prodrug was designed based on previous studies that demonstrated conjugation of an aromatic ring at C-7 lead to ASBT non-substrates. This pattern was observed here, where the prodrug designed with C-7 conjugation was not a substrate of ASBT. Additionally, two molecules of 5-ASA were conjugated to one molecule of glycoursodeoxycholic acid, allowing higher drug loading and potentially lower dose requirements. Conjugation of bile acid with two 5-ASA molecules promoted low prodrug permeability owing to three negative charges (two charges from each of the 5-ASA carboxylic acids and one negative charge from the C-24 glycine). The passive permeability was 9.67(±0.94) x 10^{-7} cm/s. Such a low passive permeability should limit systemic absorption of the prodrug after oral administration.

Patients with ulcerative colitis are at a higher risk of developing colorectal cancer and precancerous dysplasia (110). In recent studies, ursodeoxycholic acid has demonstrated colon cancer chemopreventive effects in preclinical studies. Specifically, this bile acid

reduced the risk for colorectal dysplasia or cancer in patients with ulcerative colitis (111-118). Thus conjugating 5-ASA to ursodeoxycholic acid has the added potential advantage of delivering ursodeoxycholic acid to colon.

In summary, a 5-ASA prodrug was synthesized by conjugating 5-ASA to the 3- and 7-positions of glycoursodeoxycholic acid. Prodrug design elements included a lowly permeable prodrug that would selectively release 5-ASA in the colon. In vitro results support subsequent in vivo studies to assess potential colon targeting of 5-ASA.

CHAPTER 5

Identification of novel non-steroidal compounds as substrates or inhibitors of ASBT

5.1 INTRODUCTION

The human apical sodium dependent bile acid transporter (ASBT) is a member of the solute carrier family of transporters SLC10A2 and is expressed at high levels in the terminal ileum (119). ASBT is critical in the enterohepatic circulation of bile acids. The bile acid pool (about 3-5 g) undergoes multiple cycles daily and results in a re-cycling of 12-18 g of bile acid each day. However, less than 0.5 g is lost in feces each day, reflecting the high capacity and efficiency of ASBT to reabsorb bile acids. This high capacity and efficiency affords ASBT to be an attractive prodrug target (35). As the endogenous substrates for ASBT (119), bile acids can be used as the ASBT recognition moiety (i.e. pro-moiety), to increase the bioavailability of an otherwise low permeability drug. This strategy increased the bioavailability of acyclovir in rats by conjugating chenodeoxycholic acid to acyclovir via a valine linker (120).

Although bile acids are endogenous compounds that can be expected to have low toxicity after oral dosing, an ASBT recognition moiety that is not a bile acid may be advantageous. Firstly, a bile acid has significant molecular weight compared to a typical drug molecular weight of 500-600 daltons. The molecular weight of chenodeoxycholic acid is 392 daltons and would contribute significantly to the molecular weight of a prodrug that employs a bile acid as a pro-moiety. A high molecular weight would have negative implications on the clinical dose of such a prodrug. A pro-moiety with smaller molecular weight than a bile acid would be favorable.

Secondly, bile acids are not simple detergent molecules that only serve to facilitate lipid absorption, but are complex signaling molecules capable of activating specific receptors (121). They interact with nuclear receptors like farnesoid X receptor (FXR) and are

involved in regulating bile acid, cholesterol, and glucose metabolism (122). Bile acids also activate mitogen-activated protein kinase pathways and are ligands for a G-protein-coupled bile acid receptor, TGR5. They interact with diverse signaling pathways, thereby regulating cellular ions, as well as triglyceride and energy homeostasis. Bile acids have also been suggested to play a role in immune and inflammatory reactions in enterohepatic tissues (123). Thus, in addition to their role in lipid absorption, bile acids are versatile regulatory molecules involved in key signaling pathways. Chronic administration of bile acids via a prodrug approach that employs a bile acid as a pro-moiety has the potential to modify the normal bile acid pool and impact these pathways (124). A non-bile acid pro-moiety with a non-steroidal backbone would likely minimize such impact. Thirdly, bile acids have significant lipophilic character, such that some bile acid conjugates exhibit low aqueous solubility, which generally disfavors absorption.

Despite such motivations, the molecular mechanisms underlying the interaction of ASBT with its substrates and inhibitors are not clear. In the absence of a crystal structure of the transporter, pharmacophore modeling with a series of substrates or inhibitors can facilitate the understanding of transporter-ligand interaction. A substrate-based model can explain critical features in the active site (13). However, most reported ASBT models are based on inhibition data (29, 48). Recently, our laboratory has reported 3D-QSAR models based on novel steroidal ASBT substrates (54, 55). A model based on non-steroidal substrates can aid in understanding the structural requirements of this transporter.

The objective was to identify non-steroidal, small molecules that could potentially serve as pro-moieties in the design of prodrugs that target ASBT. Computer-based similarity

searching was performed to identify bile acids analogues that were neither bile acids nor steroids. Three searches were conducted and involved molecular fingerprints as the computational tools for similarity searching, as well as traditional medicinal chemistry pattern recognition.

5.2 MATERIALS AND METHODS

5.2.1 Materials

[^{3}H]-Taurocholic acid (4.6 Ci/mmol) was purchased from PerkinElmer, Inc. (Waltham, MA). Taurocholate was obtained from Sigma Aldrich (St. Louis, MO). All the other compounds were purchased from ChemBridge Corporation (San Diego, CA), TCI America (Portland, OR), Sigma Aldrich (St. Louis, MO), Ryan Scientific Inc. (Mt. Pleasant, SC), Scientific Exchange Inc. (Center Ossipee, NH) and Princeton BioMolecular Research (Princeton, NJ). Geneticin, fetal bovine serum (FBS), trypsin, and DMEM were purchased from Invitrogen (Rockville, MD).

5.2.2 Computational pro-moiety searches

5.2.2.1 Overall approach and Search A. The overall approach is depicted in Figure 1 and was based on similarity searching for the query compounds, followed by in vitro testing of the selected molecules. Molecular fingerprints were used as the computational tools for similarity searching. In silico similarity search was performed using MOE (Molecular Operating Environment, Chemical Computing Group; Montreal, Quebec, Canada, http://www.chemcomp.com). In Figure 2, glycolithocholate (**I**) and S0382 (**II**) were the query compounds for the initial similarity search (i.e. Search A). Glycolithocholate is a representative bile acid, with only one steroidal hydroxyl group. S0382 is a non-steroidal

ASBT inhibitor that satisfies all five of the pharmacophore points for rabbit ASBT inhibition (48). S0382 has a molecular weight of 357. The search database consisted of over 3.5 million molecules from various chemical and pharmaceutical companies (Table C1 in Appendix C). The BIT_MACCS fingerprint was first applied to identify compounds that were structurally similar to GLCA or S0382 (125, 126). To facilitate the discovery of novel ligands of ASBT, no molecules with steroidal nucleus were selected. Additionally, the MP_MFP fingerprint was applied to identify the molecules that were similar to glycolithocholate and S0382 in terms of various physiochemical descriptors (127). Each the MACCS fingerprint and the MP_MFP fingerprint yielded about 100 non-steroidal molecules with at least 75% similarity to **I** or **II**.

Twenty-five compounds were selected and evaluated for their interaction with ASBT. These 25 compounds were selected since they had a molecular weight less than 375, calculated logP less than 3.5 and could be commercially obtained.

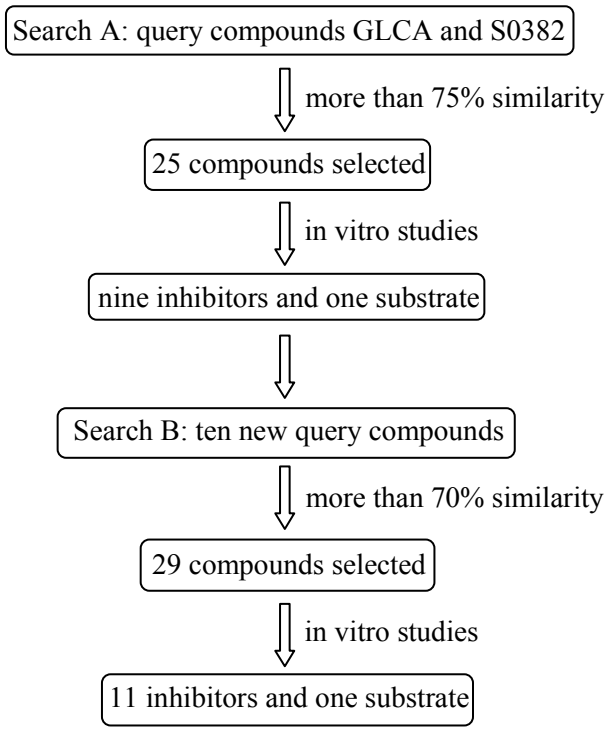

Figure 1. Overall approach.
Searches A and B were performed in series. Search A employed the query compounds glycolithocholic acid (GCLC; compound **I**) and S0382 (compound **II**), resulting in nine inhibitors, including one that was also a substrate. Search B was devised using search A findings, resulting in 11 inhibitors, including one that was also a substrate. Additionally, search C was performed in parallel to search A and B, and employed cholic acid (compound **III**) as a template.

5.2.2.2 Search B. Ten query compounds were used. Search B leveraged results from search A, in order to identify a better ASBT substrate than compound **1**., which was the most potent compound uncovered from search A Of note, Roman numbered compounds denote query compounds, while Arabic numbers denote retrieved compounds. Figure 3 illustrates the nine query compounds used in search B, including how these query compounds were arrived at from compound **1**, as well as from S0382. Compound **1**

consists of two rings (denoted A and B) connected via an amide bond. Panel A of Fig. 3 shows three ring alternatives for ring A, as well as two ring alternatives for ring B. Various combinations of these alternatives for rings A and B yielded seven query compounds for search B, which are drawn in panel B and denoted compounds **IV** through **IX**. Compound **1** and compound **X** (compound **1** with carboxylate substitution) were also among the query compounds. Compounds **XI** and **XII** were conceived as hydrophilic derivatives of S0382 (**II**). Using these ten compounds, similarity searching was performed using the BIT_MACCS fingerprint and the MP_MFP fingerprint for each compound. The search database was the same database used in search A (Table C1 in Appendix C). Each search yielded around 100 molecules with at least 70% similarity (total of 2,471 molecules). Two to four compounds were selected from each query search and evaluated for interaction with ASBT.

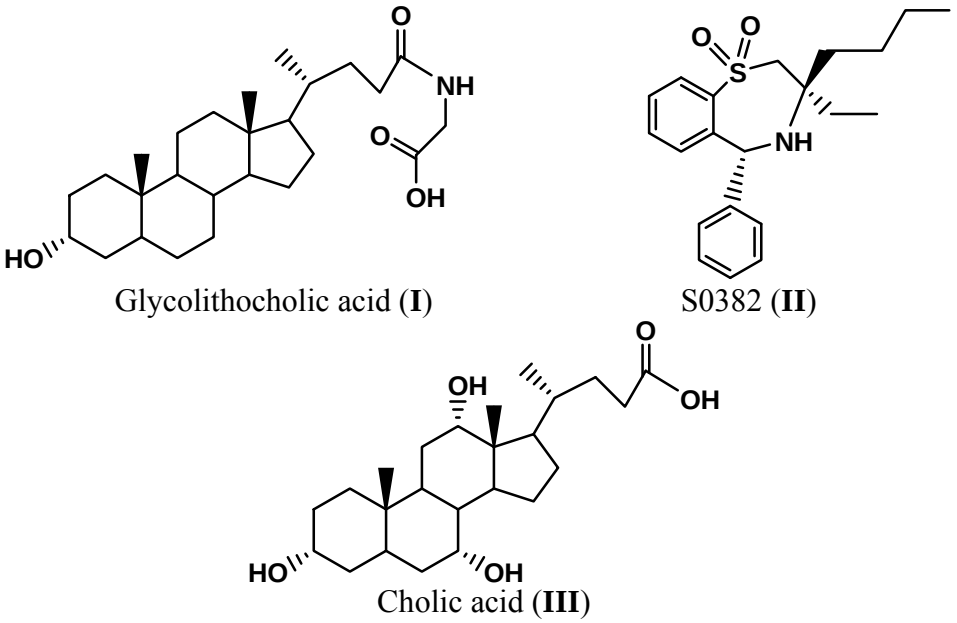

Figure 2. Structures of query compounds.
Search A query compounds glycolithocholic acid (**I**) and S0382 (**II**), along with cholic acid (**III**), the query compound in search C.

A

Compound 1

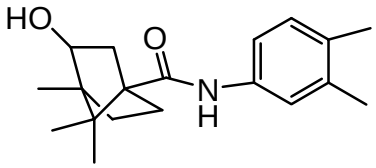

Ring A Ring B

Ring A replacement

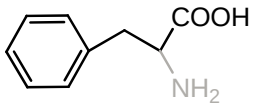

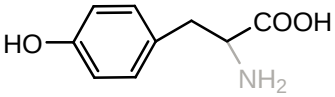

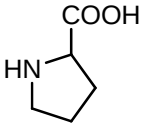

Ring B replacement

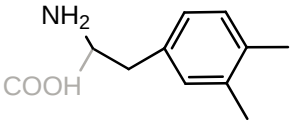

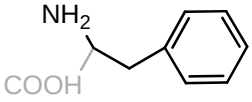

B

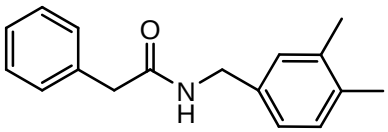

IV

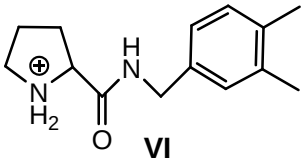

VI

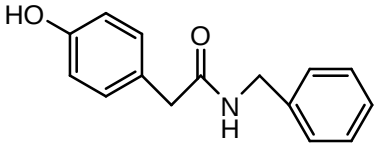

V

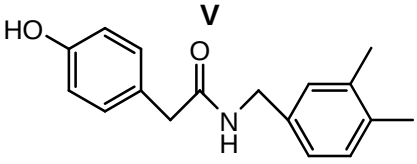

VII

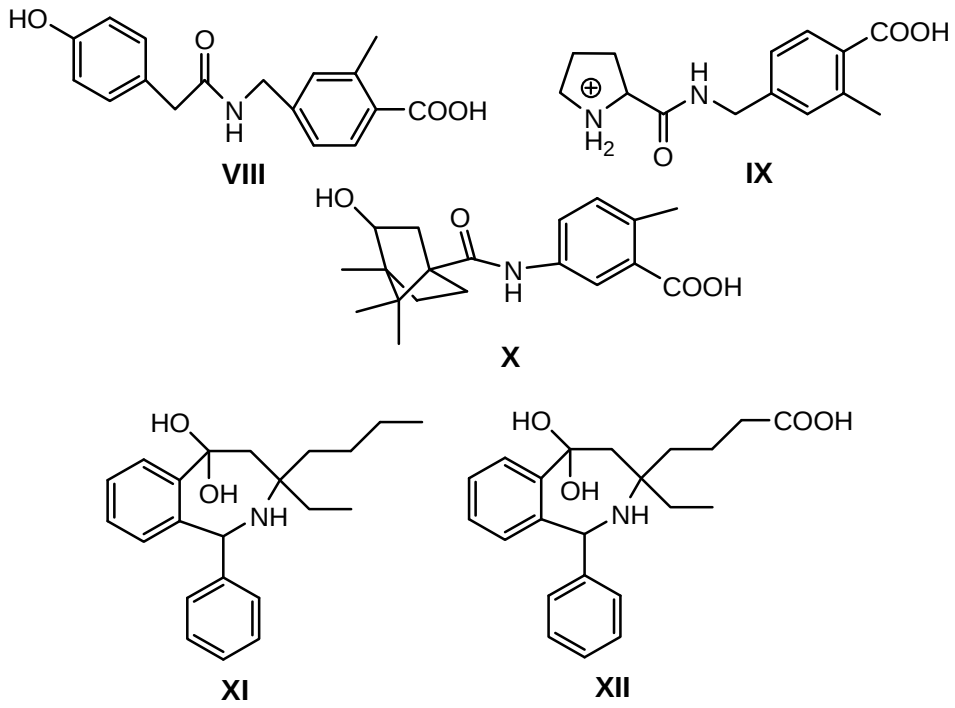

Figure 3. Query compounds in search B.
In panel A, compound **1** is drawn, including its two rings that were the basis for conceiving seven subsequent query compounds for search B. In panel B, the structures of the nine search B query compounds are drawn. Compounds **IV**-**X** were conceived from compound **1**. Compounds **XI** and **XII** were conceived as hydrophilic derivatives of S0382 (**II**).

5.2.2.3 Search C. A similarity search via a traditional medicinal chemistry method was performed, and denoted search C. Previous studies have indicated that the presence of single negative charge in the C-24 region and hydroxyl group are necessary for transport by ASBT (29, 46, 48, 51). Therefore, using SciFinder Scholar (American Chemical Society, Columbus, OH), compounds with a single negative charge connected to a reduced ring system (i.e. non-steroidal ring system) were identified via traditional medicinal chemistry pattern recognition. Figure 4 illustrates this general approach. In vitro studies were performed on nine compounds to examine their interaction with ASBT.

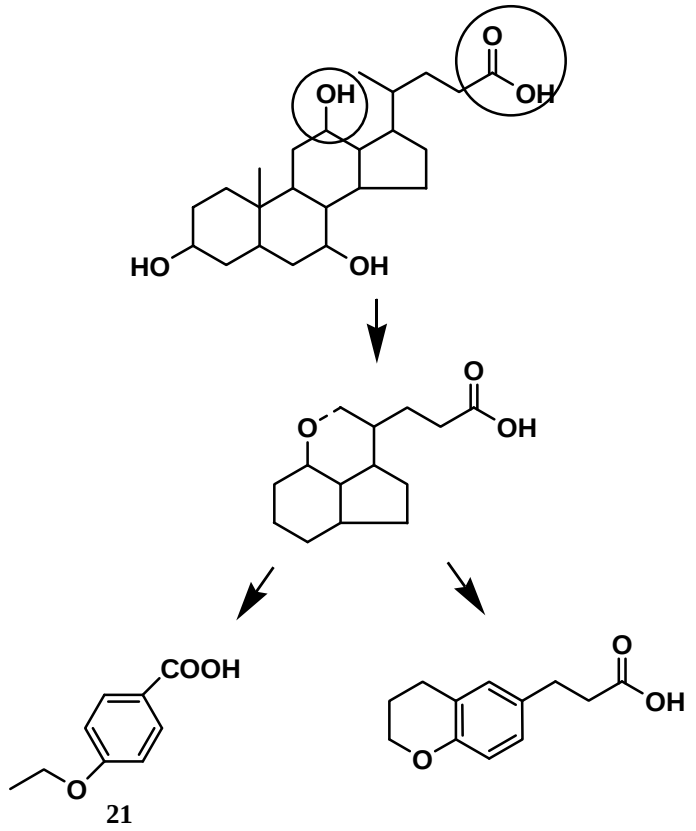

Figure 4. Schematic representation of the overall approach in conducting Search C. Cholic acid was visually conceived to be similar to a three ring structure with a carboxylate, from which nine compounds were identified and tested. Two of the nine compounds are shown. Compound **21** was shown to be an inhibitor, along with two other compounds from search C (Table 3).

5.2.3 Cell culture

Compounds were evaluated for their interaction with ASBT using stably transfected ASBT-MDCK cells. The cells were cultured as previously described (49). Briefly, cells were grown at 37 ºC, 90% relative humidity, 5% CO_2 atmosphere, and fed every two days. Culture media consisted of DMEM supplemented with 10% FBS, 50 units/mL penicillin, and 50 μg/mL streptomycin. Geneticin was added at 1 mg/mL to maintain selection pressure. Cells were passaged after four days or after reaching 90% confluency.

5.2.4 Inhibition studies

Compounds were screened for ASBT binding via a taurocholate uptake inhibition study, as previously described (52). Twenty-five compounds from search A, 29 compounds from search B, and nine compounds from search C were screened. Screening was performed in stably-transfected ASBT-MDCK cells grown on 12-well plates (3.8 cm^2, Corning, Corning, NY) under conditions described above. Briefly, cells were seeded at a density of 1.5 million/well and induced with 10 mM sodium butyrate 12–15 h prior to study on day 4. Cells were washed three times with Hank's balanced salt solution (HBSS) prior to assay. Studies were conducted at 37 °C, 50 rpm for 10 min in an orbital shaker. Uptake buffer consisted of HBSS, which contained 137 mM NaCl (pH 6.8) and was supplemented with 1 g/L of glucose. Cells were exposed to donor solutions containing substrate (2.5 μM TCA with 0.5 μCi/ml [^{3}H]-TCA) and inhibitor (500 μM or 1000 μM for screening and 0 μm to 500 μM or 1000 μM to determine Ki) in triplicate for 10 min. These concentrations of 500 to 1000 μM were employed in these screening studies in order to identify even weak inhibitors. After this time, donor solution was removed and cells were washed three times with chilled sodium-free buffer (where NaCl was replaced by 137 mM tetraethylammonium chloride). Cells were lysed using 250 μL of 1N NaOH and allowed to stand for at least 2 h. Cell lysate was then neutralized with 250 μL of 1N HCl. Lysate was counted for associated radioactivity (i.e. [^{3}H]-TCA) using an LS6500 liquid scintillation counter (Beckmann Instruments, Inc., Fullerton, CA) in Econosafe scintillation cocktail (52).

Nine compounds with diverse chemical structures from search A and the two most potent inhibitors from search B were further evaluated to measure inhibition coefficient Ki.

Inhibition data was regressed using a modified Michaelis-Menten equation (eqn 1) to determine Ki as previously described, including parallel studies on each occasion to estimate Jmax and Pp for taurocholic acid (52).

$$J = \frac{P_{ABL} \cdot \left(\frac{J_{\max}}{K_t\left(1+\frac{I}{K_i}\right)+S} + P_p \right)}{P_{ABL} + \frac{J_{\max}}{K_t\left(1+\frac{I}{K_i}\right)+S} + P_p} \cdot S \qquad \text{eqn 1}$$

where I is inhibitor concentration, Ki is inhibition constant, J is taurocholate flux, Jmax and Kt are the Michaelis-Menten constants, S is taurocholate concentration (i.e. 2.5 μM), Pp is passive taurocholate permeability, and P_{ABL} is aqueous boundary layer permeability. Kt was set to 5.03 μM, as obtained from pooled kinetic analysis of historical taurocholate uptake studies. P_{ABL} was set to 1.5×10^{-4} cm/s (86). Pp was estimated from taurocholate (TCA) uptake studies in absence of sodium. Ki was estimated by using nonlinear regression fitting performed by WinNonlin Professional. Potent inhibitors were denoted to be compounds with Ki less than 100 μM, modestly potent inhibitors as compounds with Ki between 100 and 1000 μM, and non-inhibitors with Ki above 1000 μM.

5.2.5 Uptake studies

Inhibitors were further assessed in terms of being translocated by ASBT. As ASBT is a sodium dependent transporter, studies were performed with and without sodium to assess for active transport by ASBT (45, 54). The procedure was the same as described above for inhibition studies, except donor solution contained the study compound at different

concentrations in buffer, with and without sodium. Uptake was carried out for 10 min. After 10 min, cells were washed three times with chilled sodium-free buffer. At the end of uptake experiment cells were lysed by adding 0.3 mL acetonitrile. Extraction of conjugate from cell lysate was performed by adding 1 mL of 50:50 acetonitrile:water spiked with 500 nM internal standard; plates were then sealed with parafilm. After 30 min, extract was placed into silanized vials and stored in -80 °C until analyzed by LC/MS/MS (72). For each compound, uptake data was fitted to the modified Michaelis-Menten equation (eqn 2) to yield estimates for Kt and Jmax and Pp (86).

$$J = \frac{P_{ABL} \cdot \left(\frac{J_{\max}}{K_t + S} + P_p \right)}{P_{ABL} + \frac{J_{\max}}{K_t + S} + P_p} \cdot S \qquad \text{eqn 2}$$

$$J = \frac{P_{ABL} P_p S}{P_{ABL} + P_p} \qquad \text{eqn 3}$$

Jmax of each compound was normalized against the observed taurocholate Jmax on that same occasion to yield normalized Jmax for the compound, denoted normJmax. normJmax accommodates variable ASBT protein expression across occasions. Taurocholate Jmax was measured in parallel to compound Jmax (86). Kt was estimated by using nonlinear regression fitting performed by WinNonlin Professional.

5.2.6 Statistical analysis

Experiments were performed using n = 3. Error bars denote ±SEM. T-test was used to assess for inhibition versus control ($p < 0.05$).

5.2.7 Analytical methods

Compound uptake was quantified by LC/MS/MS on a Thermo Finnigan Surveyor HPLC system, equipped with a Thermo Finnigan Surveyor autosampler and a Thermo TSQ quantum mass spectrometer (Thermo Fisher Scientific Inc., Waltham, MA). The column used was a Phenomenex Luna C8 (50 × 2.0 mm, 5µ; Phenomenex, Torrance, CA, USA). The mobile phase was water and acetonitrile for compound **1** and water and methanol for compound **11**. Formic acid (0.1%) was used as modifier in each mobile phase. Regarding mobile phase, the initial 65% organic phase was linearly increased to 95% from 0.2 min to 2 min, maintained at 95% organic for 1 min, and then reduced back to 65% over next 2 min (i.e. 5 min run time). Detection was achieved under positive ion electrospray tandem mass spectrometry in MRM mode.

5.3 RESULTS AND DISCUSSION

Overall, searches A, B, and C yielded 23 new ASBT inhibitors, where inhibitors were non-steroidal and possessed a molecular weight less than 375 daltons. As discussed below, compounds **1** and **11** were substrates and hence represent potential pro-moieties to target ASBT.

5.3.1 Search A

Search A suggested 471 compounds, about 100 from each query compound **I** and **II** (i.e. glycolithocholic acid and S0382, respectively) and from each fingerprint approach (i.e. BIT_MACCS and MP_MFP). Twenty-five compounds were selected for in vitro evaluation (Fig. 1), since they had a molecular weight less than 375, calculated logP less

than 3.5 and could be commercially obtained. Nine compounds were inhibitors. Table 1 lists their Ki values. Among the active compounds, compounds **1-8** were obtained from glycolithocholic acid, while compound **9** was obtained from S0382. Figure C1 in Appendix C shows the structures of the eight compounds obtained from glycolithocholate that were not inhibitors. Figure C2 in Appendix C shows the structures of the eight compounds obtained from S0382 that were not inhibitors. Figure 5 shows the inhibition profile of compound **1**, where Ki = 29.6 μM.

Table 1. Ki values of compounds 1-9 from search A.
Compounds **1-8** were obtained from glycolithocholic acid and compound **9** was obtained from S0382. Of the 471 non-steroidal compounds suggested from search A, 25 compounds were tested. The structures of the nine compounds that showed activity are shown. Compound **1** was also a substrate, while the other inhibitors were not.

No	Structure	MW	logP	Ki (±SEM) [μM]
1	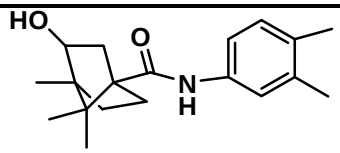	301.4	3.42	29.6±4.0
2	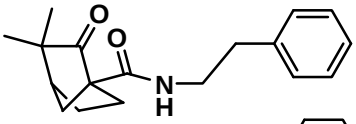	285.3	3.01	243±27
3	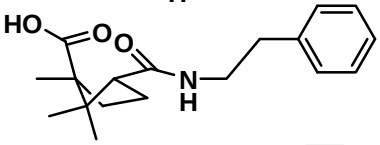	303.4	2.78	336±61
4	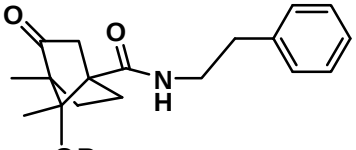	299.4	2.40	571±49
5	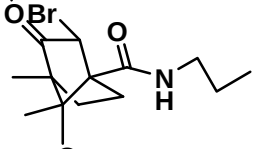	316.2	2.28	685±87
6	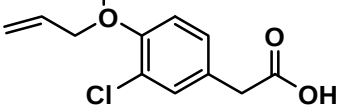	226.6	2.92	698 ±77

7	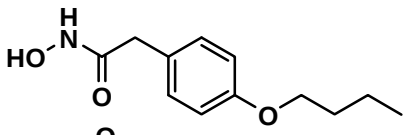	223.6	2.35	709±85
8	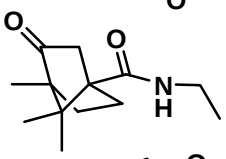	223.3	0.87	1230±200
9	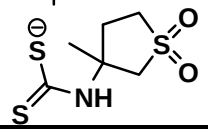	224.3	0.33	129±15

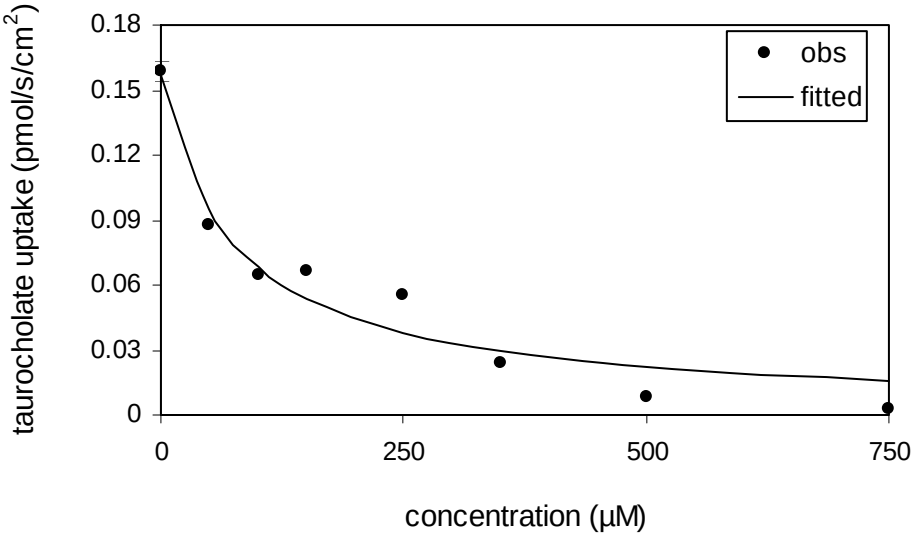

Figure 5. Inhibition profile of compound 1.

Compound **1** was the only inhibitor with Ki < 50 μM, such that only compound **1** was evaluated as a potential substrate. Figure 6 shows its uptake profile in the presence and absence of sodium. Compound **1** was a modest substrate, with Kt = 181(±48) μM, Jmax = 0.000148 nmol/s/cm^2, normalized Jmax = 0.186, and Pp = 0.301(±0.008) x 10^{-6} cm/s. Jmax was about one-fifth that of taurocholate. Also, Kt was less potent than the Kt of taurocholate.

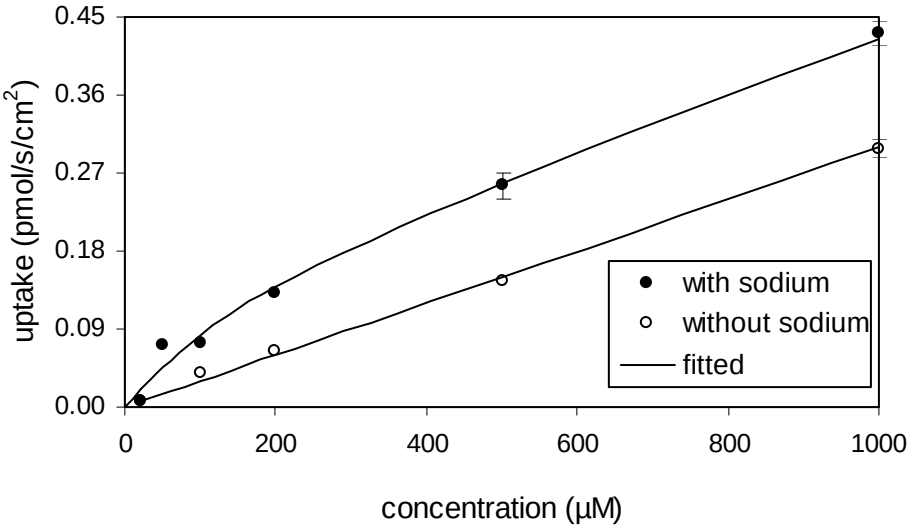

Figure 6. Concentration-dependent uptake profile of compound 1.
Uptake was greater in the presence of sodium (●) than in the absence of sodium (○), indicating compound **1** to be an ASBT substrate.

5.3.2 Search B

From Search B, about 2400 non-steroidal compounds were suggested. Twenty-nine compounds were tested (Fig. 1). Eleven compounds were inhibitors. Table 2 lists their percent uptake of taurocholate, in the presence of the compound, compared to taurocholate uptake in the absence of the compound. Compound **10** and **11** reduced taurocholate uptake to 8.02% and 26.4% of control, respectively. Other active compounds reduced uptake by less than 50%, and were not evaluated further. Figure C3 in Appendix C shows the structures of the 18 compounds that were not inhibitors.

Table 2. Structures of the 11 compounds that were found to be inhibitors from search B. Cis-inhibition studies of taurocholate (2.5 μM with spiked [^{3}H] of taurocholate) uptake were carried out in presence of 500 μM of the compound. Results are expressed in terms of percent uptake of of taurocholate (TCA), compared to of taurocholate uptake in the absence of the compound. Search B suggested 2474 non-steroidal compounds. Of the 29 compounds tested, these 11 were inhibitors (i.e. at least 20% decrease in 2.5μM taurocholate uptake by 500μM of test compound), while the other 18 were not. Compound **11** was also a substrate, while compound **10** was not a substrate.

No	Structure	MW	logP	Percent TCA uptake compared to control
10	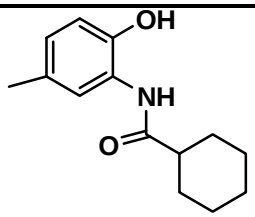	233.3	2.899	8.02±0.42
11	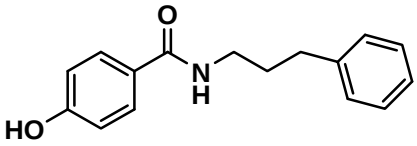	255.3	3.215	26.4±2.1
12	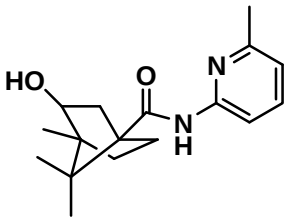	288.3	2.225	60.3±2.6
13	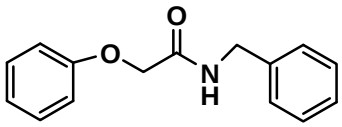	241.2	2.777	64.2±7.0
14	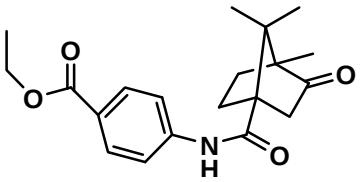	343.4	2.464	70.3±2.0
15	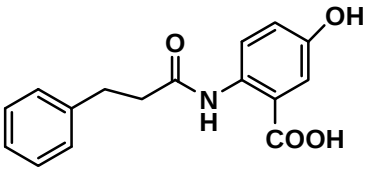	285.3	2.439	70.4±1.1

16	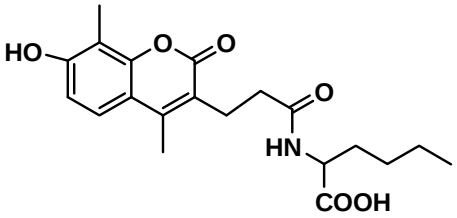	375.4	3.021	70.8±2.1
17	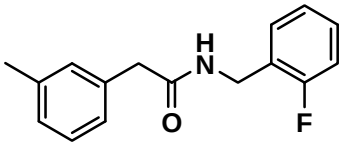	257.3	3.567	72.7±7.5
18	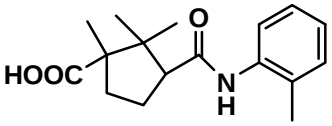	319.3	2.267	74.6±6.5
19	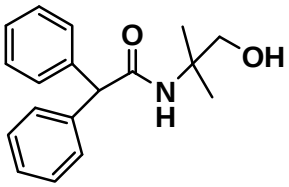	283.3	3.11	75.1±6.1
20	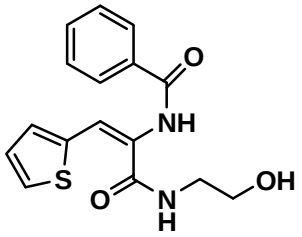	316.3	1.717	76.6±3.8

Ki determination and substrate evaluation were performed for **10** and **11**. Ki of **10** and **11** were 31.0(±4.6) μM and 199(±20) μM, respectively. Figure 7 shows the inhibition profile of compound **11**. Native bile acids exhibit very high affinity (Ki range from 1 to 25 μM) for ASBT (50). Ki of **10** and **11** reflect potent inhibition and modestly potent inhibition, respectively.

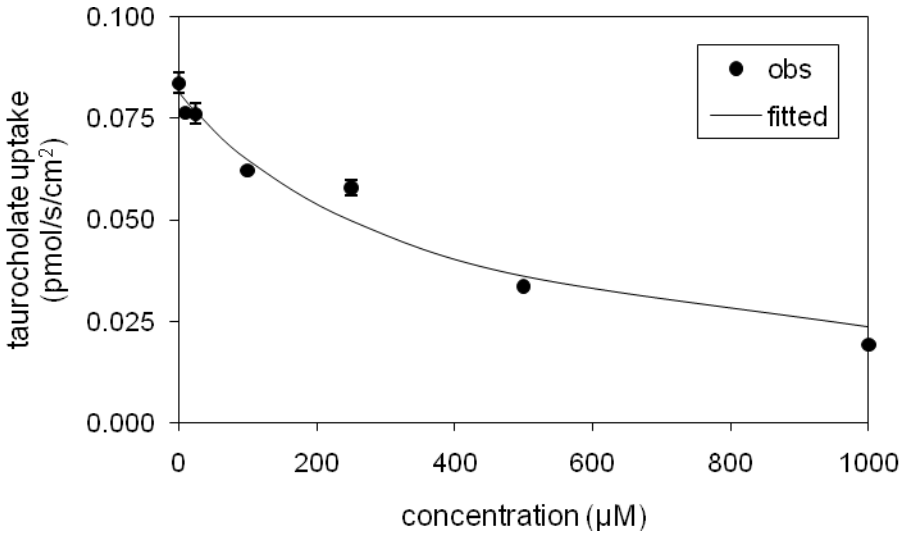

Figure 7. Inhibition profile of compound 11.

Compound **11** was a substrate, while compound **10** was not a substrate. Figure 8 shows uptake profile for compound **11** in the presence and absence of sodium. Compound **11** was a substrate, with Kt = 90.6(±20.3) µM, Jmax = 0.000457 nmol/s/cm^2, normalized Jmax = 1.089, and Pp = 3.66(±0.08) x 10^{-6} cm/s. Jmax was the same as that of taurocholate. Kt was less potent than the Kt of taurocholate.

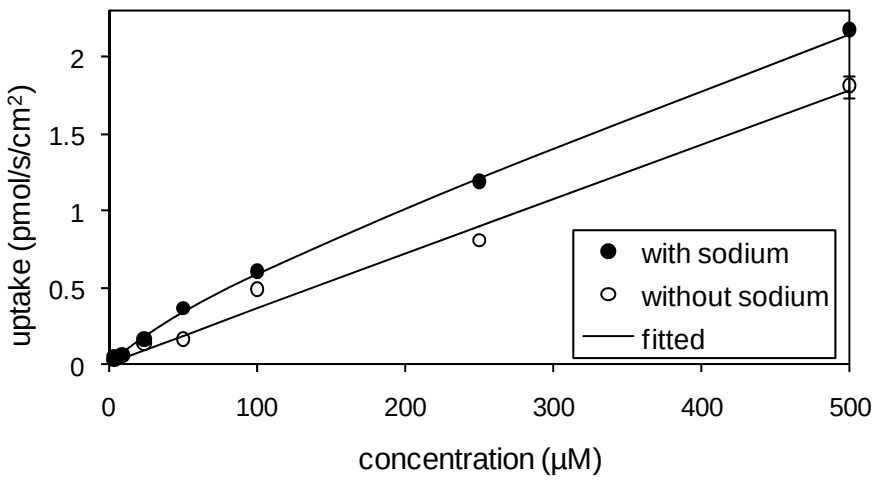

Figure 8. Concentration-dependent uptake profile of compound 11.
Uptake was marginally greater in the presence of sodium (●) than in the absence of sodium (○), indicating compound **11** to be a weak ASBT substrate.

5.3.3 Search C

Among nine compounds identified and tested, three compounds showed inhibition (Table 3). Compounds **21**, **22**, and **23** inhibited taurocholate to a modest extent. Interestingly, compound **21** reduced taurocholate uptake about 50%, even though compound **21** has a molecular weight of only 166. However, this modest level of inhibition potency did not afford compound **21** to be evaluated for uptake.

Table 3. Screening result from search C.
Cis-inhibition studies of TCA (2.5 μM with spiked [^{3}H] TCA) uptake were carried out in presence of 1000 μM of the compound. Results are expressed in terms of percent uptake of taurocholate (TCA), compared to TCA uptake in the absence of the compound. These three compounds were inhibitors.

No	Structure	MW	logP	Percent TCA uptake compared to control
21	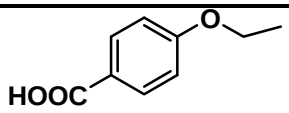	166.1	1.80	52.3±5.8
22	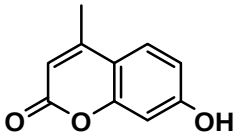	176.1	1.61	60.3±4.9
23	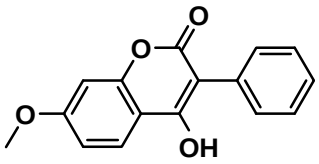	268.1	2.58	79.7±3.9

5.3.4 Overall findings

The objective was to identify non-steroidal, small molecules that could potentially serve as pro-moieties in the design of prodrugs that target ASBT. Two sequential searches were conducted and involved molecular fingerprints. Each search employed similarity to query compounds based on structure (i.e. BIT_MACCS), as well a parallel search based upon physiochemical characteristics i.e. MP_MFP). Searches were conducted for each query compound, independent of other query compounds, in order to afford a broad search. Additionally, a third, traditional medicinal chemistry search, using pattern recognition, was used. Searches excluded bile acids and steroidal compounds.

Sixty-three compounds were selected based on their molecular weight, logP (≤ 3.5), availability, and structural diversity, and evaluated for their interaction with ASBT. Twenty-three were found to be novel ASBT inhibitors. Each inhibitor possessed a molecular weight less than 375; log P ranged from 0.33 to 3.5. In the context of designing a pro-moiety that allows for ASBT targeting, a low molecular weight is desirable and would favor a lower prodrug dose. A logP less than 3.5 was considered desirable, as to avoid aqueous solubility limitations. Among the 23 inhibitors, three were selected for ASBT uptake studies, and two compounds (compound **1** and **11)** were substrates.

In search A, nine of the 25 tested compounds showed interaction with ASBT, but only compound **1** indicated strong interaction with ASBT (Ki = 29.6±4.0 μM). Compound **1** was demonstrated to be a modest ASBT substrate with Kt = 181±48 μM. Reported here, compound **1** is the first known non-steroidal substrate of ASBT and was used as a basis for subsequent search B.

In search B, query compounds were designed based on two rings joined by an amide bond (Fig. 3). Since the objective aims toward the identification of a pro-moiety for uptake by ASBT, it is desirable for ring structure to reflect small molecules with lower toxicity. Hence, search B query compounds were designed where ring A was replaced with phenylalanine-, tyrosine-, and proline-like structures; ring B was replaced with dimethylphenylalanine- and phenylalanine-like structures. Using various combinations, the two rings were joined to yield compounds **IV-VII** as query compounds (Fig 3 panel B). Since models favor a single negative charge for translocation across ASBT, query compounds also included compounds with single negative charge (**VII-IX** in Fig 3 panel B). Compound **1** and compound **X** (i.e. compound **1** with single negative charge; Fig 3 panel B) were also query compounds in search B. Additionally, the sulfone group in ASBT inhibitor S0382 was replaced with acetal group to yield to serve as query compound (i.e. compound **XI**). Also, negative charge was introduced in compound **XI** to yield query compound **XII**. Search B resulted in 11 inhibitors and one substrate (compound **11**).

This is the first report of non-steroidal substrates of ASBT. Interestingly, compound **1** and **11** lack a negative charge, which generally is considered as necessary for ASBT translocation (29, 46, 48). Compound **1** was obtained by a physiochemical-based search of glycolithocholate (search A) using the MP-MFP fingerprints. Search B was partially based on compound **1** and was successful in identifying compounds that showed interaction with ASBT. Of the 29 compounds tested in search B, 11 showed activity and among these 11 compounds, six compounds were similar to compound **1** (compounds **10**,

11, **12**, **14**, **15** and **18**). Additionally, compound **11** was also a substrate thus emphasizing the success of this new scaffold.

In addition to prodrug design, these findings have implications for the design of ASBT inhibitors. ASBT has been exploited for cholesterol lowering therapies. Bile acids are catabolic products of cholesterol metabolism. ASBT therefore plays a critical role in cholesterol homeostasis. Inhibitors of ASBT-mediated bile acid absorption is an approach towards a new class of cholesterol lowering drugs, especially when treatment targets are not achieved with statins, the currently most effective therapy (128).

Studies will be continued to improve on compound **1** and **11** to identify substrates with higher efficiency for the transport by ASBT, high aqueous solubility, and with suitable functional groups to conjugate to a drug molecule. Of course, one limitation of the present study is that the drug portion of a prodrug can impact interaction with the transporter. Never the less, this approach has promise to identify more substrates for ASBT. Results here indicate, for the first time, that the four-member bile acid steroid backbone is not required for ASBT translocation.

CHAPTER 6

CONCLUSIONS

6.1 CONCLUSIONS

Bile acid transporters apical sodium dependent bile acid transporter (ASBT) and sodium-taurocholate cotransporting polypeptide (NTCP), with their high capacity and efficiency, have potential as prodrug targets (35, 40, 80). However, the absence of crystal structures and lack of understandings of structural requirements of these transporters has impeded the design of prodrugs. The long term aim here was to understand the substrate and inhibition requirements of the two bile acid transporters ASBT and NTCP to identify the structure activity relationships to rationally design prodrugs.

The first step is identifying interaction with a transporter is inhibition study. Identifying correct type of inhibition is important to understand interaction with a transporter. Therefore, chapter two described the studies that were performed to identify methods which can correctly determine type of inhibition. Three objectives were pursued that concerned the ability to correctly identify the type of inhibition. The objectives were to compare the abilities of the competitive, noncompetitive, and uncompetitive inhibition models to best fit simulated competitive and noncompetitive data, where data reflected conventional inhibition data, Dixon-type data and nonconventional data. These objectives were pursued by simulating uptake values for each competitive and noncompetitive inhibition model under each of the conditions. The simulated data were subjected to nonlinear model fitting and the best fitting model was identified based on AIC criteria. Analysis examined the conditions and extent to which nonlinear regression results can be relied upon. For conventional inhibition data, nonlinear regression performed poorly for both the competitive and noncompetitive inhibition models. For Dixon-type data,

nonlinear regression yielded moderately better results. Interestingly, nonconventional inhibition data performed well, with higher ratio of I/Ki providing better results. Nonconventional inhibition data merits further consideration.

ASBT and NTCP are potential prodrug targets, but understanding of structural requirements for these transporters is incomplete. The objective of the study described in chapter three was to evaluate the effect of C-3 and C-7 substitution on bile acid interaction with these bile acid transporters. Nineteen bile acid analogues were tested against ASBT and NTCP for binding, as well as translocation. Results indicated that ASBT and NTCP accommodated a wide range of substituents for binding, but all major C-7 modifications resulted in analogues that did not demonstrate active uptake by either ASBT or NTCP. A C-3 modification that was not tolerated at C-7 still afforded translocation via ASBT and NTCP, confirming the relative unacceptability of C-7 modification. Both ASBT and NTCP demonstrated a generally similar binding potency. Results suggest that drug conjugation to the C-3 hydroxyl group, rather than C-7, has potential to lead to a successful prodrug targeting ASBT and NTCP.

Results from chapter three indicated that conjugation of an aromatic ring at the C-7 position of chenodeoxycholic acid or ursodeoxycholic acid resulted in molecules with low passive permeability and no translocation across ASBT. Based on this a prodrug was designed that conjugated 5-aminosalicylic acid (5-ASA), first-line therapy for treatment of ulcerative colitis, to glycoursodeoxycholic acid. In vitro studies were performed to test suitability for colon targeting. The results are discussed in chapter four. 5-ASA was conjugated to the bile acid via a linker and an azo bond. This allowed the drug to be specifically released in colon by action of azoreductase enzyme. This 5-ASA prodrug

was successfully synthesized by conjugating 5-ASA to the 3- and 7- positions of glycoursodeoxycholic acid. Prodrug demonstrated low permeability and was not a substrate of ASBT. Also in vitro studies showed selective release 5-ASA in the colon. In vitro results support subsequent in vivo studies to assess potential colon targeting of 5-ASA.

Although bile acids are endogenous molecules and are considered to be safe, there are several reasons that motivate use of a non-steroidal promoiety to target ASBT. These include high molecular weight and limited aqueous solubility of bile acids. Also bile acids are versatile signaling molecules; chronic administration of bile acids can impact these signaling pathways. Chapter five describes the similarity search performed to identify non-steroidal bile acid substrate. This successfully identified two small molecules that demonstrated active uptake via ASBT. Both these molecules lack the steroidal backbone and the negative charge that was considered essential. Results indicated, for the first time, that the four-member bile acid steroid backbone is not required for ASBT translocation.

Further studies that can identify more chemistry space and better substrates will be helpful. Design of a prodrug by conjugation of a drug to such a substrate can further highlight success of the strategy. Also identification of more substrates will enable design of a substrate based model. Such a substrate based model can explain critical features in the active site and aid in understanding the structural requirements of this transporter.

In conclusion, bile acid transporters ASBT and NTCP are prodrug targets to increase absorption of drug candidates that have insufficient oral absorption and for liver targeting, respectively. The objective was to identify structural requirements for these

transporters. The studies performed identified that conjugation of drug candidates at C-3 hydroxyl group on bile acids can lead to a successful prodrug for absorption via these transporters. Meanwhile, conjugation of drug candidates at C-7 position via a suitable linker can result in lowly permeable prodrug with potential to deliver the drug in colon as demonstrated by 5-ASA prodrug. Identification of non-steroidal ASBT substrates can lead to prodrugs with such pro-moieties to target ASBT. Overall, this work may lead to successful design of prodrugs to target ASBT and NTCP.

APPENDIX A

Supplementary information for Chapter 2.

Figure A2. **Inhibition profiles from error-free nonconventional inhibition data for the noncompetitive and uncompetitive inhibition model**.
I/Ki = 10 and S = 1 to 50 μM. This plot is the same as Fig 8 panel C, but limited to 0-50 μM substrate concentration. The noncompetitive and uncompetitive models differ at these lower substrate concentrations, but overlap at the higher substrate concentrations. This difference is not observed at I/Ki = 1, thus higher ratio of I/Ki is required to distinguish the noncompetitive model from the competitive and uncompetitive model.

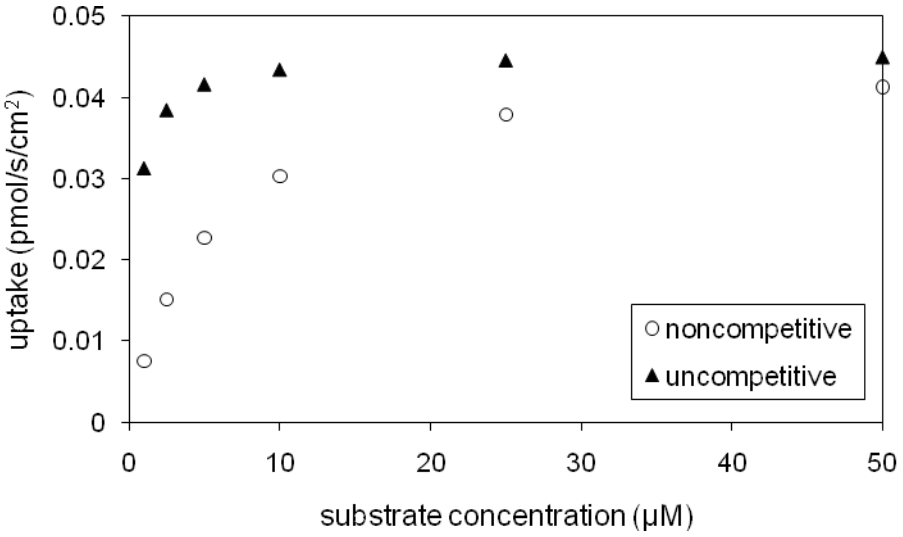

APPENDIX B

Supplementary information for chapter 3.

A

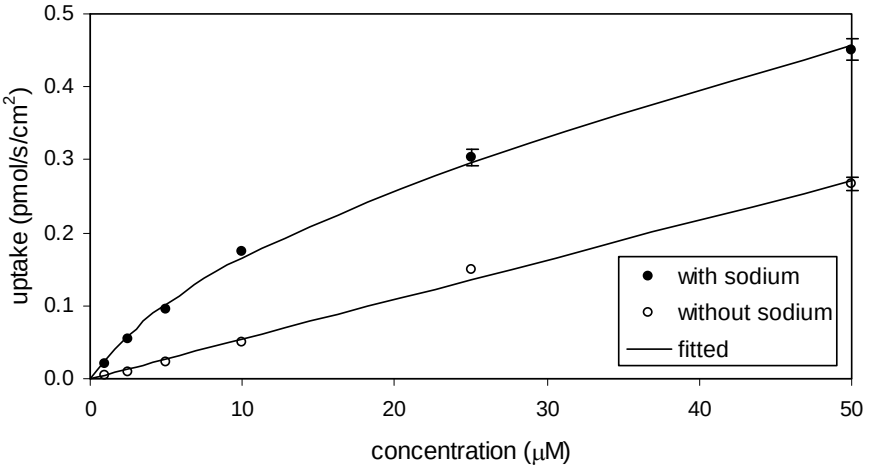

B

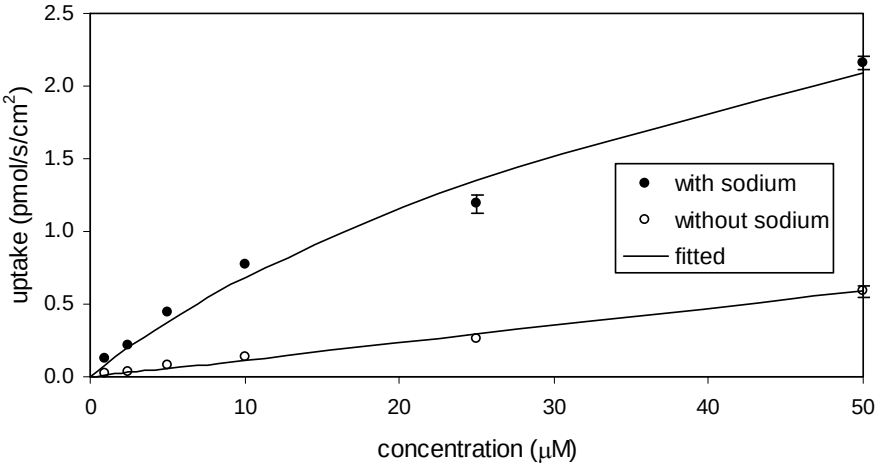

Figure B1. **Concentration-dependent uptake profile for 7-oxo glycocholanic acid [i.e. compound 12] into (A) ASBT-MDCK monolayers and (B) NTCP-HEK monolayers**. For each transporter, uptake was greater in the presence of sodium (●) than in the absence (○) of sodium, indicating this compound to be both ASBT and NTCP substrate.

APPENDIX C

Supplementary information for Chapter 5.

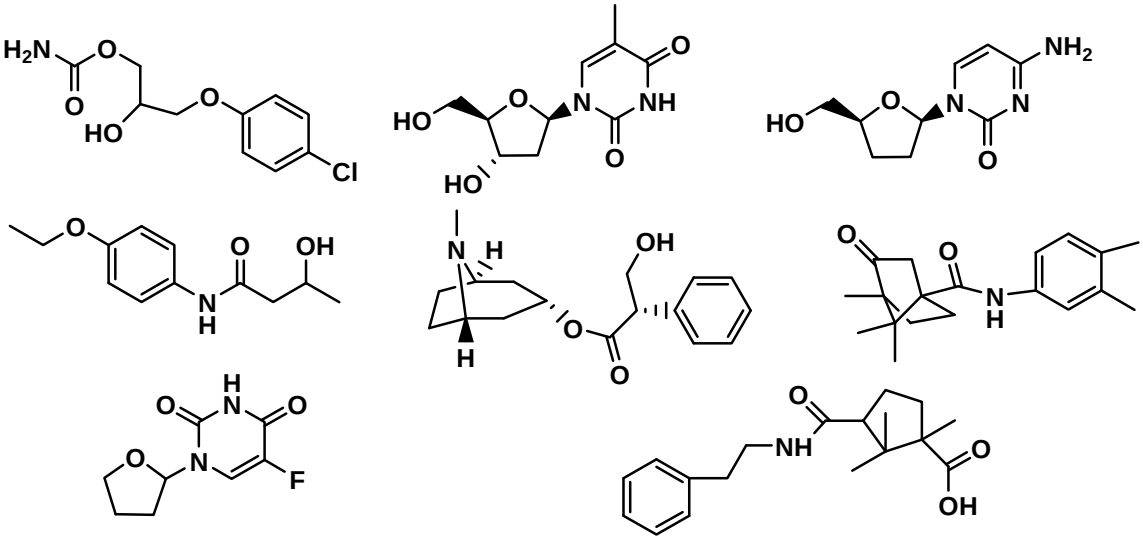

Figure C1. **Structures of the eight compounds obtained from glycolithocholic acid (I) that were not inhibitors from search A**.

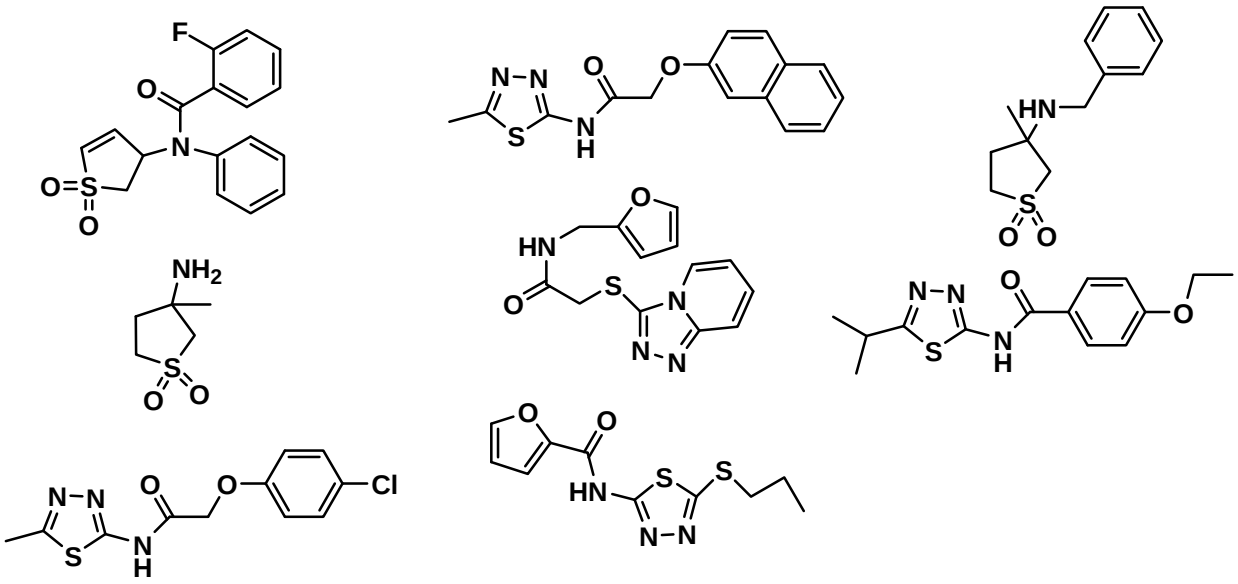

Figure C2. Structures of the eight compounds obtained from S0382 (II) that were not inhibitors from search A.

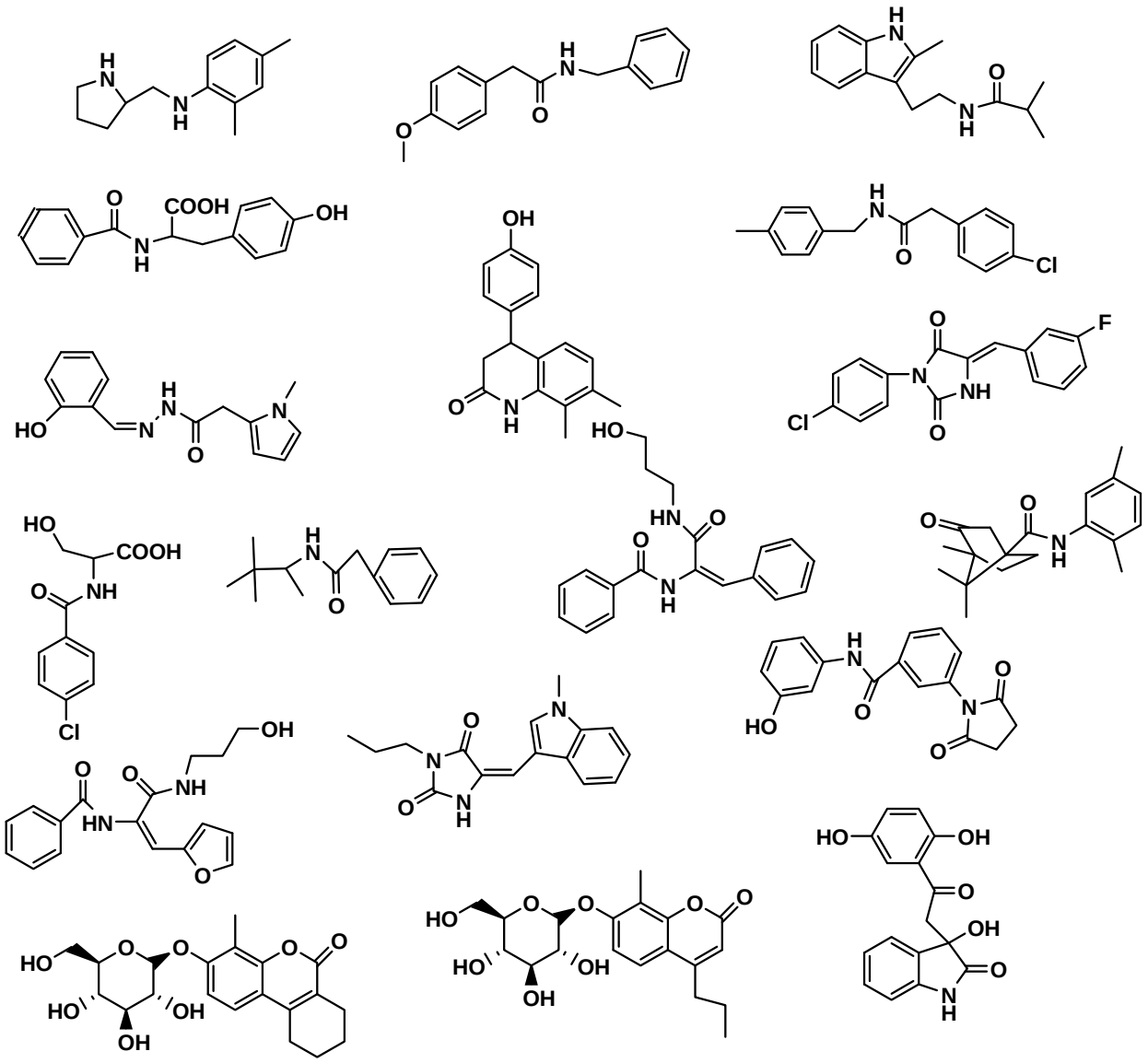

Figure C3. Structures of the 18 compounds that were not inhibitors from search B.

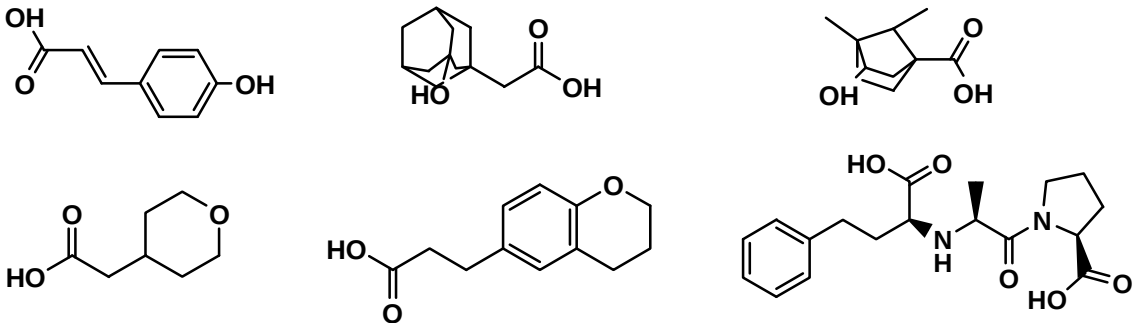

Figure C4. Structures of the six compounds that were not inhibitors from search C.

Table C1. List of companies that contributed to the database used for similarity search.

Company-Name/Country	CODEN	IDNUMBER-example
Ambinter-SARL/France	Ambinter	612 (48110, or ASKVIRT/18704)
ASDI,Inc/U.S.A	Asdi	206_3023146
AsInex,Ltd/Russia	Asinex	BAS 0349284
Bionet,Ltd/England	Bionet	10A-002
ChemBridge-Corp.	Chembridge	553395
ChemDiv,Inc./U.S.A	Chemdiv	0278-0100
ComGenex,Ltd/U.S.A	Comgenex	0000450
G&J/U.S.A	G_j	JS-1464
KEGG compounds/Japan	KeggC	C14833
Life Chemicals Inc.	lifechem	F0007-0721
Maybridge-Chemical-Company/England	Maybridge	XBX 00214
Menai/England	Menai	H86 LIST 104
MicroSource-Discovery-Systems,Inc./U.S.A	Mdsi	1501043
Molecular-Design-and-Discovery-Inc./Canada	Mdd	APX000035319
Nanoscale-Combinatorial-Synthesis-Inc-/U.S.A	Nanosyn	NS2812
NCI (National Cancer Institute)	Nci	4376
Otava/Ukrain	Otava	0100380824
Scut	Scut	404
Sherk/England	Sherk	6289
Sigma-Aldrich-Library/U.S.A	Sigma	R305170
SPECS&BioSpecs/Netherlands	Specs_s	AF-399/42874488
SPECS&BioSpecs/Netherlands	Specs_n	AF-399/42874488
Tripos,Inc./U.S.A	Tripos	1449-00052
Timtec,Inc./U.S.A	Timtec	ST040804

Table C2. Chemical names of the hit compounds 1-23.

1. Bicyclo[2.2.1]heptane-1-carboxamide, N-(3,4-dimethylphenyl)-3-hydroxy-4,7,7-trimethyl-

2. Bicyclo[2.2.1]heptane-1-carboxamide, 3,3-dimethyl-2-oxo-N-(2-phenylethyl)-

3. Cyclopentanecarboxylic acid, 1,2,2-trimethyl-3-[[(2-phenylethyl)amino]carbonyl]-

4. Bicyclo[2.2.1]heptane-1-carboxamide, 4,7,7-trimethyl-3-oxo-N-(2-phenylethyl)-

5. Bicyclo[2.2.1]heptane-1-carboxamide, 2-bromo-4,7,7-trimethyl-3-oxo-N-propyl-

6. Benzeneacetic acid, 3-chloro-4-(2-propen-1-yloxy)-

7. Benzeneacetamide, 4-butoxy-N-hydroxy-

8. Bicyclo[2.2.1]heptane-1-carboxamide, N-ethyl-4,7,7-trimethyl-3-oxo-

9. (3-methyl-1,1-dioxidotetrahydrothiophen-3-yl)carbamodithioate

10. Cyclohexanecarboxamide, N-(2-hydroxy-5-methylphenyl)-

11. Benzamide, 4-hydroxy-N-(3-phenylpropyl)-

12. Bicyclo[2.2.1]heptane-1-carboxamide, 3-hydroxy-4,7,7-trimethyl-N-(6-methyl-2-pyridinyl)-

13. Acetamide, 2-phenoxy-N-(phenylmethyl)-

14. Benzoic acid, 4-[[(4,7,7-trimethyl-3-oxobicyclo[2.2.1]hept-1-yl)carbonyl]amino]-, ethyl ester

15. Benzoic acid, 5-hydroxy-2-[(1-oxo-3-phenylpropyl)amino]-

16. 2-(3-(7-hydroxy-4,8-dimethyl-2-oxo-2H-chromen-3-yl)propanamido)hexanoic acid
CAS Registry Number: 1008697-34-4

17. Benzeneacetamide, N-[(2-fluorophenyl)methyl]-3-methyl-

18. Cyclopentanecarboxylic acid, 1,2,2-trimethyl-3-[[(2-methylphenyl)amino]carbonyl]-

19. Benzeneacetamide, N-(2-hydroxy-1,1-dimethylethyl)-α-phenyl-

20. Benzamide, N-[1-[[(2-hydroxyethyl)amino]carbonyl]-2-(2-thienyl)ethenyl]-

21. Benzoic acid, 4-ethoxy-

22. 2H-1-Benzopyran-2-one, 7-hydroxy-4-methyl-

23. 2H-1-Benzopyran-2-one, 4-hydroxy-7-methoxy-3-phenyl-

References

1. Neuvonen, P.J.; Niemi, M.; Backman, J.T. Drug interactions with lipid-lowering drugs: mechanisms and clinical relevance. *Clin. Pharmacol. Ther.* **2006,** *80,* 565-581.

2. Simonson, S.G.; Raza, A.; Martin, P.D.; Mitchell, P.D.; Jarcho, J.A.; Brown, C.D.; Windass, A.S.; Schneck, D.W. Rosuvastatin pharmacokinetics in heart transplant recipients administered an antirejection regimen including cyclosporine. *Clin. Pharmacol. Ther.* **2004,** *76,* 167-177.

3. Zheng, H.X.; Huang, Y.; Frassetto, L.A.; Benet, L.Z. Elucidating rifampin's inducing and inhibiting effects on glyburide pharmacokinetics and blood glucose in healthy volunteers: unmasking the differential effects of enzyme induction and transporter inhibition for a drug and its primary metabolite. *Clin. Pharmacol. Ther.* **2009,** *85,* 78-85.

4. Ding, R.; Tayrouz, Y.; Riedel, K.D.; Burhenne, J.; Weiss, J.; Mikus, G.; Haefeli, W.E. Substantial pharmacokinetic interaction between digoxin and ritonavir in healthy volunteers. *Clin. Pharmacol. Ther.* **2004,** *76,* 73-84.

5. Sugano, K.; Kansy, M.; Artursson, P.; Avdeef, A.; Bendels, S.; Di, L.; Ecker, G.F.; Faller, B.; Fischer, H.; Gerebtzoff, G.; Lennernaes, H.; Senner, F. Coexistence of passive and carrier-mediated processes in drug transport. *Nat. Rev. Drug Discov.* **2010,** *9,* 597-614.

6. International Transporter Consortium; Giacomini, K.M.; Huang, S.M.; Tweedie, D.J.; Benet, L.Z.; Brouwer, K.L.; Chu, X.; Dahlin, A.; Evers, R.; Fischer, V.; Hillgren, K.M.; Hoffmaster, K.A.; Ishikawa, T.; Keppler, D.; Kim, R.B.; Lee, C.A.; Niemi, M.; Polli, J.W.; Sugiyama, Y.; Swaan, P.W.; Ware, J.A.; Wright, S.H.; Yee, S.W.; Zamek-Gliszczynski, M.J.; Zhang, L. Membrane transporters in drug development. *Nat. Rev. Drug Discov.* **2010,** *9,* 215-236.

7. Jones, P.M. and George, A.M. The ABC transporter structure and mechanism: perspectives on recent research. *Cell Mol. Life Sci.* **2004,** *61,* 682-699.

8. Rees, D.C.; Johnson, E.; Lewinson, O. ABC transporters: the power to change. *Nat. Rev. Mol. Cell Biol.* **2009,** *10,* 218-227.

9. Leslie, E.M.; Deeley, R.G.; Cole, S.P. Multidrug resistance proteins: role of P-glycoprotein, MRP1, MRP2, and BCRP (ABCG2) in tissue defense. *Toxicol. Appl. Pharmacol.* **2005,** *204,* 216-237.

10. Xia, C.Q.; Milton, M.N.; Gan, L.S. Evaluation of drug-transporter interactions using in vitro and in vivo models. *Curr. Drug Metab.* **2007,** *8,* 341-363.

11. Hagenbuch, B. and Gui, C. Xenobiotic transporters of the human organic anion transporting polypeptides (OATP) family. *Xenobiotica* **2008,** *38,* 778-801.

12. Zhang, E.Y.; Phelps, M.A.; Cheng, C.; Ekins, S.; Swaan, P.W. Modeling of active transport systems. *Adv. Drug Deliv. Rev.* **2002,** *54,* 329-354.

13. Chang, C. and Swaan, P.W. Computational approaches to modeling drug transporters. *Eur. J. Pharm. Sci.* **2006,** *27,* 411-424.

14. Chang, C.; Ekins, S.; Bahadduri, P.; Swaan, P.W. Pharmacophore-based discovery of ligands for drug transporters. *Adv. Drug Deliv. Rev.* **2006,** *58,* 1431-1450.

15. Diao, L.; Ekins, S.; Polli, J.E. Novel inhibitors of human organic cation/carnitine transporter (hOCTN2) via computational modeling and in vitro testing. *Pharm. Res.* **2009,** *26,* 1890-1900.

16. Zheng, X.; Ekins, S.; Raufman, J.P.; Polli, J.E. Computational Models for Drug Inhibition of the Human Apical Sodium-Dependent Bile Acid Transporter. *Mol. Pharm.* **2009,** *6,* 1591.

17. Cer, R.Z.; Mudunuri, U.; Stephens, R.; Lebeda, F.J. IC50-to-Ki: a web-based tool for converting IC50 to Ki values for inhibitors of enzyme activity and ligand binding. *Nucleic Acids Res.* **2009,** *37,* W441-5.

18. Lin, C.J.; Akarawut, W.; Smith, D.E. Competitive inhibition of glycylsarcosine transport by enalapril in rabbit renal brush border membrane vesicles: interaction of ACE inhibitors with high-affinity H+/peptide symporter. *Pharm. Res.* **1999,** *16,* 609-615.

19. Akarawut, W.; Lin, C.; Smith, D., E. Noncompetitive inhibition of glycylsarcosine transport by quinapril in rabbit renal brush border membrane vesicles: effect on high-affinity peptide transporter. *J Pharmacol. Exp. Ther.* **1998,** *287,* 684-690.

20. Segel, I., H. Enzymes, In *Biochemical Calculations,* Second ed.; Anonymous ; John Wiley & Sons: New York, 1976; pp. 208-318.

21. Deferme, S.; Annaert, P.; Augustijns, P. In Vitro Screening Models to Assess Intestinal Drug Absorption and Metabolism, In ***Drug Absorption Studies In Situ, In Vitro and In Silico Models,*** Ehrhardt, C. and Kim, K., Eds.; Springer: New York, NY, 2008; pp. 182-215.

22. Volpe, D.A. Variability in Caco-2 and MDCK cell-based intestinal permeability assays. *J. Pharm. Sci.* **2008,** *97,* 712-725.

23. Cundy, K.C.; Annamalai, T.; Bu, L.; De Vera, J.; Estrela, J.; Luo, W.; Shirsat, P.; Torneros, A.; Yao, F.; Zou, J.; Barrett, R.W.; Gallop, M.A. XP13512 [(+/-)-1-([(alpha-isobutanoyloxyethoxy)carbonyl] aminomethyl)-1-cyclohexane acetic acid], a novel gabapentin prodrug: II. Improved oral bioavailability, dose proportionality, and colonic absorption compared with gabapentin in rats and monkeys. *J. Pharmacol. Exp. Ther.* **2004,** *311,* 324-333.

24. Tsuda, M.; Terada, T.; Irie, M.; Katsura, T.; Niida, A.; Tomita, K.; Fujii, N.; Inui, K. Transport characteristics of a novel peptide transporter 1 substrate, antihypotensive drug midodrine, and its amino acid derivatives. *J. Pharmacol. Exp. Ther.* **2006,** *318,* 455-460.

25. Sugawara, M.; Huang, W.; Fei, Y.J.; Leibach, F.H.; Ganapathy, V.; Ganapathy, M.E. Transport of valganciclovir, a ganciclovir prodrug, via peptide transporters PEPT1 and PEPT2. *J. Pharm. Sci.* **2000,** *89,* 781-789.

26. Guo, A.; Hu, P.; Balimane, P.V.; Leibach, F.H.; Sinko, P.J. Interactions of a nonpeptidic drug, valacyclovir, with the human intestinal peptide transporter (hPEPT1) expressed in a mammalian cell line. *J. Pharmacol. Exp. Ther.* **1999,** *289,* 448-454.

27. Rautio, J.; Kumpulainen, H.; Heimbach, T.; Oliyai, R.; Oh, D.; Jarvinen, T.; Savolainen, J. Prodrugs: design and clinical applications. *Nat. Rev. Drug Discov.* **2008,** *7,* 255-270.

28. Kramer, W.; Wess, G.; Schubert, G.; Bickel, M.; Girbig, F.; Gutjahr, U.; Kowalewski, S.; Baringhaus, K.H.; Enhsen, A.; Glombik, H. Liver-specific drug targeting by coupling to bile acids. *J. Biol. Chem.* **1992,** *267,* 18598-18604.

29. Swaan, P.W.; Hillgren, K.M.; Szoka, F.C.,Jr; Oie, S. Enhanced transepithelial transport of peptides by conjugation to cholic acid. *Bioconjug. Chem.* **1997,** *8,* 520-525.

30. Lin, Y.S.; Tungpradit, R.; Sinchaikul, S.; An, F.M.; Liu, D.Z.; Phutrakul, S.; Chen, S.T. Targeting the delivery of glycan-based paclitaxel prodrugs to cancer cells via glucose transporters. *J. Med. Chem.* **2008,** *51,* 7428-7441.

31. Gynther, M.; Ropponen, J.; Laine, K.; Leppanen, J.; Haapakoski, P.; Peura, L.; Jarvinen, T.; Rautio, J. Glucose promoiety enables glucose transporter mediated brain uptake of ketoprofen and indomethacin prodrugs in rats. *J. Med. Chem.* **2009,** *52,* 3348-3353.

32. Diao, L. and Polli, J.E. Synthesis and in vitro characterization of drug conjugates of l-carnitine as potential prodrugs that target human Octn2. *J. Pharm. Sci.* **2011,**

33. Luo, S.; Wang, Z.; Patel, M.; Khurana, V.; Zhu, X.; Pal, D.; Mitra, A.K. Targeting SVCT for enhanced drug absorption: Synthesis and in vitro evaluation of a novel vitamin C conjugated prodrug of saquinavir. *Int. J. Pharm.* **2011,**

34. Yan, Z.; Sun, J.; Chang, Y.; Liu, Y.; Fu, Q.; Xu, Y.; Sun, Y.; Pu, X.; Zhang, Y.; Jing, Y.; Yin, S.; Zhu, M.; Wang, Y.; He, Z. Bifunctional peptidomimetic prodrugs of didanosine for improved intestinal permeability and enhanced acidic stability: synthesis, transepithelial transport, chemical stability and pharmacokinetics. *Mol. Pharm.* **2011,** *8,* 319-329.

35. Balakrishnan, A. and Polli, J.E. Apical sodium dependent bile acid transporter (ASBT, SLC10A2): a potential prodrug target. *Mol. Pharm.* **2006,** *3,* 223-230.

36. St-Pierre, M.V.; Kullak-Ublick, G.A.; Hagenbuch, B.; Meier, P.J. Transport of bile acids in hepatic and non-hepatic tissues. *J. Exp. Biol.* **2001,** *204,* 1673-1686.

37. Pols, T.W.; Noriega, L.G.; Nomura, M.; Auwerx, J.; Schoonjans, K. The bile acid membrane receptor TGR5 as an emerging target in metabolism and inflammation. *J. Hepatol.* **2011,** *54,* 1263-1272.

38. Thomas, C.; Pellicciari, R.; Pruzanski, M.; Auwerx, J.; Schoonjans, K. Targeting bile-acid signalling for metabolic diseases. *Nat. Rev. Drug Discov.* **2008,** *7,* 678-693.

39. Li, T.; Holmstrom, S.R.; Kir, S.; Umetani, M.; Schmidt, D.R.; Kliewer, S.A.; Mangelsdorf, D.J. The G Protein-Coupled Bile Acid Receptor, TGR5, Stimulates Gallbladder Filling. *Mol. Endocrinol.* **2011,** *25,* 1066-1071.

40. Alrefai, W.A. and Gill, R.K. Bile acid transporters: structure, function, regulation and pathophysiological implications. *Pharm. Res.* **2007,** *24,* 1803-1823.

41. Alpini, G.; Glaser, S.; Baiocchi, L.; Francis, H.; Xia, X.; Lesage, G. Secretin activation of the apical Na+-dependent bile acid transporter is associated with cholehepatic shunting in rats. *Hepatology* **2005,** *41,* 1037-1045.

42. Alpini, G.; Glaser, S.S.; Ueno, Y.; Rodgers, R.; Phinizy, J.L.; Francis, H.; Baiocchi, L.; Holcomb, L.A.; Caligiuri, A.; LeSage, G.D. Bile acid feeding induces cholangiocyte proliferation and secretion: evidence for bile acid-regulated ductal secretion. *Gastroenterology* **1999,** *116,* 179-186.

43. Chignard, N.; Mergey, M.; Veissiere, D.; Poupon, R.; Capeau, J.; Parc, R.; Paul, A.; Housset, C. Bile salts potentiate adenylyl cyclase activity and cAMP-regulated secretion in human gallbladder epithelium. *Am. J. Physiol. Gastrointest. Liver Physiol.* **2003,** *284,* G205-12.

44. Banerjee, A. and Swaan, P.W. Membrane topology of human ASBT (SLC10A2) determined by dual label epitope insertion scanning mutagenesis. New evidence for seven transmembrane domains. *Biochemistry* **2006,** *45,* 943-953.

45. Weinman, S.A.; Carruth, M.W.; Dawson, P.A. Bile acid uptake via the human apical sodium-bile acid cotransporter is electrogenic. *J. Biol. Chem.* **1998,** *273,* 34691-34695.

46. Lack, L. Properties and biological significance of the ileal bile salt transport system. *Environ. Health Perspect.* **1979,** *33,* 79-90.

47. Swaan, P.W.; Szoka, F.C.,Jr; Oie, S. Molecular modeling of the intestinal bile acid carrier: a comparative molecular field analysis study. *J. Comput. Aided Mol. Des.* **1997,** *11,* 581-588.

48. Baringhaus, K.H.; Matter, H.; Stengelin, S.; Kramer, W. Substrate specificity of the ileal and the hepatic Na(+)/bile acid cotransporters of the rabbit. II. A reliable 3D QSAR pharmacophore model for the ileal Na(+)/bile acid cotransporter. *J. Lipid Res.* **1999,** *40,* 2158-2168.

49. Balakrishnan, A.; Sussman, D.J.; Polli, J.E. Development of stably transfected monolayer overexpressing the human apical sodium-dependent bile acid transporter (hASBT). *Pharm. Res.* **2005,** *22,* 1269-1280.

50. Balakrishnan, A.; Wring, S.A.; Polli, J.E. Interaction of native bile acids with human apical sodium-dependent bile acid transporter (hASBT): influence of steroidal hydroxylation pattern and C-24 conjugation. *Pharm. Res.* **2006,** *23,* 1451-1459.

51. Balakrishnan, A.; Wring, S.A.; Coop, A.; Polli, J.E. Influence of charge and steric bulk in the C-24 region on the interaction of bile acids with human apical sodium-dependent bile acid transporter. *Mol. Pharm.* **2006,** *3,* 282-292.

52. Gonzalez, P.M.; Acharya, C.; Mackerell, A.D.,Jr; Polli, J.E. Inhibition requirements of the human apical sodium-dependent bile acid transporter (hASBT) using aminopiperidine conjugates of glutamyl-bile acids. *Pharm. Res.* **2009,** *26,* 1665-1678.

53. Rais, R.; Acharya, C.; Tririya, G.; Mackerell, A.D.; Polli, J.E. Molecular switch controlling the binding of anionic bile acid conjugates to human apical sodium-dependent bile acid transporter. *J. Med. Chem.* **2010,** *53,* 4749-4760.

54. Rais, R.; Acharya, C.; Mackerell, A.D.; Polli, J.E. Structural determinants for transport across the intestinal bile acid transporter using C-24 bile acid conjugates. *Mol. Pharm.* **2010,** *7,* 2240-2254.

55. Zheng, X.; Pan, Y.; Acharya, C.; Swaan, P.W.; Polli, J.E. Structural requirements of the ASBT by 3D-QSAR analysis using aminopyridine conjugates of chenodeoxycholic acid. *Bioconjug. Chem.* **2010,** *21,* 2038-2048.

56. Kim, J.Y.; Kim, K.H.; Lee, J.A.; Namkung, W.; Sun, A.; Ananthanarayanan, M.; Suchy, F.J.; Shin, D.M.; Muallem, S.; Lee, M.G. Transporter-mediated bile acid uptake causes Ca2+-dependent cell death in rat pancreatic acinar cells. *Gastroenterology* **2002,** *122,* 1941-1953.

57. Hagenbuch, B. and Meier, P.J. Molecular cloning, chromosomal localization, and functional characterization of a human liver Na+/bile acid cotransporter. *J. Clin. Invest.* **1994,** *93,* 1326-1331.

58. Ho, R.H.; Tirona, R.G.; Leake, B.F.; Glaeser, H.; Lee, W.; Lemke, C.J.; Wang, Y.; Kim, R.B. Drug and bile acid transporters in rosuvastatin hepatic uptake: function, expression, and pharmacogenetics. *Gastroenterology* **2006,** *130,* 1793-1806.

59. Lau, A.J. and Chang, T.K. Inhibition of human CYP2B6-catalyzed bupropion hydroxylation by Ginkgo biloba extract: effect of terpene trilactones and flavonols. *Drug Metab. Dispos.* **2009,** *37,* 1931-1937.

60. Frank, H. and Althoen, S., C. *Statistics: concepts and applications.* Cambridge University Press: 1994; pp. 853.

61. Bhattacharyya, A.; Mazumdar Leighton, S.; Babu, C.R. Bioinsecticidal activity of Archidendron ellipticum trypsin inhibitor on growth and serine digestive enzymes during larval development of Spodoptera litura. *Comp. Biochem. Physiol. C. Toxicol. Pharmacol.* **2007,** *145,* 669-677.

62. Ismair, M.G.; Kullak-Ublick, G.A.; Blakely, R.D.; Fried, M.; Vavricka, S.R. Tegaserod inhibits the serotonin transporter SERT. *Digestion* **2007,** *75,* 90-95.

63. Je, J.Y. and Kim, S.K. Water-soluble chitosan derivatives as a BACE1 inhibitor. *Bioorg. Med. Chem.* **2005,** *13,* 6551-6555.

64. Martin-Venegas, R.; Rodriguez-Lagunas, M.J.; Geraert, P.A.; Ferrer, R. Monocarboxylate transporter 1 mediates DL-2-Hydroxy-(4-methylthio)butanoic acid transport across the apical membrane of Caco-2 cell monolayers. *J. Nutr.* **2007,** *137,* 49-54.

65. Narawa, T.; Tsuda, Y.; Itoh, T. Chiral recognition of amethopterin enantiomers by the reduced folate carrier in Caco-2 cells. *Drug Metab. Pharmacokinet.* **2007,** *22,* 33-40.

66. Wong, I.L.; Chan, K.F.; Tsang, K.H.; Lam, C.Y.; Zhao, Y.; Chan, T.H.; Chow, L.M. Modulation of multidrug resistance protein 1 (MRP1/ABCC1)-mediated multidrug resistance by bivalent apigenin homodimers and their derivatives. *J. Med. Chem.* **2009,** *52,* 5311-5322.

67. Kakkar, T.; Boxenbaum, H.; Mayersohn, M. Estimation of Ki in a competitive enzyme-inhibition model: comparisons among three methods of data analysis. *Drug Metab. Dispos.* **1999,** *27,* 756-762.

68. Schlamowitz, M.; Shaw, A.; Jackson, W.T. Limitations of he Dixon plot for ascertaining naure of enzyme inhibition. *Tex. Rep. Biol. Med.* **1969,** *27,* 483-488.

69. Duan, P. and You, G. Novobiocin is a potent inhibitor for human organic anion transporters. *Drug Metab. Dispos.* **2009,** *37,* 1203-1210.

70. Lan, T.; Rao, A.; Haywood, J.; Davis, C.B.; Han, C.; Garver, E.; Dawson, P.A. Interaction of macrolide antibiotics with intestinally expressed human and rat organic anion-transporting polypeptides. *Drug Metab. Dispos.* **2009,** *37,* 2375-2382.

71. Knutter, I.; Wollesky, C.; Kottra, G.; Hahn, M.G.; Fischer, W.; Zebisch, K.; Neubert, R.H.; Daniel, H.; Brandsch, M. Transport of angiotensin-converting enzyme inhibitors by H+/peptide transporters revisited. *J. Pharmacol. Exp. Ther.* **2008,** *327,* 432-441.

72. Rais, R.; Gonzalez, P.M.; Zheng, X.; Wring, S.A.; Polli, J.E. Method to screen substrates of apical sodium-dependent bile acid transporter. *AAPS J.* **2008,** *10,* 596-605.

73. Craddock, A.L.; Love, M.W.; Daniel, R.W.; Kirby, L.C.; Walters, H.C.; Wong, M.H.; Dawson, P.A. Expression and transport properties of the human ileal and renal sodium-dependent bile acid transporter. *Am. J. Physiol.* **1998,** *274,* G157-69.

74. Zheng, X. and Polli, J.E. Synthesis and in vitro evaluation of potential sustained release prodrugs via targeting ASBT. *Int. J. Pharm.* **2010,** *396,* 111-118.

75. Rais, R.; Fletcher, S.; Polli, J.E. Synthesis and in vitro evaluation of gabapentin prodrugs that target the human apical sodium-dependent bile acid transporter (hASBT). *J. Pharm. Sci.* **2011,** *100,* 1184-1195.

76. Kramer, W.; Wess, G.; Neckermann, G.; Schubert, G.; Fink, J.; Girbig, F.; Gutjahr, U.; Kowalewski, S.; Baringhaus, K.H.; Boger, G. Intestinal absorption of peptides by coupling to bile acids. *J. Biol. Chem.* **1994,** *269,* 10621-10627.

77. Kullak-Ublick, G.A.; Glasa, J.; Boker, C.; Oswald, M.; Grutzner, U.; Hagenbuch, B.; Stieger, B.; Meier, P.J.; Beuers, U.; Kramer, W.; Wess, G.; Paumgartner, G. Chlorambucil-taurocholate is transported by bile acid carriers expressed in human hepatocellular carcinomas. *Gastroenterology* **1997,** *113,* 1295-1305.

78. Kramer, W.; Wess, G.; Enhsen, A.; Falk, E.; Hoffmann, A.; Neckermann, G.; Schubert, G.; Urmann, M. Modified bile acids as carriers for peptides and drugs. *J. Controlled Release* **1997,** *46,* 17-30.

79. Sievanen, E. Exploitation of bile acid transport systems in prodrug design. *Molecules* **2007,** *12,* 1859-1889.

80. Kramer, W. Transporters, Trojan horses and therapeutics: suitability of bile acid and peptide transporters for drug delivery. *Biol. Chem.* **2011,** *392,* 77-94.

81. Kullak-Ublick, G.A.; Stieger, B.; Meier, P.J. Enterohepatic bile salt transporters in normal physiology and liver disease. *Gastroenterology* **2004,** *126,* 322-342.

82. Tserng, K.Y.; Hachey, D.L.; Klein, P.D. An improved procedure for the synthesis of glycine and taurine conjugates of bile acids. *J. Lipid Res.* **1977,** *18,* 404-407.

83. Kritchevsky, D.; Poli, G.; Scolastico, C.; Sirtori, C.R. Novel derivatives of 3 alpha,7 alpha-dihydroxy-5 beta-cholan-24-oic acid (chenodeoxycholic acid) and 3 alpha,7 beta-dihydroxy-5 beta-cholan-24-oic acid (ursodeoxycholic acid). *Steroids* **1986,** *47,* 41-48.

84. Bortolini, O.; Fantin, G.; Fogagnolo, M.; Mari, L. Two-way enantioselective control in the epoxidation of alkenes with the keto bile acid–Oxone® system. *Tetrahedron* **2006,** *62,* 4482-4490.

85. Han, Y.H.; Busler, D.; Hong, Y.; Tian, Y.; Chen, C.; Rodrigues, A.D. Transporter studies with the 3-O-sulfate conjugate of 17alpha-ethinylestradiol: assessment of human liver drug transporters. *Drug Metab. Dispos.* **2010,** *38,* 1072-1082.

86. Balakrishnan, A.; Hussainzada, N.; Gonzalez, P.; Bermejo, M.; Swaan, P.W.; Polli, J.E. Bias in estimation of transporter kinetic parameters from overexpression systems: Interplay of transporter expression level and substrate affinity. *J. Pharmacol. Exp. Ther.* **2007,** *320,* 133-144.

87. Kolhatkar, V. and Polli, J.E. Reliability of inhibition models to correctly identify type of inhibition. *Pharm. Res.* **2010,** *27,* 2433-2445.

88. Kramer, W.; Stengelin, S.; Baringhaus, K.H.; Enhsen, A.; Heuer, H.; Becker, W.; Corsiero, D.; Girbig, F.; Noll, R.; Weyland, C. Substrate specificity of the ileal and the

hepatic Na(+)/bile acid cotransporters of the rabbit. I. Transport studies with membrane vesicles and cell lines expressing the cloned transporters. *J. Lipid Res.* **1999,** *40,* 1604-1617.

89. Bhat, L.; Jandeleit, B.; Dias, T.M.; Moors, T.L.; Gallop, M.A. Synthesis and biological evaluation of novel steroidal pyrazoles as substrates for bile acid transporters. *Bioorg. Med. Chem. Lett.* **2005,** *15,* 85-87.

90. Bemis, G.W. and Murcko, M.A. The properties of known drugs. 1. Molecular frameworks. *J. Med. Chem.* **1996,** *39,* 2887-2893.

91. Trauner, M. and Graziadei, I.W. Review article: mechanisms of action and therapeutic applications of ursodeoxycholic acid in chronic liver diseases. *Aliment. Pharmacol. Ther.* **1999,** *13,* 979-996.

92. Kolhatkar, V.; Diao, L.; Acharya, C.; MacKerell, A., D.; Polli, J.E. Identification of novel non-steroidal compounds as substrates or inhibitors of hASBT *Journal of pharmaceutical sciences* **2011,**

93. Baumgart, D.C. and Carding, S.R. Inflammatory bowel disease: cause and immunobiology. *Lancet* **2007,** *369,* 1627-1640.

94. Mahmud, N.; O'Toole, D.; O'Hare, N.; Freyne, P.J.; Weir, D.G.; Kelleher, D. Evaluation of renal function following treatment with 5-aminosalicylic acid derivatives in patients with ulcerative colitis. *Aliment. Pharmacol. Ther.* **2002,** *16,* 207-215.

95. Wallace, J.L. and Sharkey, K.A. Pharmacotherapy of Inflammatory Bowel Disease, In *Goodman & Gilman's The Pharmacological Basis of Therapeutics http://www.accessmedicine.com/content.aspx?aID=16675684.* 11th ed.; Brunton, L., L., Chabner, B., A. and Knollmann, B., C., Eds.;2006;

96. Peppercorn, M.A. Sulfasalazine. Pharmacology, clinical use, toxicity, and related new drug development. *Ann. Intern. Med.* **1984,** *101,* 377-386.

97. Kolhatkar, V. and Polli, J.E. Effect of Structural Modifications of Steroidal Hydroxyl Groups on Bile Acid Interaction with Human Apical Sodium-Dependent Bile Acid Transporter. *AAPS J.* **2010,** *12,* http://www.aapsj.org/abstracts/AM_2010/M1199.pdf.

98. Annaert, P.; Kinget, R.; Naesens, L.; de Clercq, E.; Augustijns, P. Transport, uptake, and metabolism of the bis(pivaloyloxymethyl)-ester prodrug of 9-(2-phosphonylmethoxyethyl)adenine in an in vitro cell culture system of the intestinal mucosa (Caco-2). *Pharm. Res.* **1997,** *14,* 492-496.

99. Morrison, R.T. and Boyd, R.N. *Organic Chemistry.* Allyn and Bacon, Inc.: 1973;

100. Perazella, M.A. and Markowitz, G.S. Drug-induced acute interstitial nephritis. *Nat. Rev. Nephrol.* **2010,** *6,* 461-470.

101. Calder, I.C.; Funder, C.C.; Green, C.R.; Ham, K.N.; Tange, J.D. *Nephrotoxic lesions from 5-aminosalicylic Acid. Br. Med. J.* **1972,** *1,* 152-154.

102. Hamling, J.; Raedler, A.; Helmchen, U.; Schreiber, S. 5-Aminosalicylic acid-associated renal tubular acidosis with decreased renal function in Crohn's disease. *Digestion* **1997,** *58,* 304-307.

103. Courtney, M.G.; Nunes, D.P.; Bergin, C.F.; O'Driscoll, M.; Trimble, V.; Keeling, P.W.; Weir, D.G. Randomised comparison of olsalazine and mesalazine in prevention of relapses in ulcerative colitis. *Lancet* **1992,** *339,* 1279-1281.

104. Green, J.R.; Lobo, A.J.; Holdsworth, C.D.; Leicester, R.J.; Gibson, J.A.; Kerr, G.D.; Hodgson, H.J.; Parkins, K.J.; Taylor, M.D. Balsalazide is more effective and better tolerated than mesalamine in the treatment of acute ulcerative colitis. The Abacus Investigator Group. *Gastroenterology* **1998,** *114,* 15-22.

105. Cameron, A.J.; Baron, J.H.; Priestley, B.L. Erythema multiforme, drugs, and ulcerative colitis. *Br. Med. J.* **1966,** *2,* 1174-1178.

106. Di Paolo, M.C.; Paoluzi, O.A.; Pica, R.; Iacopini, F.; Crispino, P.; Rivera, M.; Spera, G.; Paoluzi, P. Sulphasalazine and 5-aminosalicylic acid in long-term treatment of ulcerative colitis: report on tolerance and side-effects. *Dig. Liver Dis.* **2001,** *33,* 563-569.

107. Batta, A.K.; Tint, G.S.; Xu, G.; Shefer, S.; Salen, G. Synthesis and intestinal metabolism of ursodeoxycholic acid conjugate with an antiinflammatory agent, 5-aminosalicylic acid. *J. Lipid Res.* **1998,** *39,* 1641-1646.

108. Hasanain, F. and Wang, Z.Y. New one-step synthesis of polyimides in salicylic acid. *Polymer* **2008,** *49,* 831-835.

109. Solomons, T.W.G. *Organic Chemistry.* John Wiley & Sons, Inc.: New York, 1992;

110. Lewis, J.D.; Deren, J.J.; Lichtenstein, G.R. Cancer risk in patients with inflammatory bowel disease. *Gastroenterol. Clin. North Am.* **1999,** *28,* 459-77, x.

111. Earnest, D.L.; Holubec, H.; Wali, R.K.; Jolley, C.S.; Bissonette, M.; Bhattacharyya, A.K.; Roy, H.; Khare, S.; Brasitus, T.A. Chemoprevention of azoxymethane-induced

colonic carcinogenesis by supplemental dietary ursodeoxycholic acid. *Cancer Res.* **1994,** *54,* 5071-5074.

112. Ikegami, T.; Matsuzaki, Y.; Shoda, J.; Kano, M.; Hirabayashi, N.; Tanaka, N. The chemopreventive role of ursodeoxycholic acid in azoxymethane-treated rats: suppressive effects on enhanced group II phospholipase A2 expression in colonic tissue. *Cancer Lett.* **1998,** *134,* 129-139.

113. Kim, H.S. Prevention of colon cancer with ursodiol in ulcerative colitis. *Inflamm. Bowel Dis.* **2001,** *7,* 279-280.

114. Pardi, D.S.; Loftus, E.V.,Jr; Kremers, W.K.; Keach, J.; Lindor, K.D. Ursodeoxycholic acid as a chemopreventive agent in patients with ulcerative colitis and primary sclerosing cholangitis. *Gastroenterology* **2003,** *124,* 889-893.

115. Serfaty, L.; De Leusse, A.; Rosmorduc, O.; Desaint, B.; Flejou, J.F.; Chazouilleres, O.; Poupon, R.E.; Poupon, R. Ursodeoxycholic acid therapy and the risk of colorectal adenoma in patients with primary biliary cirrhosis: an observational study. *Hepatology* **2003,** *38,* 203-209.

116. Tung, B.Y.; Emond, M.J.; Haggitt, R.C.; Bronner, M.P.; Kimmey, M.B.; Kowdley, K.V.; Brentnall, T.A. Ursodiol use is associated with lower prevalence of colonic neoplasia in patients with ulcerative colitis and primary sclerosing cholangitis. *Ann. Intern. Med.* **2001,** *134,* 89-95.

117. Alberts, D.S.; Martinez, M.E.; Hess, L.M.; Einspahr, J.G.; Green, S.B.; Bhattacharyya, A.K.; Guillen, J.; Krutzsch, M.; Batta, A.K.; Salen, G.; Fales, L.; Koonce, K.; Parish, D.; Clouser, M.; Roe, D.; Lance, P.; Phoenix and Tucson Gastroenterologist Networks Phase III trial of ursodeoxycholic acid to prevent colorectal adenoma recurrence. *J. Natl. Cancer Inst.* **2005,** *97,* 846-853.

118. Amaral, J.D.; Viana, R.J.; Ramalho, R.M.; Steer, C.J.; Rodrigues, C.M. Bile acids: regulation of apoptosis by ursodeoxycholic acid. *J. Lipid Res.* **2009,** *50,* 1721-1734.

119. Dawson, P.A.; Lan, T.; Rao, A. Bile acid transporters. *J. Lipid Res.* **2009,** *50,* 2340-2357.

120. Tolle-Sander, S.; Lentz, K.A.; Maeda, D.Y.; Coop, A.; Polli, J.E. Increased acyclovir oral bioavailability via a bile acid conjugate. *Mol. Pharm.* **2004,** *1,* 40-48.

121. Vallim, T.Q. and Edwards, P.A. Bile acids have the gall to function as hormones. *Cell. Metab.* **2009,** *10,* 162-164.

122. Knop, F.K. Bile-induced secretion of glucagon-like peptide-1: pathophysiological implications in type 2 diabetes? *Am. J. Physiol. Endocrinol. Metab.* **2010,** *299,* E10-3.

123. Fiorucci, S.; Cipriani, S.; Mencarelli, A.; Renga, B.; Distrutti, E.; Baldelli, F. Counter-regulatory role of bile acid activated receptors in immunity and inflammation. *Curr. Mol. Med.* **2010,** *10,* 579-595.

124. Setchell, K.D.; Rodrigues, C.M.; Podda, M.; Crosignani, A. Metabolism of orally administered tauroursodeoxycholic acid in patients with primary biliary cirrhosis. *Gut* **1996,** *38,* 439-446.

125. Brown, R.D. and Martin, Y.C. The information content of 2D and 3D structural descriptors relevant to ligand-receptor binding. *J. Chem. Inf. Comput. Sci.* **1997,** *37,* 1-9.

126. Butina, D. Unsupervised data base clustering based on Daylight's fingerprint and Tanimoto similarity: a fast and automated way to cluster small and large data sets. *J. Chem. Inf. Comput. Sci.* **1999,** *39,* 747-750.

127. Xue, L.; Godden, J.W.; Stahura, F.L.; Bajorath, J. Design and Evaluation of a Molecular Fingerprint Involving the Transformation of Property Descriptor Values into a Binary Classification Scheme. *J. Chem. Inf. Comput. Sci.* **2003,** *43,* 1151-1157.

128. El Harchaoui, K.; Akdim, F.; Stroes, E.S.; Trip, M.D.; Kastelein, J.J. Current and future pharmacologic options for the management of patients unable to achieve low-density lipoprotein-cholesterol goals with statins. *Am. J. Cardiovasc. Drugs* **2008,** *8,* 233-242.